Fall 11-16-2015

Polymeric Porphyrins as Solar Photocatalysts

Nicholas Upton Day
Portland State University

Polymeric Porphyrins as Solar Photocatalysts

by

Nicholas Upton Day

A dissertation submitted in partial fulfillment of the
requirements for the degree of

Doctor of Philosophy
in
Chemistry

Dissertation Committee:
Carl Wamser, Chair
Erik Johansson
David Stuart
Erik Bodegom

Portland State University
2015

Abstract

Research concentrated on the absorption, transformation, and storage of light energy is useful for the energy challenges faced by humanity. In particular, photocatalysis using solar energy to generate useful fuels has become a primary research goal in the drive to replace fossil fuels for the future. In this dissertation it is shown that poly-tetra(4-aminophenyl)porphyrin (pTAPP) can be oxidatively polymerized using a variety of methods, including electropolymerization, chemical oxidation, and interfacial polymerization and that pTAPP has photocatalytic ability to reduce O_2 to H_2O_2 for a storable fuel.

Organic conductive polymers such as pTAPP are attractive catalysts because of their high surface area and ability to coat electrodes. pTAPP in a mixed oxidation state is shown to have both its minimum charge transfer resistance as well as its minimum impedance to electronic conductivity in the film. The UV-vis-NIR absorption spectra of pTAPP with increased oxidative doping are similar to hyperporphyrin spectra, characteristic of a two-plus charge localized on a single porphyrin unit. This suggests the presence of a bipolaron on the individual porphyrin units, and thus a bipolaron conductivity mechanism has been proposed.

pTAPP changes color depending on its oxidation state, and therefore is a promising material for electrochromic devices. A novel Pourbaix diagram was created as a means of illustrating the redox and protonation states of pTAPP as a function of changes in pH, applied potential, electrochromic behavior, and electronic conductivity.

Both pTAPP and pCoTAPP were shown to be effective catalysts for the reduction of oxygen to hydrogen peroxide, with pCoTAPP a better catalyst than pTAPP. When pCoTAPP is irradiated, oxygen reduction occurs close to the thermodynamic potential, indicating a promising system for storage of solar energy.

Acknowledgements

First I would like to thank Dr. Carl Wamser for all of your guidance and care over the last five years. It has been an honor to work with you as both a wonderful mentor and an admirable individual. I have the utmost respect for your knowledge and how you conduct yourself on a daily basis. I could not have made a better decision when choosing an instructor from which to learn. I am honored to be one of your last graduate students and to join the elite science genealogy you embody.

Secondly, I would like to thank Dr. Erik Johansson for emboldening me with a desire to learn electrochemistry. I came here planning to be an organic chemist and am leaving as an organic electrochemist. There is no doubt in my mind that the change in my field of interest was due to your teaching and encouragement.

I would also like to thank Dr. David Reingold for pushing me to continue in academia and encouraging me to meet with many of the highly successful speakers he has brought to Portland through the ACS. I relish these opportunities and know they make me a stronger scientist at each step. Your light-hearted attitude and good sense of humor have given me the continued desire to become a professor and stay in academics. I would also like to thank you for helping to defend my position in lab meetings as well as cutting through much of the fluff which tends to appear in lab meetings. I hope the snacks were worth it.

Dr. Warren Ford, thank you for helping me understand polymers and carbon nanotubes on a higher level. I have both enjoyed and grown from many a conversation with you along rides to and from the ACS talks. It has been my pleasure to be able to pick your brain on polymers. I know that your edits to my polymer-related papers made them much stronger.

Dr. David Stuart, your arrival to our department in my third year was an exciting addition. Having been challenged with the task of organometallic catalysis, your class and expertise has allowed me to articulate my proposed reaction mechanisms to a higher level. Your availability, approachability and professionalism are admirable qualities seldom found together.

Dr. Theresa McCormick, you have been a breath of fresh air in my career here and undoubtedly to the department. Reading your papers upon your interview in my fourth year led me down an intellectually fruitful path. I would have loved to have you on my committee.

Keith James, you have been the best of informants and have always led me towards a better understanding of the fundamental chemistry involved with any experiment. Your basic knowledge of binding energies, spontaneous reactions and preparatory methods have undoubtedly made hundreds of my experiments in the lab successes when they were so often doomed for failure. I only hope to one day obtain the chemical knowledge which you hold at your fingertips.

Last but certainly not least I'd like to thank my fiancée Daphne; without your help and encouragement I could never have graduated. Thank you for reviewing countless documents and letting me work countless hours. I only hope I can return all of the inspiration and help you have given me over these last five years through the rest of our lives.

Table of Contents

LIST OF TABLES

LIST OF FIGURES

LIST OF ABBREVIATIONS

α	Dispersion coefficient for constant phase elements
APS	Ammonium persulfate
CoTAPP	Cobalt-Tetrakis-5,10,15,20-(4-aminophenyl)porphyrin
CoTCPP	Cobalt-Tetrakis-5,10,15,20-(4-carboxyphenyl)porphyrin
C_{HOP}	Capacitances due to hopping between conjugated segments
$C_{combined}$	Distributed capacitance at film solution interface
CPE	Constant phase element
CPE_{hop}	Capacitances due to hopping between conjugated segments
CPE_{dl}	Capacitances due to double-layer capacitance
CPE_{DL}	Bulk capacitance of the double layer between polymer and solution
CPE_{ps}	Capacitances due to pseudocapacitance
CPE_{PS}	Bulk pseudocapacitance of the film
CV	Cyclic voltammetry
DCM	Dichloromethane
EIS	Electrochemical impedance spectroscopy
FTO	Fluorine-doped tin oxide
LSV	Linear sweep voltammetry
ORR	Oxygen Reduction Reaction
pAni	Polyaniline

pCoTAPP	Poly-Cobalt-tetrakis-5,10,15,20-(4-aminophenyl)porphyrin
pTAPP	Poly-tetrakis-5,10,15,20-(4-aminophenyl)porphyrin
PV	Photovoltaic
R_{conj}	Impedances between conjugated segments of polymer
R_{ct}	Charge transfer impedances at the polymer/solution interface
R_{CT}	Bulk charge transfer impedance within the polymer film
$R_{electronic}$	Impedance through the polymer film
R_{hop}	Impedances between conjugated segments of polymer
R_{HOP}	Bulk impedance between conjugated segments of polymer
R_{ion}	Ohmic impedances due to ionic transport
R_{ionic}	Ohmic impedances due to ionic transport
R_{OHM}	Combined ohmic impedance within the bulk film and ionic solution
RC	Resistor and capacitor in parallel
RDE	Rotating disk electrode
SEM	Scanning electron microscopy
TAPP	Tetrakis-5,10,15,20-(4-aminophenyl)porphyrin
TBAP	Tetrabutylammonium perchlorate
TCPP	Tetrakis-5,10,15,20-(4-carboxyphenyl)porphyrin
TiOTPyP	Titanium-oxo-tetrakis-5,10,15,20-(4-pyridyl)porphyrin
TON	Turnover number
TOF	Turnover frequency

VitC	Citric Acid (Vitamin C)
ZnTAPP	Zinc-tetrakis-5,10,15,20-(4-aminophenyl)porphyrin

1 INTRODUCTION

1.1 Motivation

The need for alternative renewable energy stems from the environmental instability caused by our current fuel sources. As of April 2013, multiple agencies have measured atmospheric CO_2 at or above 400 ppm, 150 ppm above historic levels.(*1*),(*2*),(*3*) It is projected that global CO_2 emissions will continue to increase to 37.2 gigatons, leaving the earth on track for an increase in temperature of 3.6 ºC.(*4*) Considering current energy demands heavily outweigh the amount of carbon-neutral energy utilized, we must implement new ways to harvest renewable energy more efficiently or greatly reduce our energy demand.(*4*)

As global economic development continues to grow, an increase in energy demand is inevitable. Developing nations, led by China and followed by India, Brazil, and the rest of South America and Asia, will account for an increase in global energy consumption more than doubling current usage. Since the industrial revolution we have seen that with an increase in wealth, the demand for goods, services, and energy also increases.(*5*) Ayres et al. argue that manufacturing processes become more energy efficient with time, which causes production costs to decrease. However, as market prices for these products decrease, demand increases, leading to an increase in energy consumption to supply the demand. Interestingly it is the increase of demand that overbalances the decrease in energy consumption as manufacturing processes are always

being improved to become more energy efficient. Therefore it is unlikely that we will be able to rely on decreasing energy demand through simply increasing the efficiency of manufacturing processes, leaving us with the task of producing enough renewable energy for the world to not only sustain itself but also to grow.

According to the International Energy Agency the world produced 17 TW of power in 2011 and used 12 TW of this power globally.(*4*) This is similar to the estimate of 15 TW by Lewis et al. in 2006.(*6*) Global energy demand is expected to increase by approximately 33 percent by 2035.(*4*) Even though all forms of energy are projected to increase, the total percentage of energy demand from fossil fuels is projected to decrease from 82 to 76 percent.(*4*) Progress towards renewables has already begun to offset and is projected to account for approximately half of the increased electricity gain globally.(*4*) Unfortunately oil and coal are projected to continue their dominance in the transportation sector and creating a storable fuel becomes increasingly important. Recently the price of oil has dropped from around $115 per barrel to $45 per barrel, significantly changing the target cost of renewable fuels.(*7*) This suggests that as a new type of fuel enters the market oil producers may simply produce significantly more oil. This will force any renewable technology to be able to compete at costs less than the current energy prices in order to compete for customers not persuaded by the negative effects of using fossil fuels.

The diversification of renewable energy production is currently considered the best way to achieve the complete replacement of fossil fuels. Potential renewable energy sources include solar, wind, geothermal, hydropower, biomass, and wave/tidal power.

Excluding biomass, in 2011 only about 3 percent of the world's energy came from these renewable sources.(*4*) Biomass contributed approximately 10 percent of our energy in 2010 but it is difficult to estimate how much of that energy was replenished and thus is really sustainable.(*4*) In 2011, 32 percent of the world's energy came from oil, 22 percent from gas, and 27 percent from coal, resulting in approximately 30 gigatons of CO_2 being released into the atmosphere.(*4*) Nuclear energy accounts for about 6 percent of global energy supply and is carbon neutral; unfortunately it has other risk factors which make it undesirable, such as the production of environmentally hazardous waste. Concentrating efforts to harvest more solar, wind, and geothermal power will allow the replacement of more fossil fuels with both carbon-neutral and renewable energy sources.

As the world moves towards a global approach to fighting climate change there will likely be implementation of monetary incentives to discourage the use of fossil fuels. Whether these deterrents are directly imposed as fees or through mitigation efforts, the cost of polluting will continue to rise steadily in the future. Wind generation has reached purchasing power equivalence with natural gas in the interior of the United States.(*8*) Reports have started to appear showing silicon solar energy is now cheaper than fossil fuels in select locations around the globe.(*6*),(*9*),(*10*),(*11*) Silicon photovoltaics (PV) should continue to drop in price through a decrease in government regulation as well as decreased installation costs.(*12*) Subsidies for solar PV will continue to be needed until the associated cost of using non-renewable resources rises and the cost of using renewable resources becomes more balanced. The US should take an active role in

producing renewable energy. It will not only benefit us now but also allow us to maintain our role as a leader in the future.

1.2 Photocatalysis for the Storage of Light Energy

Some scientists believe the technology to produce enough renewable energy to power the planet exists with silicon PVs.(*13*),(*14*) If silicon PVs can produce enough power, then the problem for global renewable energy changes from production to storage. A viable and cost efficient way to store energy during times of high production from both solar PVs and wind generation will hopefully lead to a carbon neutral future.

Solar and wind energy suffer from fluctuations in production.(*15*),(*16*) This variability in power supply causes problems with the energy grid. There are many possible solutions to this problem, such as offering cheaper power at times of high output and even linking multiple locations on the planet together so that solar energy is always being produced.(*17*),(*18*),(*19*) Energy providers have already installed new plants which can be turned on and off faster in order to save money during times of high production. Coal plants are understandably slow to turn on and off but natural gas plants can be started and stopped relatively quickly.(*20*) Recently, California passed a new mandate requiring energy companies to install storage facilities to match the renewable energy systems being installed throughout the state, and Tesla released a battery designed for home storage.(*21*)(*22*) Energy storage is the next major step for the energy security of society and the major hurdle continues to be for transportation. The most realistic option is to efficiently store renewable energy locally to be used in periods of low production.

One of the best ways to store energy for long periods is in chemical bonds.(*6*) Plants, batteries, and fossil fuels are all great examples of chemical storage. Many scientists believe one of the best molecules for energy storage will be H_2.(*23*),(*24*) If it can be produced on demand it easily holds ample energy for our purposes. Fuels such as methanol, methane, and H_2O_2 may prove to be better molecules to store energy as they are easily stored for long periods of time.(*25*) Many other organic, inorganic, and metal ions have been proposed and tested for energy storage. All systems have advantages and disadvantages, but the most promising systems typically employ small molecules for optimum energy density.

1.3 H_2, CH_3OH and H_2O_2

H_2, CH_3OH, CH_4, and H_2O_2 are all desirable molecules to store light energy in chemical bonds. The reduction of H^+ to hydrogen is relatively easy and happens readily at a platinum electrode.(*26*) Research concerning the production of H_2 for energy is an active and thriving area.(*27*) The most commonly used and best method for H_2 production is currently various reformation methods.(*28*) The energy density of oxidizing H_2 to H_2O is shown in Equation 1.1. Because of the inability to store H_2 in a compact nature, the energy density of a liter of H_2 gas at ambient temperature is only 10.7 kJ despite its high energy density. The United States Department of Energy has determined that this number is three times too low for feasibly storing energy for use.(*29*)

$$H_2 + 1/2\ O_2 \longrightarrow H_2O \qquad = 120\ kJ/g \qquad \text{Eq. 1.1}$$

In order for CH_3OH or CH_4 to be carbon neutral we must reduce atmospheric CO_2. The reduction of CO_2 to methane or methanol has proven to be a relatively difficult task. CO_2 is a linear, stable molecule and is the most oxidized form of carbon. As a linear molecule it has no dipole moment even though it has two polar carbon-oxygen double bonds.(*30*) In order to reduce CO_2 many researchers believe we first must activate it; activation often involves a single bonding interaction (η^1) or a side-on carbon-oxygen (η^2) interaction with a metal or an organometallic reagent allowing CO_2 to take on a bent configuration.(*31*) Once CO_2 is activated, the carbon atom will take a partial positive charge creating a place for attack by nucleophiles. Coordination of CO_2 by metals and other molecules has been postulated to occur in many fashions.(*30*) No matter the coordination site, number, or mechanism, CO_2 still proves rather difficult to reduce. Many reactions use CO_2 as a substrate but few reduce CO_2 efficiently, without high energy reactants and conditions.(*30*) If CO_2 could be efficiently reduced to methanol, it would contain about half the energy density of gasoline.(*25*) In addition a liter of either fuel contains ample energy to be a viable source of stored energy once efficient carbon dioxide reduction is achieved.

$$CH_3OH + 3/2\ O_2 \longrightarrow CO_2 + 2\ H_2O \qquad = 22\ kJ/g \qquad \text{Eq. 1.2}$$

$$C_8H_{18} + 12.5\ O_2 \longrightarrow 8\ CO_2 + 9\ H_2O \qquad = 48\ kJ/g \qquad \text{Eq. 1.3}$$

The decomposition of H_2O_2 to O_2 and H_2O is catalyzed by many transition metals.(*32*) Today over 3.5 Mtons of H_2O_2 is produced industrially, primarily for bleaching purposes. H_2O_2 is typically produced today using H_2, anthraquinone and a Pd

catalyst.(*32*) The mechanism is still under debate but the process is highly efficient. Currently H_2O_2 is considered a green oxidant and industrially desirable. H_2O_2 holds less energy than both H_2 and CH_3OH, as can be seen in Equation 1.4, yet still has only water and O_2 as byproducts. The energy density of H_2O_2 per volume is also high enough to be a viable way to store energy today. One liter of 50 percent H_2O_2 holds 1350 kJ which is high enough to be a realistic option for today's demands. Currently the US government considers any concentration of H_2O_2 over 50 percent to be hazardous, but in comparison with nuclear reactors hazards H_2O_2 is safe.

$$H_2O_2 \longrightarrow \tfrac{1}{2}\ O_2 + H_2O \quad = 2.7\ kJ/g \qquad \text{Eq. 1.4}$$

H_2O_2 is a stable molecule and can be stored readily in liquid form. The reduction of O_2 to hydrogen peroxide is possible at low overpotentials, making it an energy efficient process. While H_2 and methanol hold higher energy densities, the inability to store H_2 at a reasonable volume and the inability to make methanol from carbon dioxide prevent their use as storable fuels. H_2O_2 is considered by some to be the molecule of choice for storage of clean energy today, with the main problem being the development of an efficient and durable fuel cell to release the stored energy.(*33*)(*34*)

1.4 Methods to Use Stored Energy

There are many available options for using stored energy and each has its own advantages and disadvantages. Fuel cells are reactors, which take chemical energy, in the form of molecules and covert it to electrical energy. Fuel cells normally rely on the

oxidation of a high-energy reactant. The most commonly used reactants in fuel cells are H_2 and O_2 with water as the byproduct.(*35*) Water as a byproduct is very desirable environmentally and the recombination of water molecules can give 1.23 V of potential as shown below.

Anode: $H_2 \longrightarrow 2\,H^+ + 2\,e^-$	0.0 V vs. NHE	Eq. 1.5
Cathode: $O_2 + 4\,H^+ + 4\,e^- \longrightarrow 2\,H_2O$	1.23 V vs. NHE	Eq. 1.6
Overall Reaction: $O_2 + 2\,H_2 \longrightarrow 2\,H_2O$	1.23 V	Eq. 1.7

One major downside to these systems is the catalysts used to oxidize H_2 or reduce O_2 as they typically contain platinum which is expensive and can become contaminated leading to decreased reactivity.(*36*) Another drawback is the storage of H_2 as a feedstock due to its size and permeability through many materials.(*37*)(*38*) Storage of H_2 as a gas or as a liquid in tanks or molecules to enable release of large quantities of H_2 on demand is heavily researched.(*37*)

Direct methanol fuel cells are also well researched, but they also have major limitations. One of the largest issues concerning operation is methanol crossover through the selective membrane. Because of the methanol crossover, direct methanol fuel cells have a low lifetime and high cost leading to the lack of deployment as a replacement for batteries.(*39*)

Recently flow cell reactors have also begun test implementations. Similar to fuel cells, the main advantage of flow cells comes from the storage of redox-active chemicals

in large reservoirs.(*40*),(*41*) This allows a large amount of energy to be stored without increasing the expensive electrode materials necessary for collection. Current flow cells typically use vanadium, iron, chromium, and bromine as redox active ions, but recently all-organic molecules have gained interest.(*40*),(*41*),(*42*)

Batteries and capacitors are another currently implemented and heavily researched method to store renewable energy. Batteries are implemented in many of the electronics used on a daily basis by the developed world.(*43*) Cost effective and reasonably consumer friendly, they are currently the best way to store readily accessible power for applications. The only reasonable alternative to batteries would be capacitors, and most importantly the electrochemical capacitor, also known as a supercapacitor. While traditional capacitors do not hold enough energy density to be replacements for batteries, supercapacitors can hold ample energy for small devices and have the potential to be more consumer friendly. The drawbacks associated with batteries are recharge time and cost. Supercapacitors hold the ability to be charged very quickly and if not for the inability to hold charge, known as leakage current, they would quickly become more popular than batteries.(*44*) Still both of these energy storage devices are considered too expensive for grid-scale storage, they are likely to remain at the consumer level for most applications. There is at least one test facility being built by business magnate Warren Buffet to store grid scale energy using batteries, which may encourage more power companies to build similar systems.(*45*) Although batteries currently control the market,

fuel cells hold significant advantages. In particular fuel cells have potential for many larger scale applications today.

The oxidation of H_2O_2 to O_2 and the reduction of H_2O_2 to H_2O yields an achievable potential of 1.09 V.(*46*) This is shown below by the following anodic and cathodic reactions.

Anode: $H_2O_2 \longrightarrow O_2 + 2\,H^+ + 2\,e^-$	0.68 V vs. NHE	Eq. 1.8
Cathode: $H_2O_2 + 2\,H^+ + 2\,e^- \longrightarrow 2\,H_2O$	1.77 V vs. NHE	Eq. 1.9
Overall Reaction: $2\,H_2O_2 \longrightarrow O_2 + 2\,H_2O$	1.09 V	Eq. 1.10

This is a slightly lower theoretically obtainable potential than the commonly targeted hydrogen fuel cell at 1.23 V.(*47*) Like the major advantage of the hydrogen fuel cell, the H_2O_2 fuel cell has no toxic byproducts.

H_2O_2 fuel cells have a few significant advantages over other types of fuel cells. First, H_2O_2 acts as both the reductant and the oxidant.(*33*) This allows the fuel cell to bypass the need for an ion-selective membrane to keep the reactants separated (Figure 1.1). In addition, as can be seen in the reduction equations above, H_2O_2 has a higher standard reduction potential than O_2, 1.77 V vs. 1.23 V. This would allow higher energy densities if paired with other standard reductants.(*48*) Lastly, but possibly most importantly, H_2O_2 can be easily stored as a liquid, even in plastic containers.(*34*) In order to bring H_2O_2 fuel cells into competition, the anodic and cathodic electrode catalysts need to be optimized. Along with certain metals and recently Prussian blue, Co-porphyrins have shown good activity for the anodic reaction.(*46*)(*49*)(*50*)

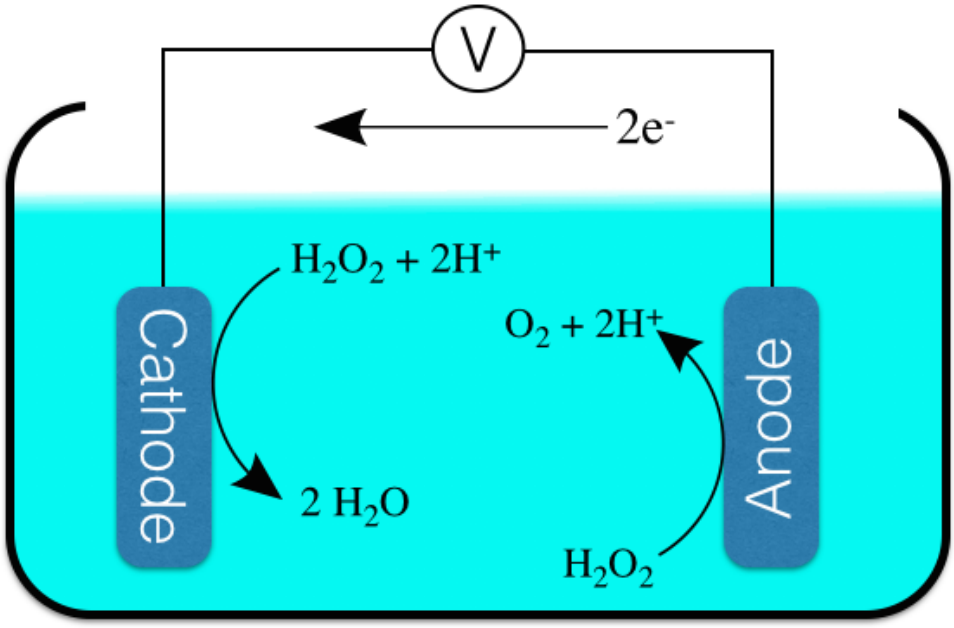

Figure 1.1 Typical H_2O_2 fuel cell. Only H_2O_2 is needed for both the reductant and the oxidant, circumventing the necessity of an internal membrane to keep the anolyte and catholyte separate.

1.5 Cobalt Metallated Porphyrins for Oxygen Reduction

The oxygen reduction reaction (ORR) (Eq. 1.5) has slow reaction kinetics even on Pt catalysts and is cited as one of the major limitations of efficiency with some fuel cells.(*51*)(*52*) ORR catalysts which do not use Pt are highly desirable. Cobalt metallated porphyrins are known to have high activity towards O_2 reduction.(*52*) In addition there has recently been significant interest in metal-free ORR catalysts, and it has been found that N-containing conjugated systems show good activity.(*52*) Studies show cobalt porphyrins to be able to reduce O_2 by only two electrons to H_2O_2 or by four electrons to

H_2O.(*53*)(*54*) Both reactions are highly desirable depending on the fuel cell architecture and electrode materials. A few studies attempted to drive the H_2O_2 fuel cell using light.(*55*) Using light energy to reduce O_2 may allow energy collection along with the creation of a storable fuel. It is unlikely that the reaction would proceed efficiently enough to be driven solely by light but the combination of light with applied potential may lead to an underpotential.

One good H_2O_2 catalytic porphyrin is cobalt-tetrakis-5,10,15,20-(4-carboxyphenyl)porphyrin (CoTCPP).(*56*) CoTCPP has been shown to reduce O_2 to H_2O_2 both selectively and with high turnover numbers. The Fukuzumi research group has proposed using CoTCPP to produce H_2O_2 from O_2 on a scale large enough to store energy for grid scale demand. They have also shown linking cobalt porphyrins with silicon photovoltaic systems in order to reduce O_2 to H_2O_2.(*56*) These types of systems, if proven to be highly efficient, would be a realistic way to produce storable fuel today.

1.6 Porphyrins as Light Energy Collectors and Catalysts

Porphyrins have been studied since their discovery as a replacement for royal purple, a purple dye made from indigo, by BASF in 1897.(*57*) The characteristic strong blue absorption, high heat resistance, fully conjugated structure, and adjustable properties, make them prime research candidates for a variety of applications, including catalysis, solar energy, photodynamic therapy, telecommunications, antibacterial and antifungal treatments, and conductive polymers to name a few.(*58*)

As a light absorber, porphyrins have an extinction coefficient greater then 250,000 $M^{-1}cm^{-1}$ at their Soret peak, typically between 420 to 450 nm.(*58*) To put this into perspective, this means a solution of only 4 mM will absorb 90 percent of the blue light within 1 mm. A free base porphyrin (non-metallated) typically has four absorbance peaks beyond the Soret band known as Q-bands. These absorbances are much weaker than the Soret peak but still absorb considerable light. Upon metallation the four Q-bands are replaced by two Q-bands which are typically at shorter wavelengths. Figure 1.2 shows the absorption spectra of 5,10,15,20-tetrakis(4-aminophenyl)porphyrin (TAPP) and zinc metallated TAPP (ZnTAPP) for comparison. In addition to monomeric porphyrins as photocatalysts, many polymeric systems have been studied.(*59*)

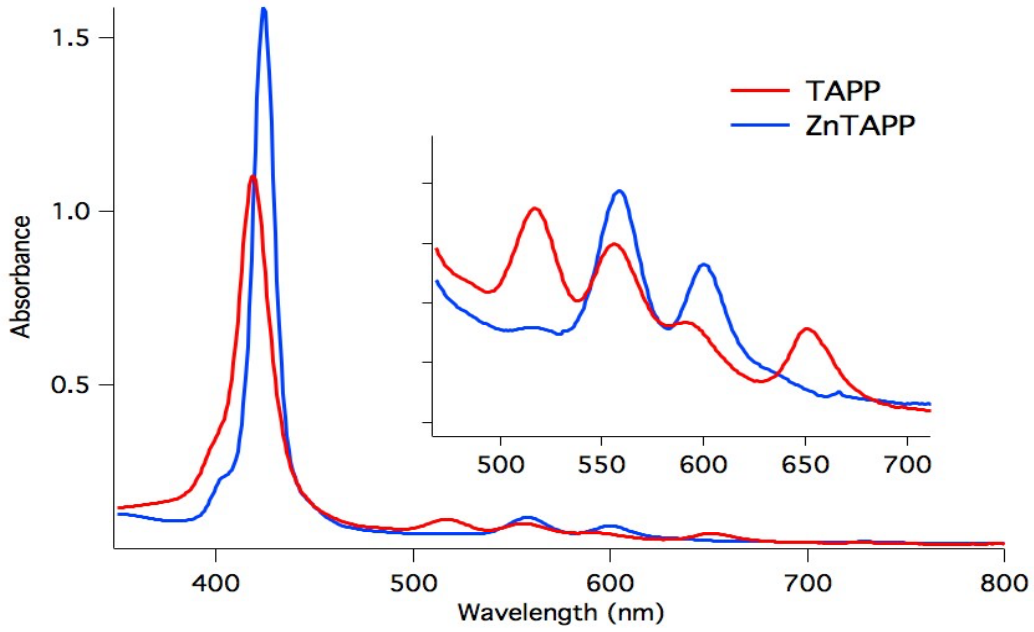

Figure 1.2 Absorbance spectra of TAPP and ZnTAPP in acetonitrile approximately 4 μM. The inset emphasizes the four Q-band to two Q-band absorption change upon metallation.

Metallated porphyrins allow coordination and activation of many small molecules. Porphyrin metallation is relatively easy and a typical procedure can be seen in Figure 1.3. Metals inside of porphyrins take on a square planar configuration with the metal ion typically having a two plus charge. Above and below the ring are open axial coordination sites. The major limitations of porphyrins as catalysts are structural decomposition and catalyst poisoning. We hope using a heterogeneous polymeric porphyrin catalyst with a conductive structure can alleviate these problems.

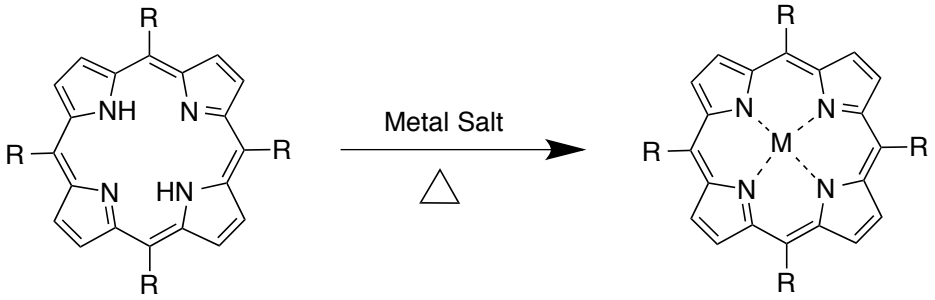

Figure 1.3 Generalized reaction scheme for porphyrin metallation.

1.7 Porphyrin 2D and 3D Polymers as Photocatalysts

There are a vast array of porphyrin-based polymers which extend in both two- and three-dimensional space.(*59*) Polymers can extend through both covalent bonds and coordination networks. The coordination networks are often referred to as covalent organic frameworks (COFs) or metal organic frameworks (MOFs) depending on the types of linkages contained within the system. The work contained within this thesis will largely be related to a single covalently linked porphyrin polymer, poly-TAPP (pTAPP).

The motivations behind studying porphyrin 2D and 3D networks are as vast as the types of networks created. Applications include solar cells, membranes, small molecule adsorption, catalysis, two-photon absorption, water purification, contrast imaging agents, and small structural templating to name the major areas.(*59*) The optimal properties of the polymer networks are different depending on the targeted application. For solar cells, optimal light absorption, and electronic conductivity or large exciton diffusion lengths are necessary. These requirements typically encourage full conjugation between porphyrin units. On the other hand, contrast imaging agents are optimized to keep the porphyrins

electronically separated in order to maintain optimal fluorescence from individual units.(*59*)

pTAPP was initially created to use as a p-type polymer replacement for the hole transport medium in dye-sensitized solar cells (DSSC).(*60*) Its conductivity is highly sensitive to its oxidation state, and this balance of reduced and oxidized species is difficult to maintain in systems which rely on redox reaction processes. As such it was decided to concentrate on its catalytic properties for targeted applications. The strong light adsorption, ability to be metallated and grown on various electrodes, as well as its high surface area gives it a great deal of potential as a heterogeneous catalyst.

1.8 pTAPP Background

As previously reported by Walter et al., the oxidative electropolymerization of pTAPP at fluorine-doped tin oxide electrodes occurs in dichloromethane (DCM) at a potential around +0.53 V vs. $Ag/AgNO_3$.(*61*) The polymer grows uniformly with successive oxidations in cyclic voltammetry, Figure 1.4, as well as during fixed potentiometry.

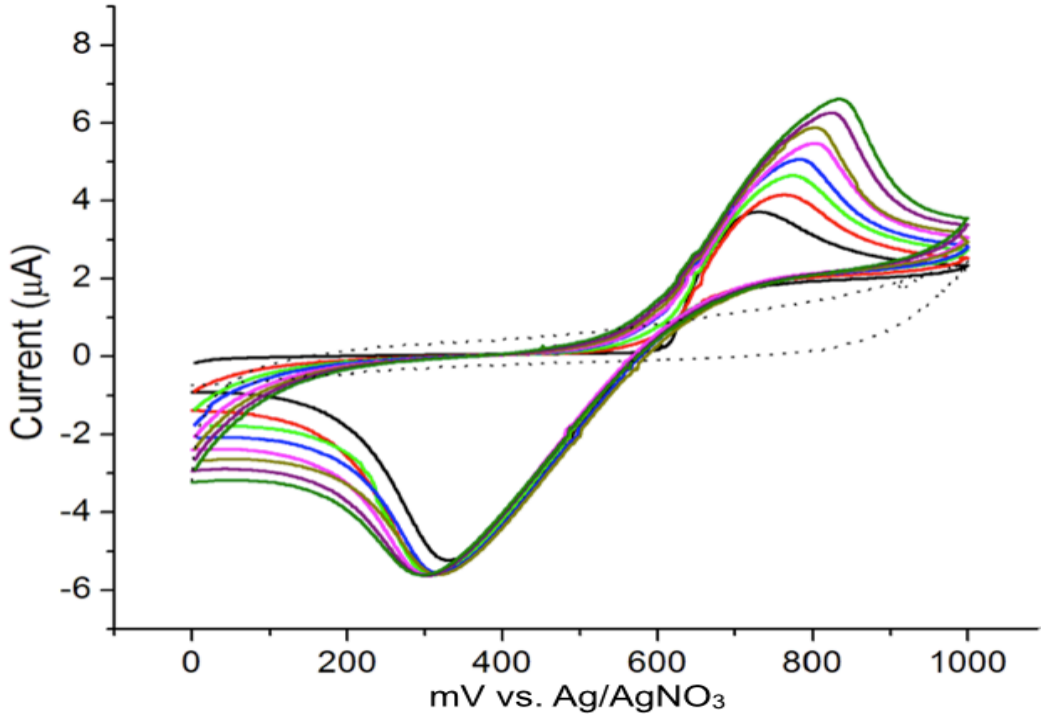

Figure 1.4 Electrochemical polymerization of pTAPP in DCM. The growing oxidation peak is an indication of increased surface area of the electrode caused by the extension of the conductive polymer network on the electrode.

The predominant form of pTAPP is nanofibers in all methods of polymerization. At a macromolecular level, nanofibers can be considered the physical extension of polymer growth through a quiescent solution as monomer is depleted in the nearby environment.

Electropolymerization generates a thick interconnected web of nanofibers with diameters about 40 - 100 nm, as previously reported (Figure 1.5a).(*61*) Interfacial polymerization generates spherical globules of polymer, within which nanofibers are clearly visible (Figure 1.5b). The globular morphology is commonly observed in

interfacial polymers; it is attributed to thermal effects at the interface in which convection and density gradients cause bubble formation.(*62*)

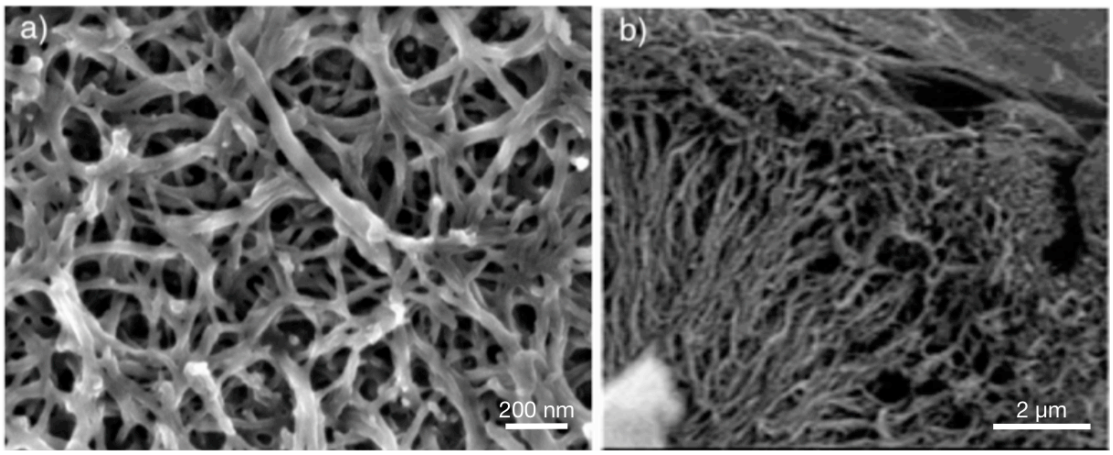

Figure 1.5 SEM images of nanostructured pTAPP grown by a) electropolymerization and b) interfacial polymerization.(*63*)

Whereas electropolymerization or interfacial polymerization generates a thin film of polymer, generation of bulk quantities can be accomplished by chemical oxidation. Bulk oxidation of TAPP with APS was carried out in an unstirred solution at constant temperature, conditions that have been shown to facilitate nanofiber formation in polyaniline.(*64*)(*65*)(*66*) In order to optimize the morphology of the nanofibers, reaction conditions at room temperature were explored including concentrations, reaction time, and dialysis time.

pTAPP harvested after slow addition of oxidant, i.e., titration, showed the evolution of modified nanofibers (Figure 1.6). Before dialysis, the nanofibers tend to

aggregate together (Figure 1.6a), possibly caused by the relatively high ionic strength and acidity (50 mM HCl) at that point. After overnight dialysis, the nanofibers tend to become overlaid with clumps of material (Figure 1.6c), possibly caused by slow continued growth of additional polymer overnight. However, if dialysis is performed quickly (1 hour) and the polymer harvested, the structure is primarily well separated individual nanofibers (Figure 1.6b).

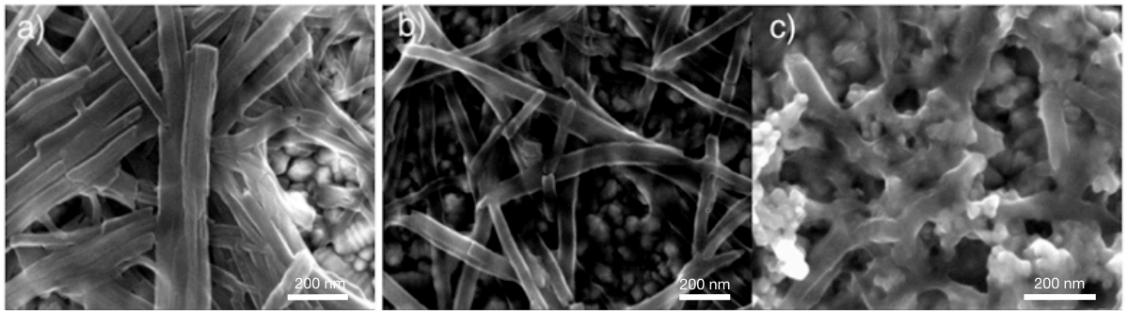

Figure 1.6 a) SEM images of pTAPP formed by slow addition of APS, before dialysis; b) same preparation, after one hour dialysis; c) same preparation, after overnight dialysis. The underlying granular structure is the FTO substrate.

An alternative method to chemically polymerize TAPP is at an aqueous/organic interface. Earlier it was shown that TAPP can be polymerized at an interface with several different poly(acyl chlorides), including the acid chloride derivative of tetrakis-5,10,15,20-(4-carboxyphenyl)porphyrin (TCPP).(*62*) Kaner has also shown that the interfacial polymerization technique can be used to generate polyaniline nanofibers.(*64*)(*65*)(*66*) Experiments were performed using 0.15 mM TAPP in DCM and

an excess (8 mol equivalents) of APS per TAPP dissolved in water at 3.4 mM. The results were dramatic; a thin (approximately 2 μm), durable film was produced in 12 hours at the interface accompanied by complete disappearance of TAPP in solution (Figure 1.7a). The black films could be harvested with an FTO electrode or a glass microscope slide, air dried, and then handled as a free-standing film on the substrate. If the solution is not stirred, the oxidation of monomer is rapid enough to form a detectable depletion region just below the surface of the film after two hours, and complete reaction takes about 12 hours. We conclude that under unstirred conditions, the rate of polymerization is controlled by TAPP monomer diffusion after the initial oxidation and film formation.(*63*)

Experiments were also performed in which the lower reaction solution was gently stirred to ensure that the solution concentration remained uniform throughout. TAPP monomer concentration was monitored over time as TAPP diffuses to the interface for oxidation and polymerization. In these experiments, fresh monomer was continuously available for oxidation and polymerization, and the disappearance of monomer followed a first-order decay and was more rapid than in the unstirred case, coming to completion in about 6 hours (Figure 1.7).(*63*)

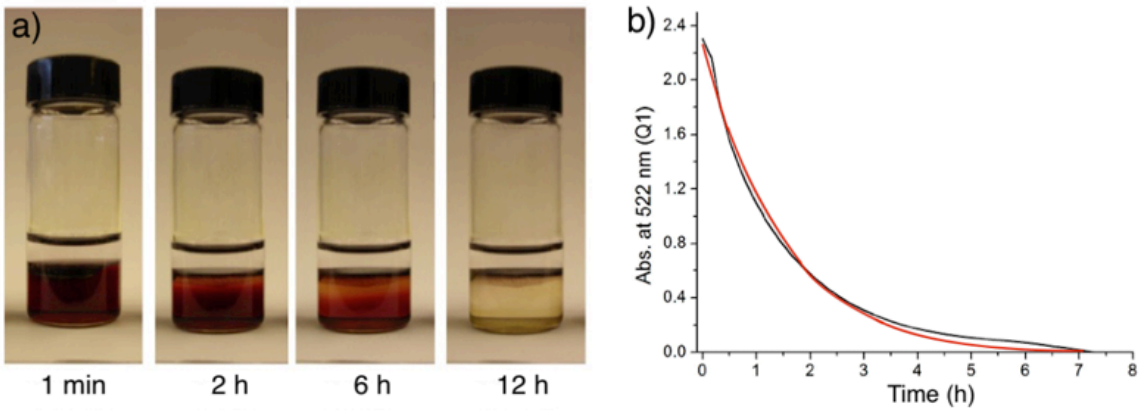

Figure 1.7 a) Interfacial polymerization of TAPP in DCM with aqueous APS over 12 h, b) relative concentration of TAPP in solution (a gently stirred solution, unlike that in part (a)), with first order decay fit (red line).

The connections between the monomeric porphyrin units were shown to consist largely of phenazine linkers, Figure 1.8, formed by an analogous mechanism as with polyaniline, in which the oxidation of aniline results in the activation of the carbon para to the amino group and the formation of a N-H bond between the para position on the oxidized aniline and the amino group on another aniline. In the case of TAPP the para position is occupied, leading to an ortho attack of the amino group. This first results in a diphenylamine linkage between monomeric units, which was also seen, but with successive oxidations the diphenylamine is oxidized further to a dihydrophenazine and finally a phenazine linkage. Phenazine linkages have also been shown by solid state ^{15}N NMR in cross-linked polyaniline samples.(*67*)

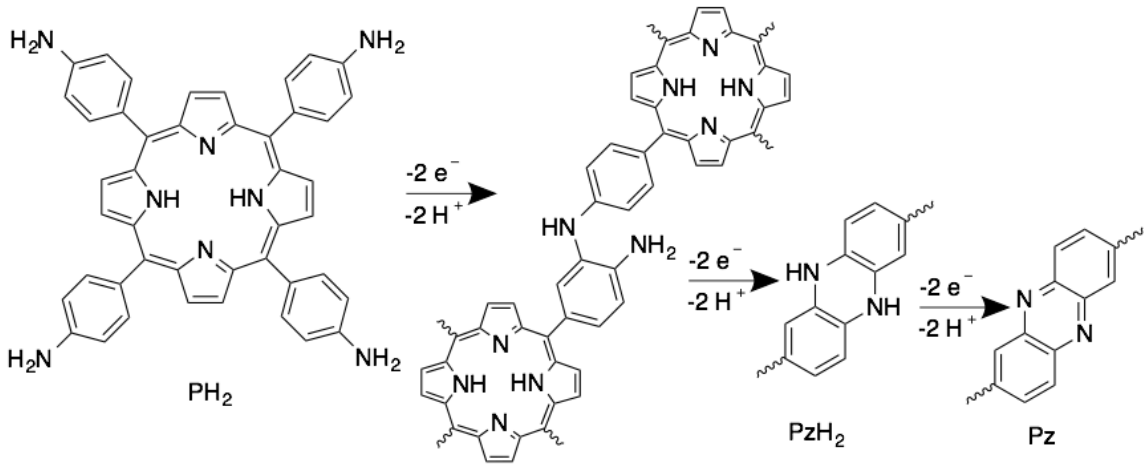

Figure 1.8 Proposed oxidation of TAPP to pTAPP through successive two-electron oxidations, ending in a phenazine linkage.

Regardless of the growth conditions, pTAPP has always shown a nanofibrous morphology. Although the structure and morphology of pTAPP have been published,(*61*) the properties and characteristics were not fully elucidated. In order to use the polymer as a photocatalyst, determining the conductivity and electrochemical properties, as well as preparing metallated derivatives was necessary.

2 EXPERIMENTAL METHODS

2.1 Materials

5,10,15,20-Tetrakis(4-aminophenyl)porphyrin (TAPP) was purchased from TCI America and used as received. Aniline was purchased from Sigma-Aldrich, vacuum distilled over Zn dust, and stored under inert atmosphere in the freezer. Ammonium persulfate (APS) was purchased from Mallinckrodt and used as received. Dialysis tubing was regenerated cellulose (12-14 kD) purchased from Fisher. Fluorine-doped tin oxide (FTO) electrodes (Tek15) were purchased from Pilkington Glass. Zinc chloride and zinc acetate were purchased from TCI America and used as received. Cobalt acetate was purchased from Sigma Aldrich and used as received. Ascorbic acid was purchased from Baker Analyzed Biochemical and used as received. MilliQ water (18 Mohm) was used for all catalysis experiments. Nitrosonium tetrafluoroborate was purchased from Acros Organics and used as received. Electrochemical-grade tetrabutylammonium perchlorate was purchased from Sigma-Aldrich and used as received. Dichloromethane was reagent grade from OmniSolve and was used as received. Ti(IV)-oxo-tetrakis-5,10,15,20-(pyridyl)porphyrin was synthesized according to previously published procedures.(*68*)

2.2 Instrumentation

UV-visible spectra were taken on a Shimadzu UV 3600 spectrophotometer. Scanning electron microscopy (SEM) was performed on an FEI Sirion XL30 instrument or Zeiss instrument, typically at 5 kV. Electrochemical and conductivity measurements were performed with a Gamry Reference 600 potentiostat. Electrochemical impedance spectroscopy (EIS) analyses were performed using Gamry Echem Analyst software. Thickness of the prepared samples was determined with a DekTak profilometer. Dynamic light scattering was taken using a Horiba LB-550 instrument.

2.3 Spectrophotometric Oxidative Titration of TAPP

a) Using APS

An aqueous solution of 3.75 μM TAPP in 50 mM HCl (2.5 mL) was titrated with 2 μL aliquots of aqueous APS (5 mM to 625 mM) in 50 mM HCl. After each addition of 2 μL of APS solution, the solution was thoroughly stirred and a full spectrum (300 - 1200 nm) was taken.

b) Using $NOBF_4$

A solution of carbon tetrachloride was saturated with $NOBF_4$ overnight. A TAPP solution of 10 μM in CCl_4 was prepared. The saturated $NOBF_4$ solution was titrated into the TAPP solution with 2 μL additions. After each addition of 2 μL of $NOBF_4$ solution, the solution was thoroughly stirred and a spectrum from 300 - 1100 nm was taken.

2.4 Preparation of pTAPP by Interfacial Polymerization

Thin films of pTAPP were grown at the interface of dichloromethane (DCM)/water solutions using aqueous APS as oxidant and TAPP in DCM solution. In a typical experiment, an aqueous solution of 3.4 mM APS was carefully layered on top of an equal volume of 0.15 mM TAPP in DCM in a 20 mL sample vial. After 12 hours, a thick black film formed at the interface leaving minimal TAPP dissolved in the DCM solution. The films were washed by replacing most of the aqueous layer with isopropyl alcohol, then harvested using an FTO conductive electrode to initially break through the side of the film, followed by scooping it out of the solution with the side of the film exposed to the aqueous/alcohol phase facing up. The films adhered well to both FTO conductive electrodes and glass microscope slides. Films could be refloated onto distilled water and rinsed with DCM and acetone. Films exhibited no visible change during storage under ambient conditions for over a year.

2.5 Preparation of pTAPP and pAni by Electrochemical Polymerization

FTO working electrodes (1 x 6 cm) were cleaned for 10 minutes by sonication in Sparkleen soap solution followed by 15 minutes of sonication in deionized H_2O. All electrochemical preparations used a Pt coil or Pt flag counter electrode (2 cm^2) and a Ag/AgCl or Ag/$AgNO_3$ reference electrode. For polyaniline films the electrode was immersed in aqueous 1 M H_2SO_4 with 0.3 M aniline and cycled between -0.2 V and +0.8 V vs. Ag/AgCl for 20 cycles at a rate of 20 mV/s. pTAPP films were prepared from 0.15

mM TAPP in DCM with 20 mM tetrabutylammonium perchlorate (TBAP), typically using multiple cycles between 0.0 V and +0.9 V and a 10 second delay at +0.9 V vs. Ag/AgCl or equivalent potentials vs. $Ag/AgNO_3$. Alternatively, pTAPP films were prepared using only one pass from 0.0 V to +0.9 V with a 10 to 150 second delay at +0.9 V, then cycling back to +0.45 V, and finally ending at +0.6 V vs. Ag/AgCl or equivalent potentials vs. $Ag/AgNO_3$.

2.6 Cyclic Voltammetry and Electrocatalytic Testing

Glassy carbon electrodes were constructed using silver paint and tinned copper wire for ohmic contact. The electrode was encased in a 1 cm glass tube with Loctite 1C epoxy and exposed through grinding with 300 grit sandpaper. Glassy carbon and gold electrodes were polished using 600 grit sandpaper, followed by 1200 grit, then 1.0 micron alumina paste, 0.3 micron alumina paste and finally 0.05 micron alumina paste from Beuhler all on microcloth polishing cloth from Beuhler, with sonication in deionized water between polishing. The final electrode surface was determined to be 0.04 cm^2 using Image J software.

Cyclic voltammograms (CV) of pTAPP films were taken in 0.5 M KCl, electrochemical grade from Sigma Aldrich, in MilliQ (18 Mohm) water at various pH values, adjusted with concentrated HCl, 4 M HCl or 10 M NaOH. The working electrode was a pTAPP film on glassy carbon, gold or an FTO electrode immersed so that no bare FTO contacted the solution. A 2 cm^2 Pt electrode or a Pt coil electrode were used as counter electrodes along with a Ag/AgCl reference electrode in solution. All solutions

were bubbled with nitrogen or argon for 20 minutes before adjusting for each pH and again before each cycle was run. Nitrogen or argon was blanketed over the solution during CV scans. Typical samples were run at several scan rates including 20 mV/s, 50 mV/s, 100 mV/s, and 1 V/s. Oxygen and air were bubbled through solutions for 10 minutes with stirring before relative tests.

2.7 Impedance Measurements

Capacitance and impedance of the pTAPP films were determined by electrochemical impedance spectroscopy (EIS) with the film on FTO and in contact with aqueous 5 M NaCl with a Ag/AgCl reference electrode. All samples were run at room temperature with an excitation signal of 10 mV from 0.1 Hz to 1 MHz. To standardize the distance between the reference electrode and the working electrode, the reference electrode was affixed to the working electrode so that its glass frit was fixed at a uniform distance (approximately 1 mm) from the film on the working electrode for every run. EIS spectra were obtained at various bias potentials and pH values typically ranging from 0 V to +0.7 V vs. Ag/AgCl and pH 3 to pH 8.

2.8 Metallation of pTAPP

pTAPP films were metallated using cobalt acetate. pTAPP films were immersed in 10 mM cobalt acetate solution in methanol and heated to 80 °C and then held there for 5 minutes, after which complete metallation was seen by UV-Vis analysis.

2.9 SEM Images

All samples for SEM were mounted on FTO glass and electrically connected to the aluminum mount using conductive copper tape. All samples were placed under vacuum for 24 hours prior to imaging.

2.10 Rotating Disk Electrode Linear Sweep Voltammetry

A glassy carbon rotating disk electrode (RDE) was polished by 1200 grit, then 1.0 micron alumina paste, 0.3 micron alumina paste, and finally 0.05 micron alumina paste from Beuhler. The electrode surface was determined to be 0.17 cm^2 using Image J software. The metal electrode was contacted during rotation by two graphite electrodes connected to the working electrode contact through metal springs. Overall resistance of the contacts during rotation was measured to be approximately 200 ohms.

Linear sweep voltammograms (LSV) of pTAPP and pCoTAPP films were taken in 0.1 M KCl, electrochemical grade from Sigma Aldrich, in MilliQ 18 Mohm water at various pH values, adjusted with concentrated HCl, 4 M HCl or 10 M NaOH. The working electrode was a pTAPP film on a glassy carbon electrode. A Pt coil counter electrode along with a Ag/AgCl reference electrode were also in solution. All solutions were bubbled with nitrogen or argon for 20 minutes before adjusting for each pH and again before each LSV was run. Nitrogen or argon was blanketed over the solution during LSV scans. All samples were run at scan rates of 20 mV/s and rotation rates of 0,

50, 100, 200, 400, 800, 1600, and 3200 rpm. Oxygen and air were bubbled through solutions for 10 minutes with stirring before relative tests.

2.11 H_2O_2 Testing

pTAPP and pCoTAPP samples were synthesized using fixed potentiometry holding for 200 seconds at 0.6 V vs. $Ag/AgNO_3$. The samples were all approximately 2 cm^2 in size. Samples were submerged in a 3 mL cuvette along with a Ag/AgCl reference electrode and an electrochemical grade graphite counter electrode. All samples were held at 0 V bias vs. Ag/AgCl and illuminated with a 5000 K 500 lumen LED light approximately 0.5 cm away from the cuvette. This illumination source and distance were tested with a silicon radiometer to give approximately 2 suns of irradiation. The samples were placed in the cuvette so that light entered the cuvette and went through the FTO glass before striking the sample which faced the solution. The graphite counter electrode has an approximate surface area of 3 cm^2. The cuvette was filled with 0.1 M acetate buffer at pH 3.0. Oxygen was continuously bubbled through the solution for the entire experiment. Experiments lasted from 30 to 120 minutes. Samples tested for 30 minutes had 10 μL aliquots removed on a 2 minute basis for the first 20 minutes and then one aliquot at 30 minutes. Samples tested for 120 minutes had 10 μL aliquots removed every 10 minutes up to 40 minutes then 60, 90 and 120 minute aliquots were also taken.

Samples were tested for H_2O_2 using double recrystallized titanium(IV)-oxo-tetrapyridylporphyrin (TiOTPyP) which was synthesized according to previously published procedures.(*68*) Testing of each aliquot was performed as follows with

procedures for the determination of H_2O_2 optimized from previously published procedures.(*69*) To a scintillation vial 5 mL of a 15 μM TiOTPyP solution in aqueous 50 mM HCl, was added then 5 mL of 6.0 M perchloric acid and 5 mL of deionized H_2O were also added. The solution was then mixed by vortexing and let stand for 5 to 20 minutes. 990 μL aliquots of this solution were transferred into test tubes. Then a 10 μL aliquot of the oxygen reduction sample was added to the cuvette, thoroughly mixed and allowed to stand for 10 minutes. After the 10 minute incubation a spectrum was taken from 350 to 650 nm. The quantity of H_2O_2 was determined using the decrease in absorbance at 433 nm relative to a sample prepared with only 10 μL of the acetate buffer solution.

The quantitative determination of H_2O_2 was done using oxo[5,10,15,20-tetra(4-pyridyl)porphyrinato] titanium(IV) (TiOTPyP) as a colorimetric reagent for H_2O_2. TiOTPyP has been shown to be able to accurately determine the presence of H_2O_2 between 0.1 μM to 10 μM.(*69*) The results shown in Figure 2.1 suggest a linear range from 0.1 μM to 3 μM as optimal for quantitation with the method used for testing pTAPP and pCoTAPP. This range was determined by taking 10 μL aliquots of hydrogen peroxide urea at carefully prepared concentrations of 5.0, 4.0, 3.0, 2.0, 1.0, and 0 mM and placing in a 1 mL cuvette as described above, then determining the absorbance change at 433 nm (blue curve). This was repeated in the linear range, shown in Figure 2.1 as the red curve. Finally 0.1 mM solution increments were prepared at each end of the linear range first at concentrations of 0.1, 0.2, 0.3, 0.4 and 0.5 mM, shown as the green curve and 2.8,

2.9, 3.0, 3.1 and 3.2 mM shown as the yellow curve. The four curves shown in Figure 2.1 had an average slope of 0.11 ± 0.01 absorbance units per nmol of hydrogen peroxide urea, which is shown as the black curve on each graph in Figure 2.1. The linear fit equation was used to determine the concentration of H_2O_2 in all samples tested.

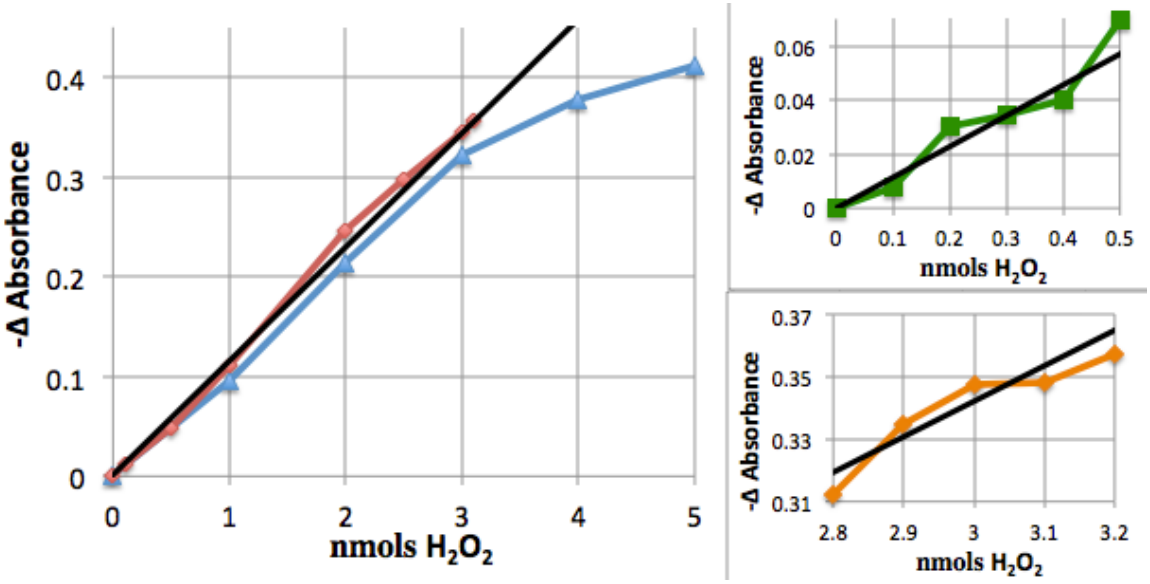

Figure 2.1 Titrations of TiOTPyP with standard solutions of hydrogen peroxide urea. The blue curve shows the linear response from 0 to 3 nmols. The green and orange curves show 0.1 nmol increments at each end of the linear range. The black line in all graphs is the average of all four curves which was used to calculate the concentration of H_2O_2 produced.

3 CHARACTERIZATION OF pTAPP

Initial reports of pTAPP proposed certain properties based upon its structure and behavior during polymerization. In order to ascertain whether pTAPP could be a useful material, additional characterizations needed to be performed, in particular the ability to conduct charge carriers. pTAPP had been attempted in a solid-state dye-sensitized solar cell but was only able to achieve an efficiency of 0.02%.(*60*) This could be attributed to its inability to conduct holes or an inappropriately aligned band gap, properties which could be characterized using electrochemistry and spectroscopy.

3.1 UV-Visible Absorption Spectroscopy

UV-Vis spectral data relevant to pTAPP can be determined by UV-Vis spectroscopy of either the polymer or oxidative titrations of the monomer. In the latter case the polymer forms in situ during the experiment. The polymer has a strong electrochromic behavior which will be discussed after structure and redox properties.

3.1.1 Titration of TAPP with Oxidants

The oxidation of monomeric TAPP was observed by titration with aqueous APS (Figure 3.1). The initial spectrum of TAPP in aqueous 50 mM HCl shows a sharp Soret (B) band at 431 nm and Q bands at 593 and 645 nm, as expected for fully protonated $TAPPH_6^{+6}$.(*70*) APS oxidation leads to a decrease and broadening of the Soret band at 431 nm and growth of a new band at 527 nm, with an isosbestic point at 456 nm; a new peak around 710 nm grows larger and broadens during the oxidation. With excess APS,

porphyrin material begins to precipitate out of solution as indicated by decreasing absorption at all peaks in the spectrum combined with a rising baseline indicating light scattering. The precipitation event is presumably caused by the formation of pTAPP, although at these concentrations it is not visibly detectable.

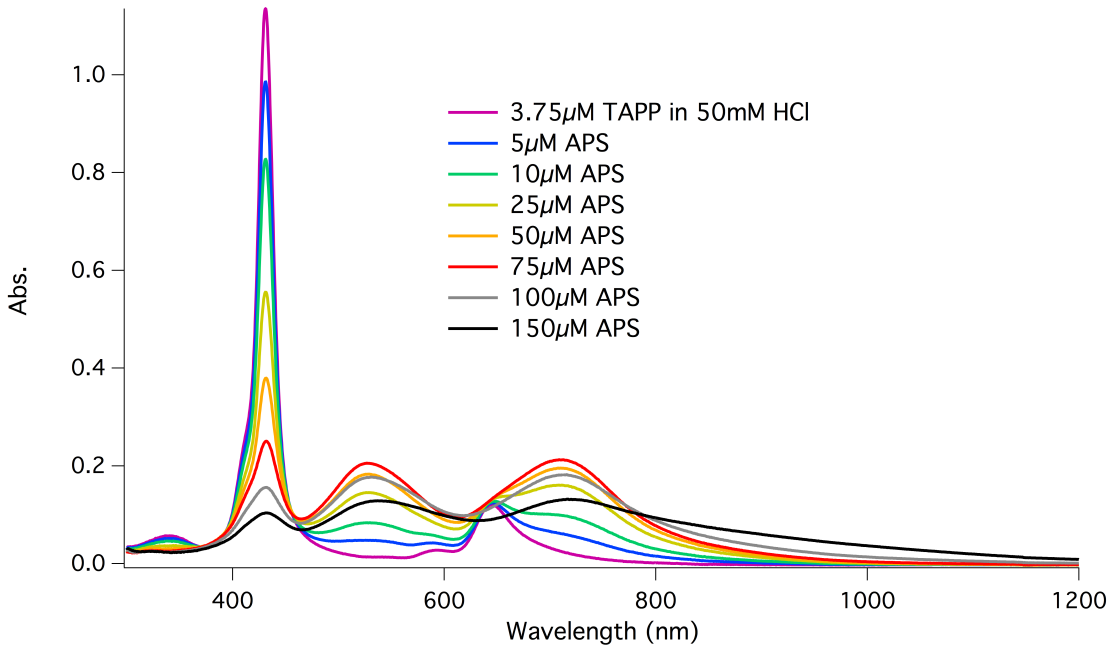

Figure 3.1 UV-Vis absorption spectra of TAPP (3 mL of 3.75 μM TAPP in 50 mM HCl) titrated with APS. The legend indicates APS concentration in the cuvette after each addition of APS.

It is notable that the titrations must be performed with a great stoichiometric excess of APS in order to observe the initial oxidation. Presumably the +6 protonation state of TAPP renders it relatively resistant to oxidation. Stoichiometrically, the simplest oxidation of $TAPPH_6^{+6}$ to $TAPPH_4^{+6}$ would require one equivalent of APS. Oxidative dimerization of two TAPP units to generate an oxidized phenazine linkage would require

three equivalents of APS. The most definitive spectrum (Figure 3.1 - red) is observed when the APS concentration is about 75 μM, which corresponds to about 20 equivalents of APS relative to TAPP. This spectrum we tentatively assign to $TAPPH_4^{+6}$. The strong red band at 710 nm is consistent with a hyperporphyrin structure,(*70*)(*71*)(*72*)(*73*) i.e., the cross-conjugation of two aminophenyl groups with the oxidized porphyrin as shown in Figure 3.2.

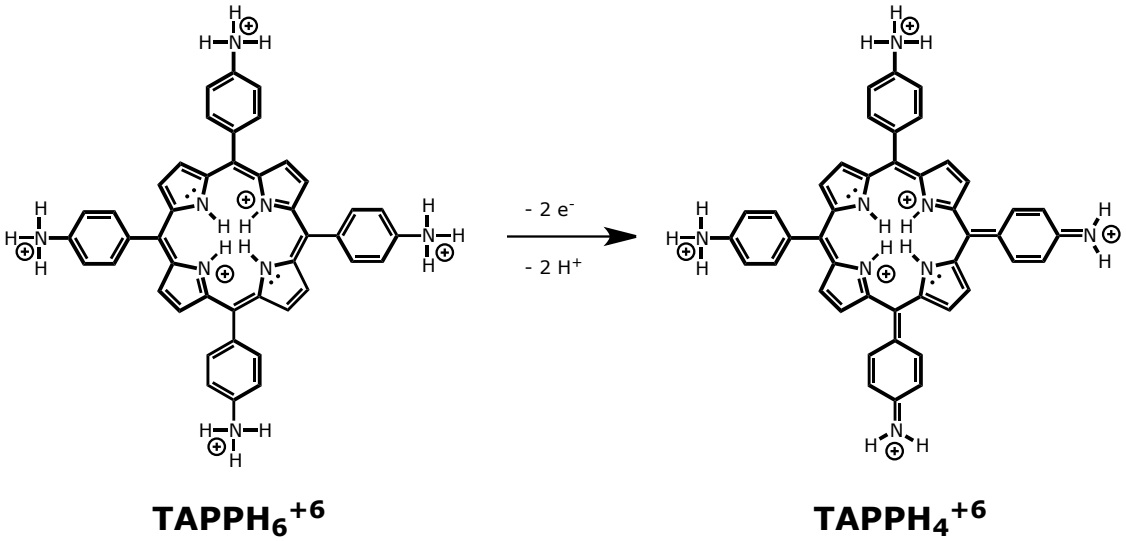

Figure 3.2 Proposed oxidation of fully protonated TAPP by APS in aqueous acid.

Over time, pTAPP precipitation can occur even at low concentrations of APS. Thus the titrations were carried out quickly; presumably the low porphyrin concentration slows the polymerization process so that it is possible to observe the oxidation process before precipitation occurs. The observation of a clean isosbestic point at 456 nm (Figure 3.1) suggests that this strategy is successful in the earliest stages of the titration.

A similar titration was performed in carbon tetrachloride in order to ascertain the effects of excess acid on the titration, Figure 3.3. Here the porphyrin is initially in the typical unprotonated state. $NOBF_4$ was found to have limited solubility in carbon tetrachloride and the concentration of free base porphyrin was increased to 10 μM. A typical free base porphyrin shows a Soret band and four Q-bands. TAPP in CCl_4 shows a Soret maxima at 427 nm and Q-bands at 522 nm, 561 nm, 599 nm and 656 nm. Upon oxidation with nitrosonium tetrafluoroborate the Soret band decreases and broadens. The Q-bands all quickly decrease and two new peaks grow in, one at 467 nm and another typical broad absorbance at 767 nm. Relative to the aqueous titrations, the difference in absorbance maxima is attributed to solvatochromic behavior.

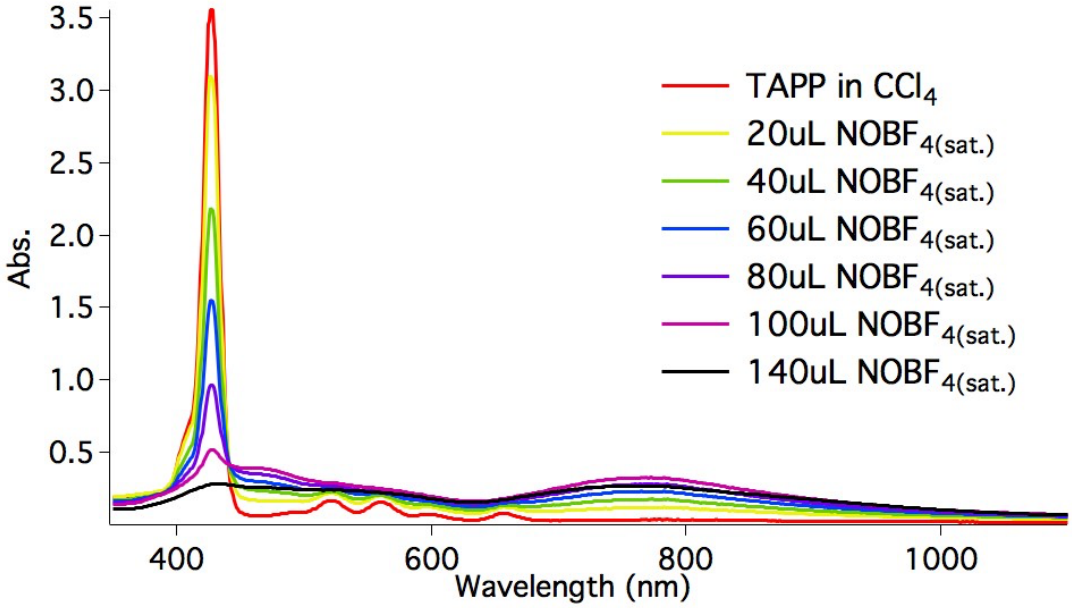

Figure 3.3 UV-Vis absorption spectra of TAPP (3 mL of 10 μM TAPP in CCl_4) titrated with $NOBF_4$. The legend indicates the total quantity of $NOBF_4$ (saturated solution in CCl_4) in the cuvette after each addition.

3.2 Cyclic Voltammetry

pTAPP films immersed in aqueous electrolyte consistently show two major waves. The largest peak near +0.5 V vs. Ag/AgCl is attributed to the oxidation of the porphyrin units in the polymer (Figure 3.4). This peak occurs at a location close to where monomeric TAPP undergoes oxidation.(*74*)(*61*) The peak shape is similar to that of an adsorbed species, which would be consistent with a conductive polymer film on the electrode. However, the polymer film is not conductive or homogeneous under all circumstances, and this leads to variable peak shapes and positions. As shown in Figure

3.4, the cyclic voltammogram at pH 4 presents a sharp oxidation wave with a peak at about +0.48 V. The current drops sharply after the peak because the film is substantially less conductive when in its fully oxidized form. The reverse wave at pH 4 peaks at about +0.31 V, well separated from the oxidation peak because the film is not initially conductive. In general, the positions of the oxidation waves for pTAPP do not vary significantly with pH, but their shape is quite variable depending on thickness, preparation method, and pH. The peaks are relatively broad and somewhat variable due to inhomogeneity of the polymer film, especially in its less-conductive states.

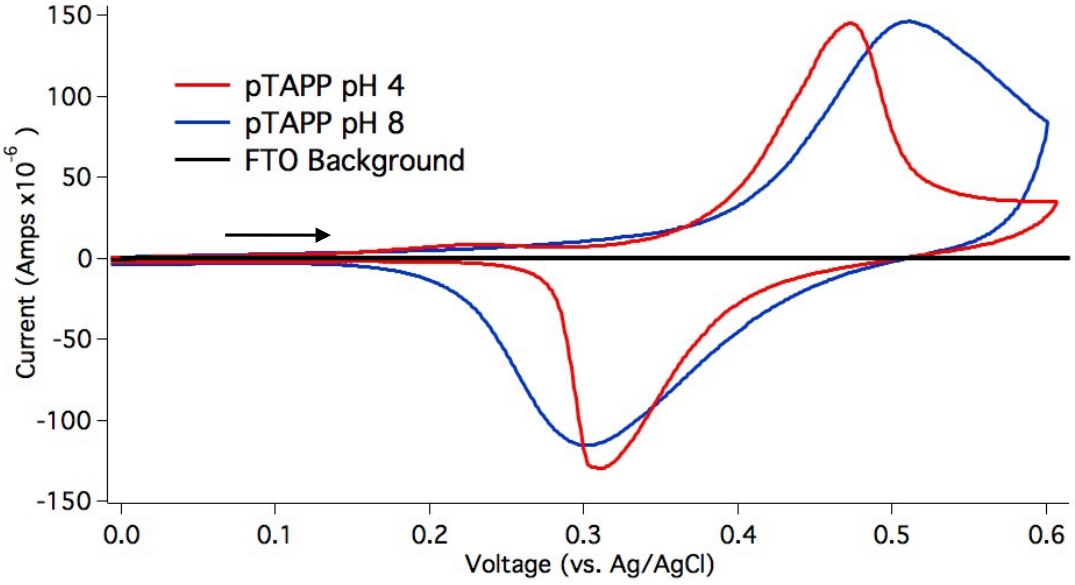

Figure 3.4 Cyclic voltammograms of a pTAPP film in aqueous 0.1 M KCl adjusted to pH 4 (red) or pH 8 (blue) at a scan rate of 20 mV/s.

The main reduction wave occurs in the range of -0.4 to -0.7 V vs. Ag/AgCl. This wave varies with pH and is proposed to correspond to the reduction of phenazine to

dihydrophenazine. The reduction of phenazine to dihydrophenazine is considered to be two one-electron processes at low pH which merge to a single two-electron process at higher pH.(*75*) We see a similar trend with the proposed phenazine reduction peaks in the polymer. The reduction at pH 4 shows two peaks, at approximately -0.5 V and -0.65 V vs. Ag/AgCl, each peak indicating a one-electron process. At pH 8, the reduction peak is a single broad peak similar to that seen for the reduction of phenazine at corresponding pH values by Bailey et al. These peaks are considerably more negative than those reported, which we believe is due to the resistive nature of the film at these potentials. The peak potential and the shape of this wave also varies significantly with the thickness and preparation method for different polymer films. Additional representative cyclic voltammograms including the negative potential range are shown in Figure 3.5.

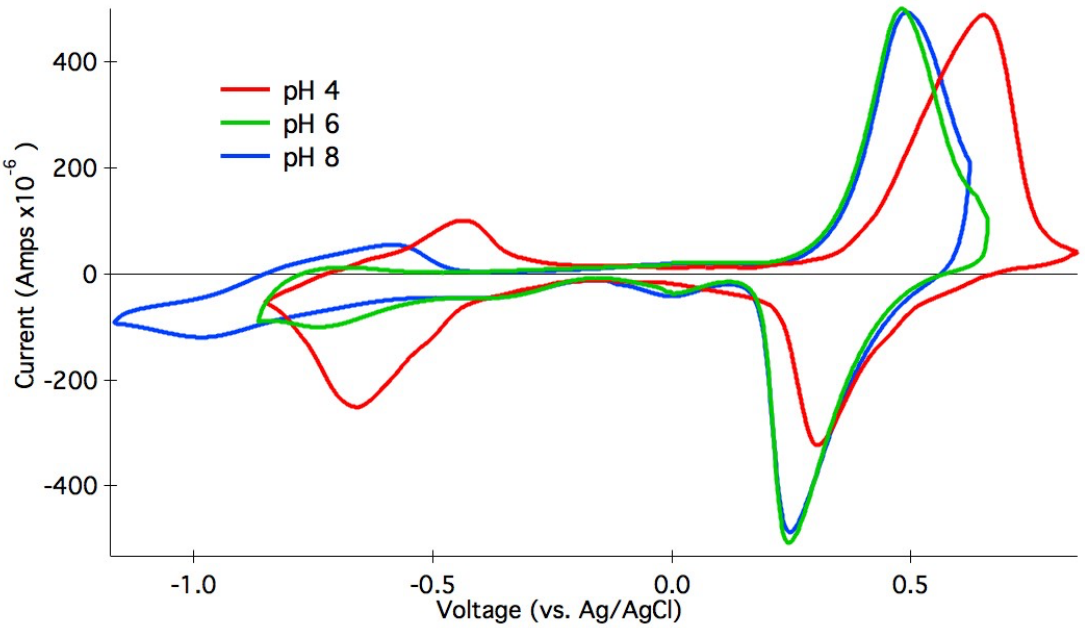

Figure 3.5 Cyclic voltammograms of a pTAPP film in aqueous 0.1 M KCl adjusted to pH 4 (red), pH 6 (green) or pH 8 (blue) at a scan rate of 20 mV/s showing both oxidation and reduction potentials.

Since both oxidation and reduction potentials have been determined the band gap of pTAPP can be estimated. With a half-wave oxidation potential close to +0.42 V vs. Ag/AgCl and a half-wave reduction potential close to -0.50 V vs. Ag/AgCl we estimate the band gap of pTAPP to be approximately 0.92 V. Using the Planck-Einstein relation, Equation 3.1, we can calculate that a band gap of 0.92 V would lead to a long wavelength absorbance near 1350 nm, where h is Planck's constant, c is the speed of light, and λ is the wavelength of light in meters. UV-Vis-NIR spectra of pTAPP films were performed out to 1800 nm in order to look for a broad absorbance in this region. As can be seen

from Figure 3.6, a broad long-wavelength absorbance is centered at 1300 nm, very close to the observed band gap of the pTAPP films tested.

$$E(eV) = hc/1.602x10^{-19}\lambda \qquad \text{Eq. 3.1}$$

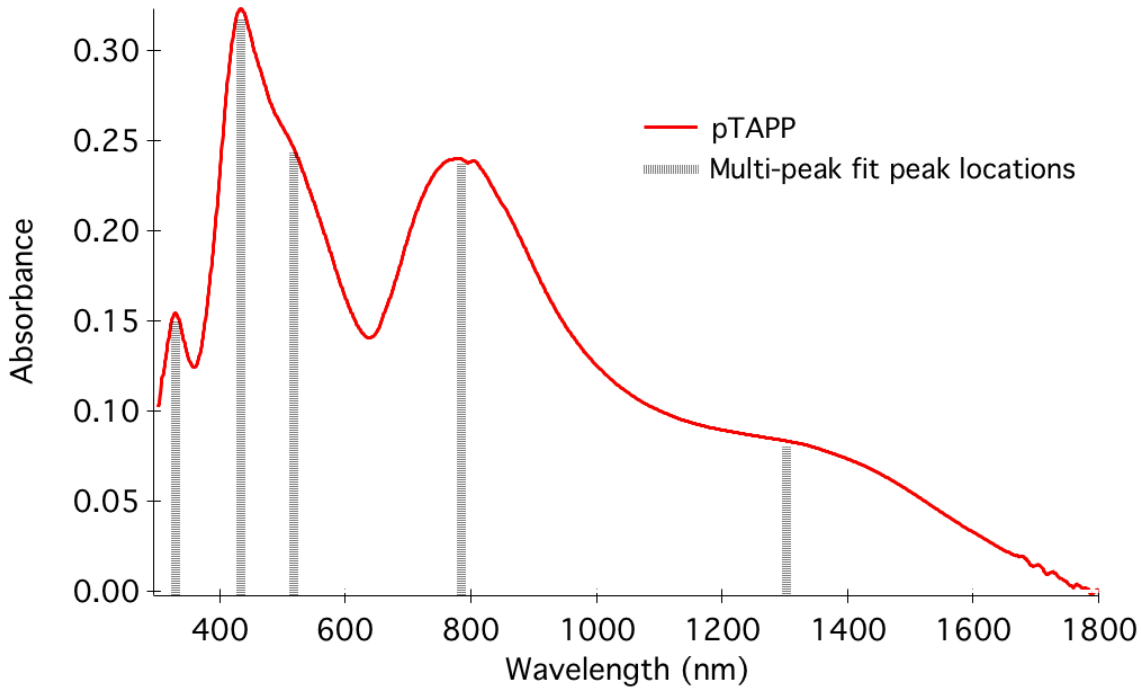

Figure 3.6 UV-Vis-NIR of pTAPP film from 300 to 1800 nm. IgorPro multi-peak fit package shows a long wavelength peak centered at 1300 nm, very close to the expected wavelength calculated from the band gap.

In comparison, the longest wavelength absorption of TAPP in CCl_4 is at 656 nm, corresponding to a band gap of 1.89 eV. This is close to the electrochemically determined band gap in DMSO of 1.66 eV.(*74*) The relatively small band gap of pTAPP helps to explain many experimental results, including its conductive nature, poor

performance in dye-sensitized solar cells, as well as it lack of fluorescence which will be discussed later with metallated derivatives.

3.3 Electrochemical Impedance Spectroscopy

Polymers are used in a wide array of electronic applications,(*76*)(*77*) in which electronic conductivity can be modulated using a variety of doping methods, including redox doping, acid-base chemistry, photo-doping, and charge-injection doping.(*78*)(*79*) Given the conjugated structure proposed for pTAPP, all of these doping types are conceivable. Oxidative p-doping and doping through acid-base chemistry can be clearly demonstrated for pTAPP using electrochemical impedance spectroscopy (EIS) by adjusting either bias potential or pH.

Using electrochemically grown films and following procedures outlined by Rubinstein et al., impedance was studied over a range of potential and pH values.(*80*) In general, lowest impedance values were observed when the film was closest to the half-wave oxidation potential (around +0.4 V vs Ag/AgCl with a scan rate of 20 mV/s). This indicates a conductivity mechanism similar to polyaniline, i.e., electronic conductivity through polaron hopping, in which optimum doping and minimum resistivity occur with half of the monomeric units in an oxidized form and the other half in a reduced form.(*78*)(*80*)

3.3.1 Equivalent Circuit Models

A recent review emphasizes that polyaniline exists in numerous different nanostructured forms, quoting Alan MacDiarmid, "there are as many different types of polyaniline as there are people who make it!"(*66*) In general, conductive polymers can be formed in a wide variety of morphologies, presumably with corresponding variations in properties such as electronic behavior. A recent review of the electrochemistry of conducting polymers outlined the wide variety of different models that have been used to describe the electrochemical behavior of conductive polymers.(*81*) A widely accepted equivalent circuit for porous films on metal electrodes is the transmission line model.(*82*)(*83*)(*84*)(*85*) The generic transmission line model proposed by Fletcher for porous polymers on a metal electrode is shown in Figure 3.7a, specifically illustrating three sets of repeating units.(*85*) There are two fundamental ways to interpret the results obtained from EIS measurements. The primary simplified circuit is shown in Figure 3.7b; this interpretation of the results is widely accepted and conductive polymers of many types have been analyzed this way. An alternative interpretation of the results has been applied to polyaniline and polypyrrole.(*86*) This more specialized interpretation of the EIS results will be discussed in section 3.3.6.

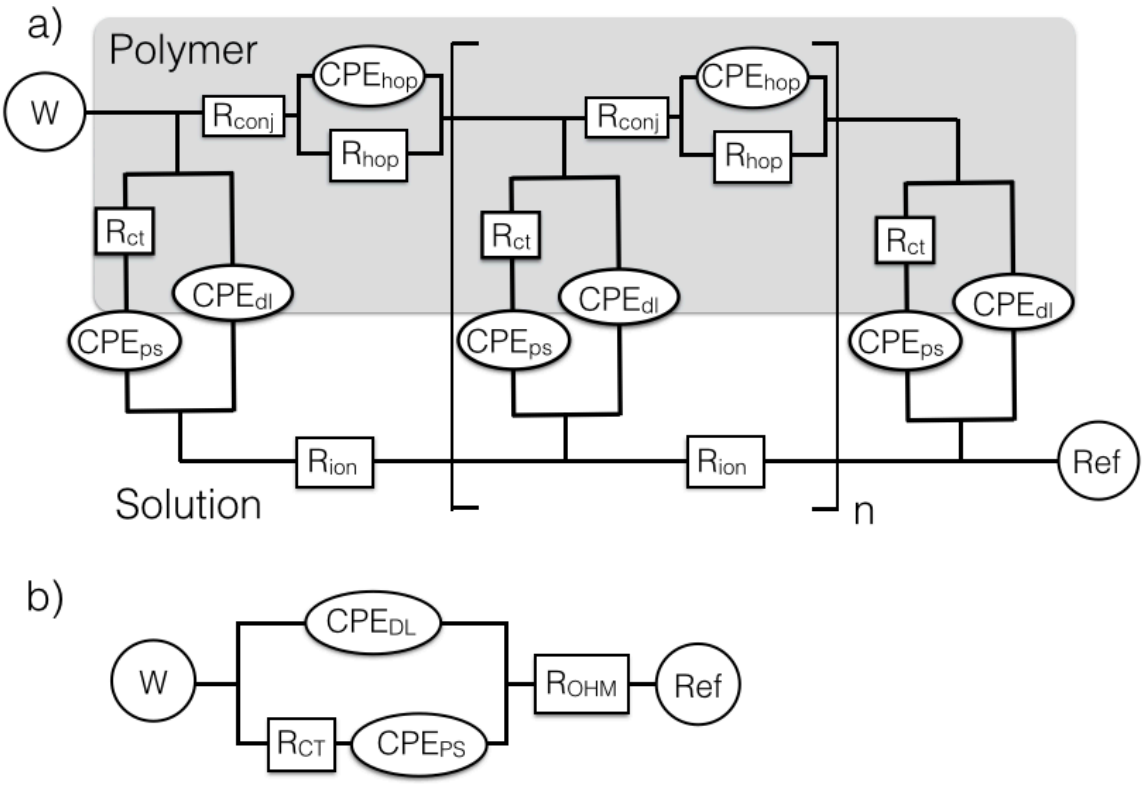

Figure 3.7 a) Typical transmission line model used to evaluate porous polymer films on metal electrodes, with individual elements defined in the text. b) Equivalent circuit model used to analyze Nyquist and Bode plots. CPE_{DL} is representative of the capacitance of the film/solution double layer, R_{CT} is the resistance of charge transfer within the pTAPP film, CPE_{PS} is representative of the pseudocapacitance of the pTAPP film, R_{OHM} is combination of the ionic and solution resistance (5 M NaCl), W is the working electrode, and Ref is the reference electrode.

The fundamental elements in Fletcher's transmission line model include resistance within the polymer due to conjugated segments (R_{conj}) as well as resistance and capacitance due to hopping between conjugated segments (R_{hop} and CPE_{hop}). Subsequent

elements represent the polymer/solution interface with charge-transfer resistance (R_{ct}), double-layer capacitance (CPE_{dl}), and pseudocapacitance (CPE_{ps}). Finally, the solution phase is represented by ohmic resistance due to ionic transport (R_{ion}).(*82*) By using a high concentration of supporting electrolyte (5 M NaCl) and an absence of electroactive species, we intentionally minimized solution resistance and minimized redox reactions at the polymer/solution interface, i.e., leakage current.(*85*) We simplified the transmission line model by treating the repeating elements as one, giving overall bulk properties (Figure 3.7b), specifically bulk charge-transfer resistance (R_{CT}) within the film, bulk capacitance of the double layer between the polymer film and solution (CPE_{DL}), and the pseudocapacitance of the film (CPE_{PS}). The ohmic resistance in the film and the ionic resistance in solution are not distinguishable and are combined to a single ohmic resistance (R_{OHM}). Polymer films on metal electrodes have often been modeled with similarly simplified equivalent circuits.(*80*)(*82*)(*85*)(*87*)

Constant phase elements (CPE) were used in the equivalent circuit model instead of capacitors, as is commonly done when the capacitive elements of a system are imperfect. In many cases films on solid electrodes behave as imperfect capacitors; this is typically attributed to variation in the thickness of the film, surface roughness, porosity, reactivity, or surface potential distributions.(*88*)(*89*) It should be noted that the units for CPE are Siemens times seconds raised to the exponent α (S s^{α}), where α is known as the dispersion coefficient. The impedance of a CPE can be defined as in Equation 3.2.(*90*)

$$Z_{CPE} = 1/Q_a(j\omega)^{\alpha} \qquad \text{Eq. 3.2}$$

In Equation 3.2, Z_{CPE} is the impedance of the constant phase element, Q_a is a coefficient with units of $\Omega^{-1}m^{-2}s^{\alpha}$, j is the imaginary number equal to $\sqrt{-1}$, and ω is the angular frequency. CPEs can display four limiting cases, described as follows: 1) if α is equal to 1, then the CPE displays a limiting behavior as a capacitor, and the units would be equal to Farads, 2) if α is equal to 0.5, the CPE displays limiting behavior as a Warburg element, which is often used to model linear diffusion, 3) if α is equal to 0, then the CPE displays limiting behavior as a resistor, and 4) if α is equal to -1, then the CPE displays limiting behavior as an inductor. A thorough explanation of CPEs and all of the limiting conditions has been published, offering insights into the versatility of CPEs and the limiting behaviors is important to their use in equivalent circuits.(*90*)

3.3.2 Bode and Nyquist Analyses of EIS Data

Several electrochemically prepared samples of pTAPP films were tested using EIS with bias potential values ranging from +0.1 V to +0.6 V (vs. Ag/AgCl). Impedance values of the films were determined by fitting to the equivalent circuit shown in Figure 3.7b for both Bode and Nyquist plots. The pTAPP films analyzed in Figure 3.7 showed relatively constant ohmic resistance (R_{OHM}) of about 70 ohms and charge-transfer resistances (R_{CT}) as low as 13 ohms at pH 4. Even lower impedances were observed with thinner films generated under different conditions, but these thicker films clearly showed the key elements in the Bode diagrams and were chosen for detailed analysis.

Figure 3.8a shows Bode phase plots of pTAPP films at various bias potentials. For reference, a phase of 0 degrees indicates an ideal resistor, and a phase of -90 degrees indicates an ideal capacitor. The large peak seen at +0.1 V bias near 50 Hz indicates a predominantly capacitive element due to the relatively high resistance of the film at this potential. As the potential is increased to +0.4 V, this peak decreases and shifts towards 1000 Hz. Simultaneously the impedance values decrease by almost an order of magnitude over the same frequency range. At potentials above +0.4 V, the film becomes more resistive again and the capacitive peak begins to grow back but is less well defined, likely due to increased leakage current through CPE_{DL} as indicated by the decreased dispersion coefficient (α).

Figure 3.8b shows data for the identical pTAPP film and EIS runs but illustrated as Nyquist plots. Figure 3.8d shows the interpretation of the Nyquist plots correlated to the equivalent circuit model of Figure 3.8c. Unlike the Bode plots, frequencies decrease from left to right in Nyquist plots. The Nyquist plots all begin with an intercept of about 70 ohms of resistance that is indicative of the total ohmic resistance (R_{OHM}). The RC arc which extends from 70 to 83 ohms and then to increasingly large impedance values is characteristic of the film charge-transfer resistance (R_{CT}), indicative of the film doping/dedoping process. The smallest arc occurs at +0.4 V bias, where the film is most highly doped and R_{CT} is only 13 ohms. The charge-transfer resistance increases at both larger and smaller positive potentials.

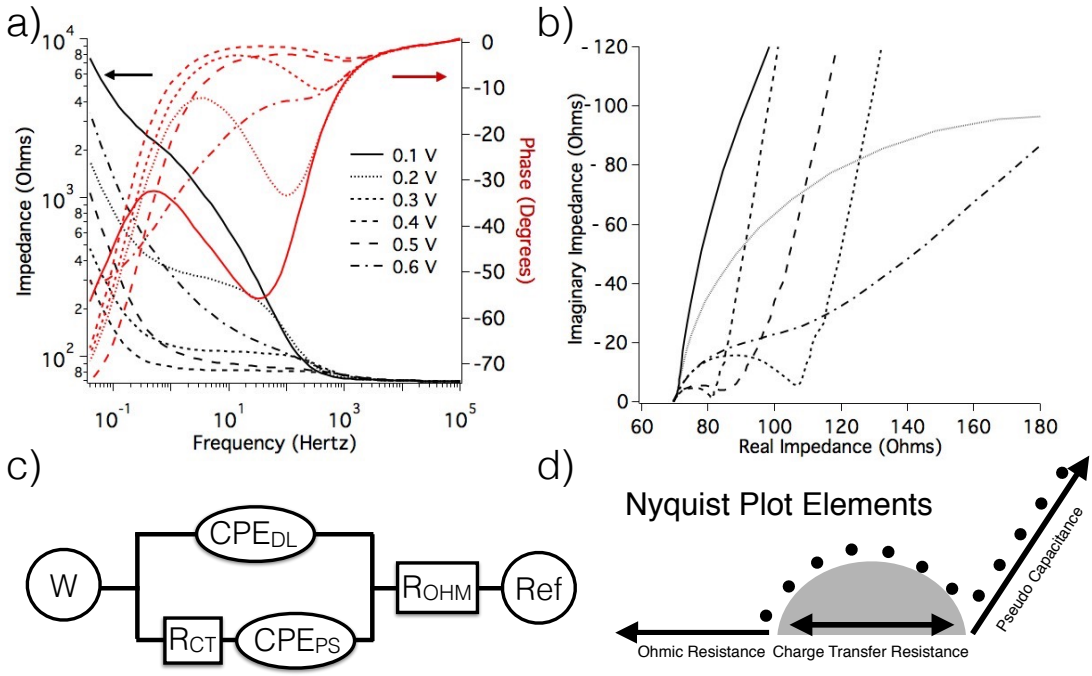

Figure 3.8 a) Bode plots of impedance and phase for an electrochemically polymerized pTAPP film at pH 4. b) Nyquist plots of the same data, where the legend for potential applies to both plots. c) Equivalent circuit used to model the EIS data, simplified from a segmented transmission line model. d) Interpretation of features of the Nyquist plots based on the equivalent circuit model.

Table 3.1 summarizes the results of fitting the EIS data to the equivalent circuit model, with resistance values in ohms and CPE values in S s^{α}. The data were fit using a non-linear least squares method. Chi-squared values were determined and used to test how well the model fit the experimental data. All chi-squared values are less than 10^{-2}

which represents a good fit. As the CPE elements act more like capacitors, the chi-squared fits are even better, with values less than 10^{-3}.

Table 3.1 Data for the pTAPP films analyzed and fitted to the equivalent circuit model in Figure 3.8.

	Bias vs. Ag/AgCl					
Element	+0.1 V	+0.2 V	+0.3 V	+0.4 V	+0.5 V	+0.6 V
R_{OHM} (Ω)	69	69	70	70	68	69
CPE_{PS} (S s^{α})	0.00037	0.0021	0.0075	0.013	0.0039	0.0015
α_{PS}	0.66	0.86	0.88	0.91	0.89	0.63
R_{CT} (Ω)	1600	252	38	13	19	68
CPE_{DL} (S s^{α})	3.9×10^{-5}	3.7×10^{-5}	4.0×10^{-5}	6.7×10^{-5}	6.5×10^{-5}	8.1×10^{-5}
$\boldsymbol{\alpha}_{DL}$	0.86	0.87	0.86	0.80	0.77	0.71
χ^2	0.0018	0.0005	0.00011	0.00019	0.0026	0.0074

Recall that when the dispersion coefficient, α, is equal to 1, the CPE shows limiting behavior as a capacitor, when α is equal to 0.5, the CPE shows limiting behavior as a Warburg element and when α is equal to 0, the CPE shows limiting behavior as a resistor. This is an important consideration when attempting to determine the capacitance of the film or interface.(*88*) As indicated by the relatively high values of α, CPE_{DL} can be

considered to have largely a capacitive nature when potentials are between +0.1 V to +0.4 V, where the values of CPE_{DL} are all relatively high. At potentials larger than +0.4 V, the capacitive nature breaks down and there is likely an increase in leakage current. Many models of similar electroactive polymers contain a Warburg element, which does not appear to be present in our system, except possibly at higher applied potentials. Albery and Mount attribute the lack of Warburg behavior seen in polyaniline to a special case in which ionic resistance in the polymer pores is approximately equivalent to the electronic resistance to hopping between polymer segments.(*81*)(*91*) As ionic and electronic conductivity measurements have been performed separately for many polymers, it has been shown that electronic conductivity through conductive polymers is typically much faster than ionic conductivity.(*92*)(*93*) Unfortunately a clear understanding of this behavior is still not fully developed. An alternative way to analyze the impedance spectroscopy will be discussed in a later section to address this topic.

The pseudocapacitance (CPE_{PS}) is largely due to redox processes within the film.(*80*)(*81*) In order to verify the values of CPE_{PS} the pseudocapacitance was also determined from cyclic voltammograms such as those shown in Figure 3.4 and Figure 3.5. Pseudocapacitance can be determined by scanning at a slow rate (20 mV/s) and dividing current by scan rate.(*94*) The pseudocapacitance calculated at the peak oxidation potential in the cyclic voltammograms had an average value of 8 mF, relatively consistent with the pseudocapacitance values determined by EIS at that potential (Table 3.1).

3.3.3 Comparative EIS Data for Related Systems

Comparable EIS experiments were run on electrochemically grown polyaniline (pAni) films for comparison with pTAPP films on FTO substrates. Figure 3.9 shows Nyquist plots of both types of films run at three different potentials, with bare FTO as a reference. Both polymer films exhibited similar trends at identical potentials, supporting the understanding of pTAPP as a conductive polymer similar to pAni.

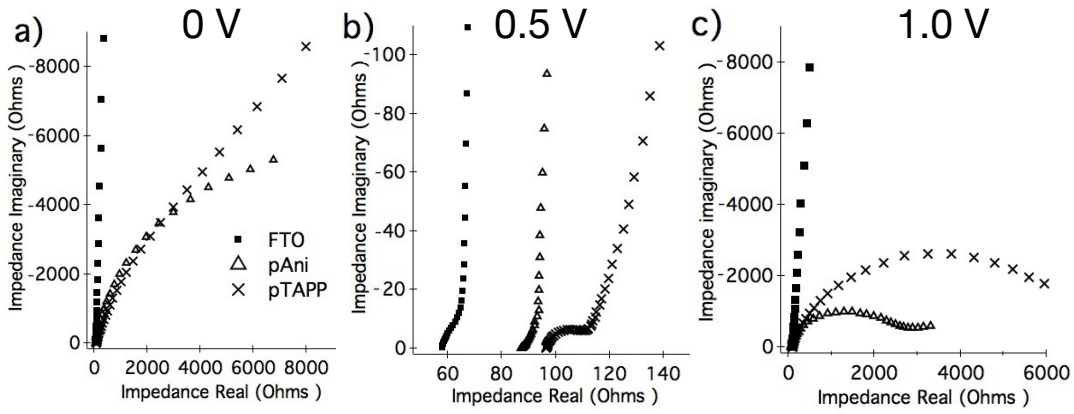

Figure 3.9 Nyquist plots of FTO (square), pAni (triangle) and pTAPP (x) showing the similarities between the conductive and insulating states at identical potentials. Graph (a) is at 0 V bias, (b) is at +0.5 V bias and (c) is at +1.0 V bias (vs. Ag/AgCl in 5 M NaCl at pH 4).

Interfacially polymerized films tested under similar conditions exhibit impedance (R_{CT}) values higher than those of electrochemically prepared films of comparable thickness. Interfacially grown films are considerably thicker when compared with typical electrochemically grown films. In order to decrease the difference between films due to

thickness effects, films grown electrochemically were made as thick as possible with long delays at oxidizing potentials. Figure 3.10 shows EIS impedance results (R_{CT}) for both electrochemically and interfacially grown films of pTAPP on FTO electrodes. Both types of films showed an optimal oxidatively doped state between +0.3 and +0.5 V, but interfacially grown films show greater divergence at limiting potentials. This is likely due to increased charge-transfer resistance between the electrode and the films; interfacial films are laid upon the electrode while still wet from synthesis and rinsing steps, as compared to the electrochemical films grown directly on the electrode. In order to test this, cyclic voltammetry of the films in a clear, monomer-free electrolyte solution was performed to visibly observe the effect on the film. Because of the electrochromic behavior of the film, discussed later, it is easy to visually detect which areas of the polymer are electrically connected. For the interfacial film, only a small amount of the black film changed color (became reduced) at less oxidizing potentials, suggesting that only a relatively small fraction of the interfacial film is effectively connected to the electrode. Electrochemically grown pTAPP films show uniform electrochromic behavior.

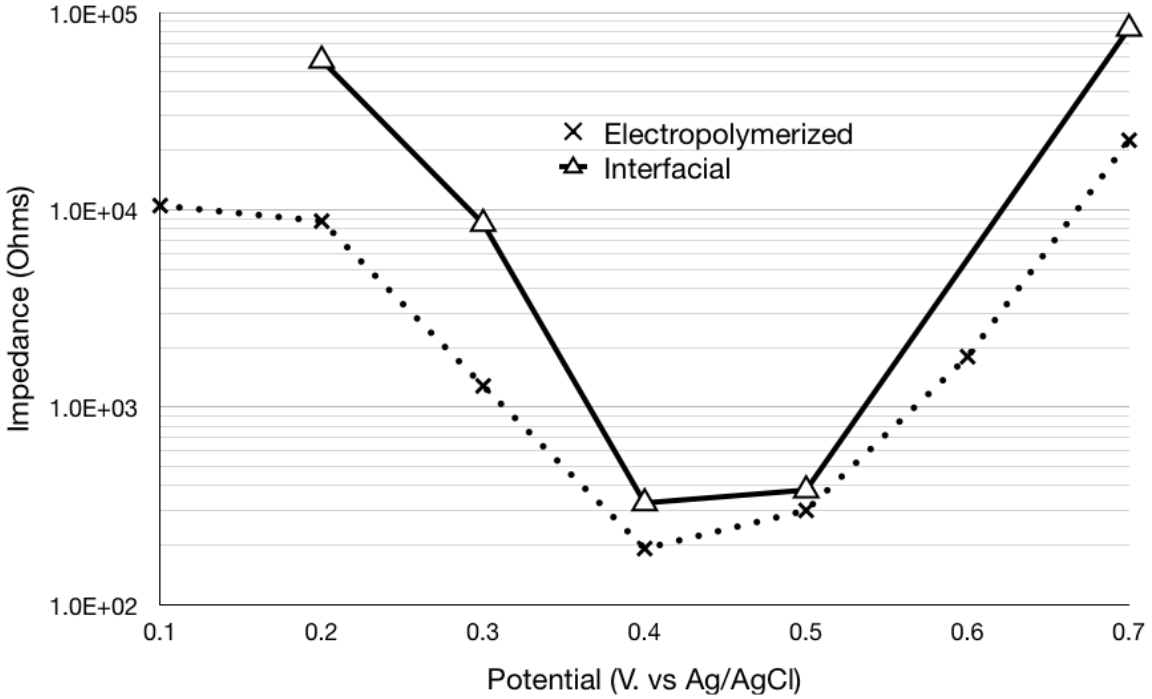

Figure 3.10 Impedance values (R_{CT} from EIS Nyquist plots) for pTAPP films. X markers and the dotted line represent electrochemically grown pTAPP films, and triangles and the solid line represent interfacially grown pTAPP films.

3.3.4 Film Thickness Effects on Impedance

Considering impedance as a bulk property, it is important to verify that it correlates with the size of the sample. The active area of all EIS runs was controlled to 1 cm^2 as closely as possible; as such the impedance should scale linearly with the thickness of the sample according to Pouillet's law.(*95*) This was tested with two pTAPP films prepared by holding a fixed potential of +0.9 V vs Ag/AgCl for 20 s and 150 s. Both samples were measured on a profilometer at three different places in order to determine an average thickness. The sample polymerized for 20 seconds had a mean thickness of

0.4 ± 0.1 μm while the sample polymerized for 150 seconds had a mean thickness of 1.2 ± 0.2 μm. Identical EIS sweeps were run on both samples and R_{CT} in the thicker sample was always greater. Of the five potentials run, including 0.1 V steps between +0.2 and +0.6 V vs. Ag/AgCl, the thicker film was on average 3.2 times more resistive than the thinner film, in agreement with the relative thickness.

3.3.5 pH Effects on Polymer Electrochemical Properties

As with polyaniline, it is expected that the conductivity of pTAPP films can be influenced by doping through acid-base chemistry.(*79*) The most conductive pTAPP samples are produced by optimizing both the potential and the pH. EIS studies were carried out with pTAPP films prepared by electropolymerization, using applied potentials between +0.2 and +0.6 V and pH values from 3 to 9 (Figure 3.11). Lowest values of R_{CT} are observed at a potential of about +0.4 V vs. Ag/AgCl and at low pH.

Unlike films tested for comparison of interfacial and electropolymerized films, pTAPP samples tested for conductivity and pH were purposely kept relatively thin. This resulted in the much lower minimum impedances seen in Figure 3.11 as compared with Figure 3.10. The intent was to minimize the differences between the outside of the film and the inside due to diffusional aspects. When the film is oxidized or reduced counterions must be driven into or out of the film. This can cause pH gradients to form within the film and could lead to inaccurate measurements. By keeping the film thin we can minimize the pH gradients formed, uniformly apply pH to the film and accurately determine the effects of pH on R_{CT}.

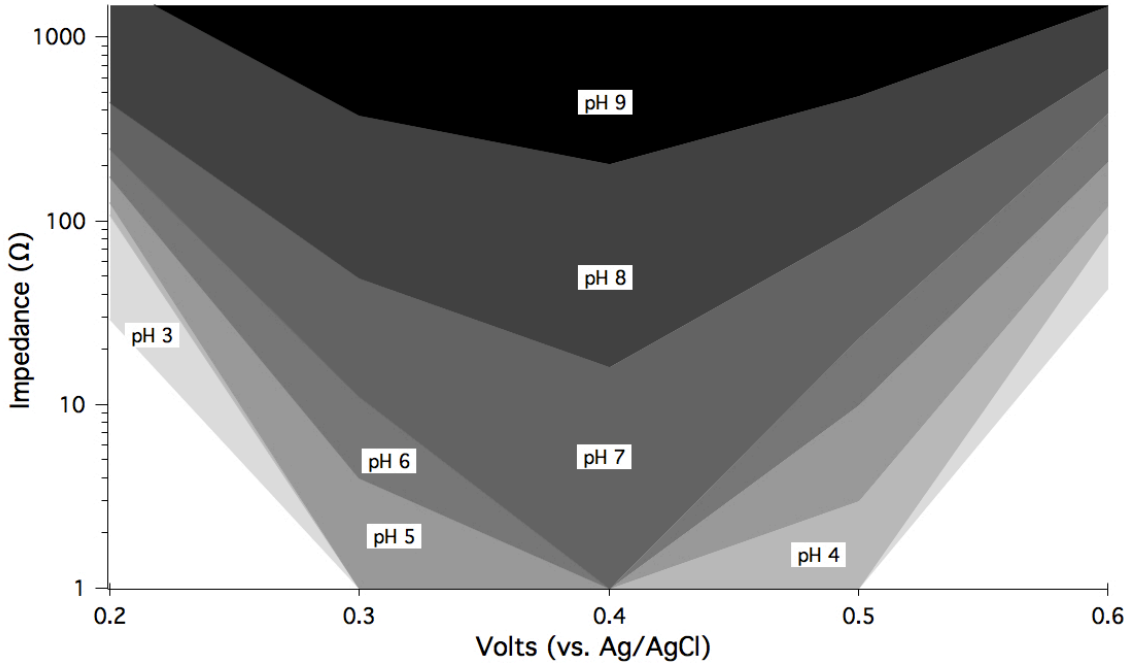

Figure 3.11 Variation in impedance values (R_{CT} from EIS Nyquist plots) for an electropolymerized pTAPP film as a function of applied potential at different solution pH values.

Figure 3.11 shows that R_{CT} values of the pTAPP film decrease at all potentials as pH decreases. Note that the minimum impedance value we could determine was about 1 ohm. The pH effect may be caused by higher concentrations of smaller, more mobile counterions (H^+), facilitating charge transfer via hopping through the polymer. Because the pK_a of protonated phenazine is around 1.2,(*96*) it is possible that even lower R_{CT} values might be observed at pH lower than 2. Although the pH effect on impedance is

reversible between pH values of 3 to 9, out of this range irreversible changes occur, so that testing these films below a pH of 3 or greater than a pH of 9 is difficult.

At pH 2 and below, the film changes to a dark purple/black color. We attribute this to the protonation of the interior of the porphyrin units giving neutral porphyrin units a +2 charge. The observed color is similar to the fully oxidized state of the polymer film. At pH 2, application of a reduction potential negative enough to reduce the phenazine linkers to dihydrophenazine causes the film to turn to a red/orange color and detach from the electrode into solution.

At pH 10 and above, the film quickly undergoes a change to a green color. This is attributed to the oxidized (+2) porphyrin units being deprotonated and returning to a neutral state.

3.3.6 EIS Interpretation Based on pAni as a Special Case

The classical transmission line model when interpreted for pAni, polypyrrole, and pTAPP shows a specialized case suggesting the polymer is highly conductive. Fletcher's generalized transmission line model is derived from a classical transmission line model and is of a type known as the segmented transmission line.(*86*) It is referred to as segmented as the RC circuits are segmented from each other and are proposed to act individually leading to a theoretical Nyquist plot with two RC time constants. Although this equivalent circuit is widely accepted for many electroactive polymers, there is a major problem applying this model to films which lack a Warburg element in the Nyquist plots. The only way the segmented model can correctly match a system which lacks a

Warburg element is if the electronic resistance through the polymer matches the ionic resistance through the solution phase. Unfortunately it has been shown that the electronic resistance in conductive polymers is typically much less then the ionic resistance.(*97*) Thus segmented transmission lines are unable to correctly model systems such as pAni and pTAPP.

Warburg elements are commonly used to model diffusion of ions through solution between the working electrode and the reference electrode. Although interpretation of a Warburg element is quite complex, identifying them is done easily as they are represented as a 45° line on a Nyquist plot.(*98*) When either pAni or pTAPP is measured using EIS there is no identifiable Warburg region in the Nyquist plots. In order to explain how this is possible and find a model which does fit these systems, we must look back at the classical transmission line model.

A classical transmission line model is shown in Figure 3.12.(*99*) The model consists of two repeating resistive elements connected in series by repeating capacitors. The classical transmission line model lacks the RC circuit seen in our Nyquist plots. In order for it to be an appropriate model for our system the C_{DL} capacitance and a resistor representing the R_{CT} would need to be inserted parallel to one of the resistive elements.(*91*) In addition since the Nyquist plots typically only show one RC circuit and an ohmic resistance at high frequencies then either the resistive element due to electron movement through the polymer or ionic diffusion would need to be much faster than the other so that one element is represented by the ohmic resistance and the other the RC

resistor. From this analysis it can be determined that upon placement of the capacitor in parallel with one of the resistive elements the other resistive element will be attributed to the ohmic resistance and as such will be the more resistive of the two systems. Next we will look at each separate case and determine the appropriate transmission line set-up for pTAPP.

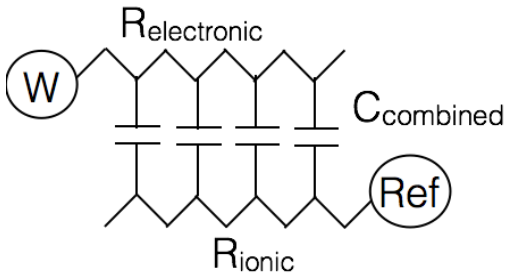

Figure 3.12 Classical transmission line model in which $R_{electronic}$ is the resistance of charges through the polymer, R_{ionic} is the resistance due to ions moving through solution and $C_{combined}$ is the distributed capacitance at the film/solution interface.

The insertion of C_{DL} and R_{CT} elements can be done in four places, bringing about four distinct cases as shown in Figure 3.13. Cases 1 and 2 have the RC circuit connected to the lower resistance line. Case 1 shows the RC circuit in parallel with the resistive element representing the polymer film, case 2 puts the RC circuit in parallel with the ionic diffusion resistance. Cases 3 and 4 have the capacitor in a place where it can shunt both of the resistances; shunting both resistances would be expected primarily at high frequencies. Theoretical modeling of these four cases indicate that cases 1 and 2 would

lack a Warburg element while cases 3 and 4 would show a distinct Warburg element. This suggests that pTAPP fits in either case 1 or 2.

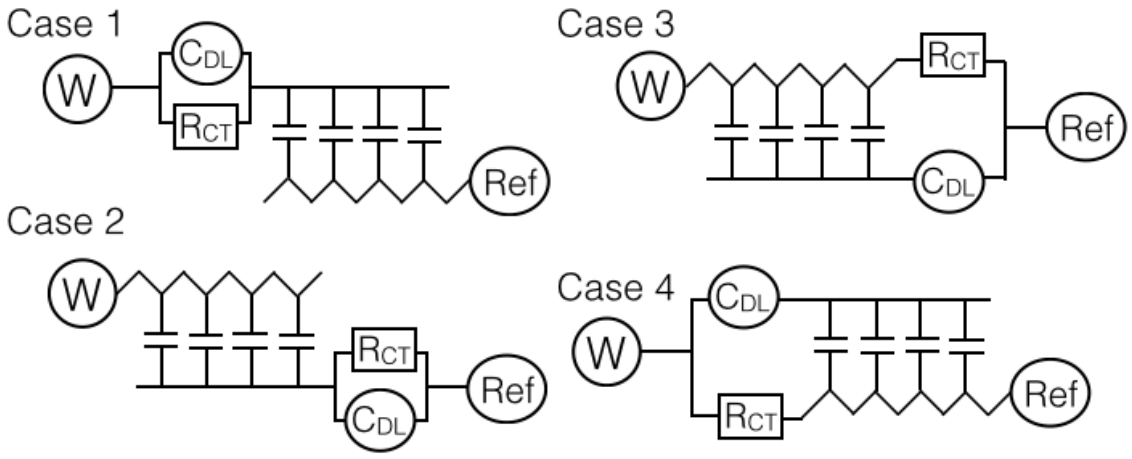

Figure 3.13 Albery and Mount modified transmission line models indicating the four possible positions for the RC circuit in typical analyses of conductive polymer films.(*91*)

Further considering cases 1 and 2 we can identify whether the ohmic resistance is dominated by the solution resistance or by the polymer resistance. If pTAPP falls into case 1 then the ohmic resistance is dominated by solution and pTAPP can be shown to be very conductive. On the other hand if pTAPP falls under case 2 then the polymer is dominating the ohmic resistance and pTAPP would be considered less conductive.

To differentiate between case 1 and case 2 it must determined if pTAPP or the solution is more conductive. One way to determine this is to purposely lower the conductivity of the polymer so that the polymer itself appears in the EIS measurements. By raising the pH of the solution at which the EIS was performed another element appears in the Nyquist plot, correlating with the conductivity of the film. Figure 3.14

contains three Nyquist plots of an electropolymerized sample of pTAPP at pH 7.0 which show two RC circuits at potentials of +0.2 V and +0.3 V vs. Ag/AgCl. The first RC circuit corresponds to the film elements at these pH and potential values. The second RC circuit is the identical double layer capacitance and resistance as seen before. Once the polymer is highly conductive at potential 0.4 V vs. Ag/AgCl, the RC circuit due to pTAPP can no longer be accurately recognized. Polypyrrole films have also been reported showing two RC circuits without a Warburg element.(*86*)

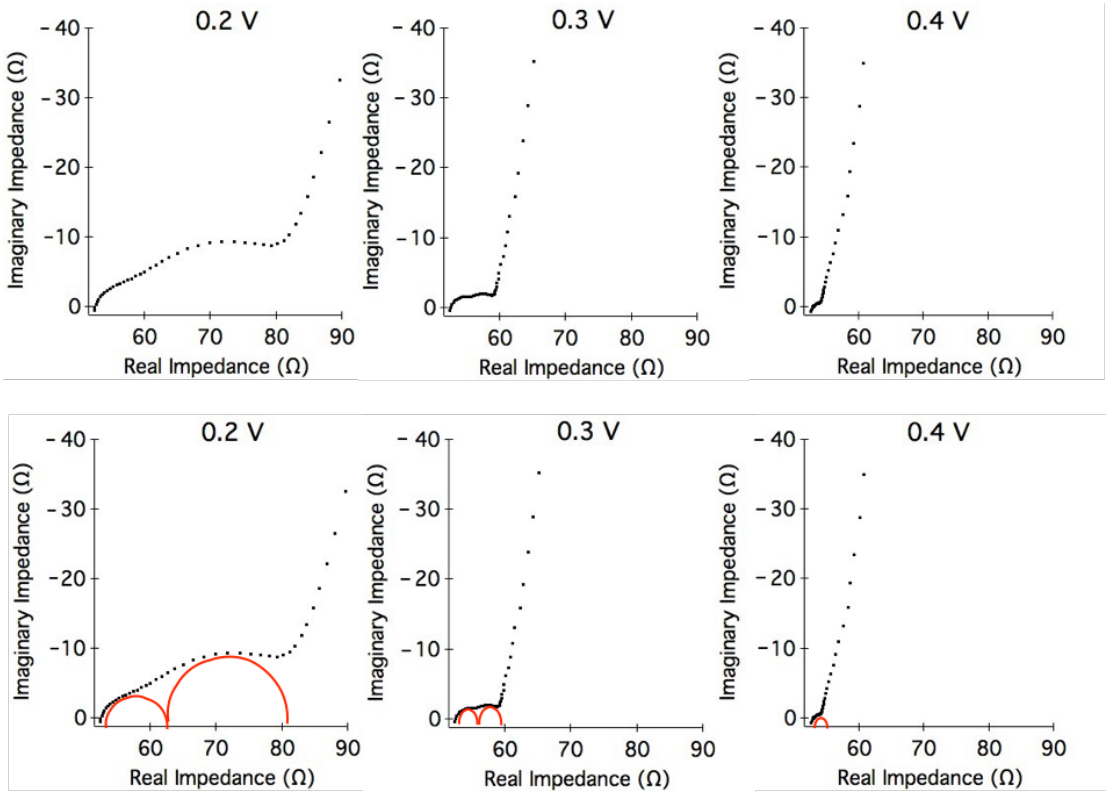

Figure 3.14 Nyquist plots of an electropolymerized pTAPP film at different potentials all at pH 7. The increased pH reduces the conductivity of the film leading to the development of two RC circuits. The lower plots show the same Nyquist plots with red-half circles emphasizing the two RC time constants.

To analyze the Nyquist plots with two RC circuits we must either put another RC element into the classical transmission line model or go back to Fletcher's model. For simplicity we will refer back to Fletcher's model and re-simplify it to contain both of the RC circuits seen. Figure 3.15 shows the simplified transmission line model used to analyze the lower conductivity films shown in Figure 3.14. Using the new equivalent circuit we can estimate the film's impedance to be approximately 10 ohms, from the

Nyquist plot taken at 0.2 V bias vs. Ag/AgCl. As the bias potential is increased both the film's resistance as well as the charge transfer resistance decreases. This is caused by an increase in the number of charge carriers within the film upon oxidation. Now the ohmic resistance of the system at high frequency can be attributed only to solution resistance, which in these films can be estimated at 52 ohms. If we can also estimate the maximum resistance of the film to be around 10 ohms then we can conclude that the film is much more conductive than the solution. This also confirms pTAPP can be classified as case 1 using the Albery and Mount classifications.

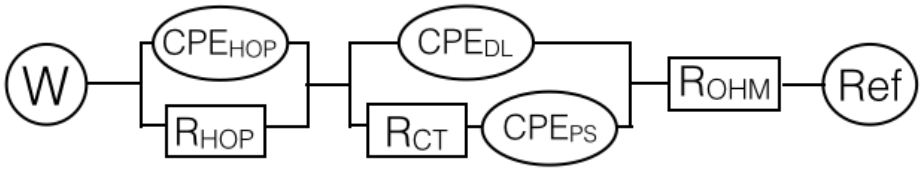

Figure 3.15 Simplified Fletcher model to fit pTAPP films at pH 7 from Figure 3.14. Model assigns both RC circuits seen in the Nyquist plots to the resistance and capacitance within the film (R_{HOP} and CPE_{HOP}) and the resistance and capacitance of the double layer (R_{DL} and CPE_{DL}).

With the system fully characterized through the use of both the Fletcher generalized model and a modified classical transmission model, we can now determine the interface at which the charge transfer resistance and capacitance occurs. There are two charge transfer interfaces, one between the electrode and the film and the other between the film and the solution.(*100*) As pTAPP has been classified as case 1 in the Albery and Mount method it suggests that the charger transfer resistance and capacitance

seen in the typical Nyquist plots is due to the double layer between the electrode and the polymer film.(*86*) Previously we attributed the double layer capacitance to the interface between the polymer and solution. This is largely due to the fact that the interface between the polymer and the electrode is not modeled in Fletcher's generalized transmission line model. If the Albery and Mount cases hold correct then Fletcher's generalized model needs to be adjusted to take both interfaces into account. On the other hand the Albery and Mount models lack a good element to truly model the pseudocapacitance as described by Fletcher's model. It can be concluded that a good equivalent circuit which can be used for conductive polymers is yet to be fully developed.

3.4 Electrochromic Behavior

Electrochromic systems are currently used for a wide variety of applications and have great potential for future applications.(*101*) A distinct electrochromic behavior is observable upon oxidation and reduction of pTAPP films. This has been characterized both electrochemically and chemically, using the oxidizing agent APS and reducing agent ascorbic acid. At -0.7 V vs Ag/AgCl or in ascorbic acid, the film is a golden yellow to green color, which slowly changes to reddish-brown and then a black color as more positive oxidation potentials are applied or when placed in APS. It should be noted that ascorbic acid is not powerful enough as a reductant to fully reduce the film, so that cycling to negative potentials is optimal to fully remove the strong absorbance near 750 nm. Figure 3.16 shows the film color and absorbance spectra on an FTO electrode, as synthesized (stopped at the half-wave potential of +0.45 V), in the oxidized state after

treatment with APS, and in the reduced state cycling to negative potentials. The films show reversible transitions between the three forms shown. The reduced spectra are similar to spectra of the films at pH 10 and above while the oxidized spectra are similar to the film at pH 2 and below. Considerably different spectra are seen when strongly reducing potentials are applied to the films at low pH; the film becomes bright red and tends to come off the electrode.

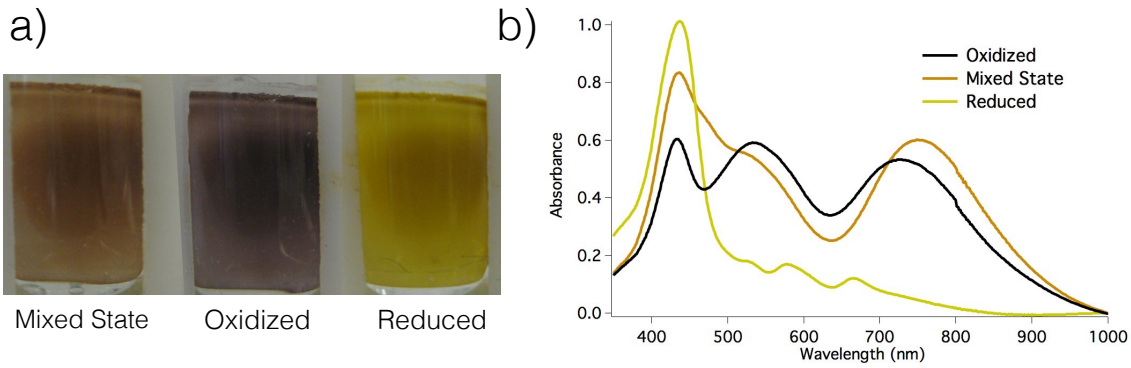

Figure 3.16 a) Single electrochemical pTAPP film, shown in order as the reddish brown film as synthesized, black film in 10 mM APS solution and yellow-brown film in 10 mM ascorbic acid solution. b) Absorbance measurements of a single pTAPP film on FTO glass. The film was synthesized electrochemically and left at a mixed state, then potentiometrically cycled to -0.7 V vs. Ag/AgCl to leave the film in the reduced state, and then cycled to +0.8 V vs. Ag/AgCl to produce the oxidized state.

3.5 Pourbaix Diagram

Pourbaix diagrams can be useful tools to help describe the equilibrium state of a system at a given pH and potential. In determining which species to include in the Pourbaix diagram, we applied the following data. The oxidation potential for conversion of dihydrophenazine to phenazine(*75*)(*102*)(*103*) occurs at potentials less positive than that of oxidation of TAPP, so we consider that the linkage between the porphyrin units is in the oxidized (phenazine) form. Phenazine is a very weak base with reported pKa values for the diprotonated and monoprotonated species as -4 and 1.2.(*96*)(*104*) Thus the linker is represented as unprotonated phenazine at all pH and potential values studied. Interestingly, the polymer film becomes unstable at very low pH and highly negative potentials, as discussed earlier, suggesting that reduced phenazine may facilitate depolymerization or other solubilization of the polymer film. The general scheme that describes the conductivity of the polymer film is illustrated below, using a representative dimer of TAPP (Figure 3.12).

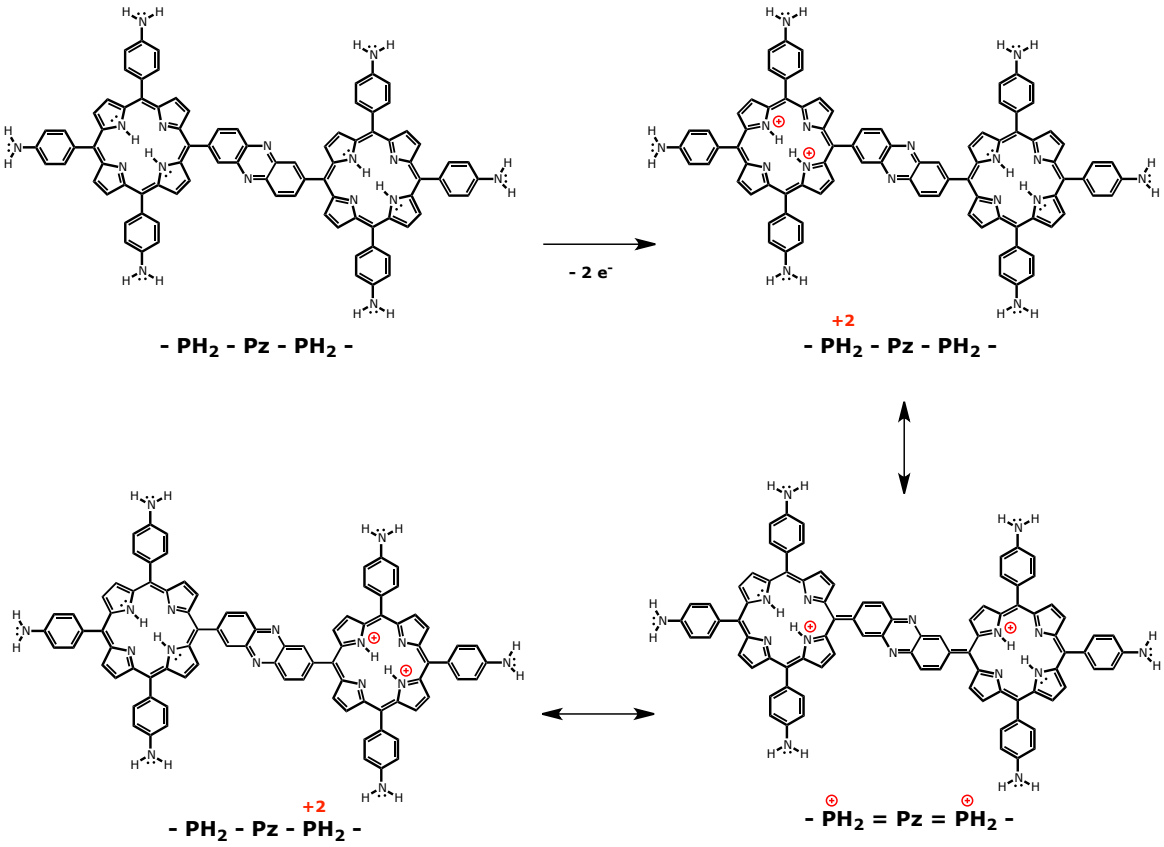

Figure 3.17 Representation of the electronic conductivity between porphyrin units via resonance forms in an oxidized TAPP dimer. All N lone pairs that are shown are part of the extended π system and generally are available to delocalize positive charges.

Considering the electrochromic behavior of pTAPP, we thought it would be convenient to generate a Pourbaix diagram that also correlates the perceived color of the film with the pH and potential range in which that system exists, Figure 3.18.

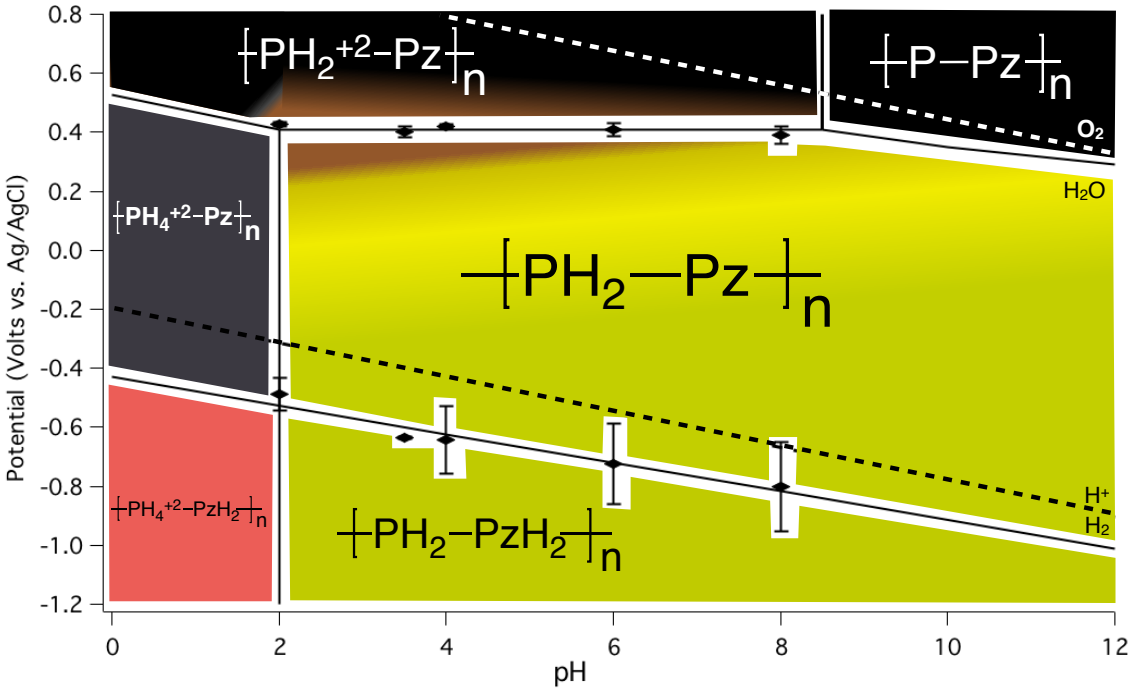

Figure 3.18 Pourbaix diagram showing the species present and the generalized color of pTAPP films on FTO at the given pH and potential values. Abbreviations are as shown in Figure 1.8 and Figure 3.17.

In a Pourbaix diagram, a vertical line can be considered to delineate a process dependent only on pH, typically correlating with the pK_a of a species. The apparent pK_a of TAPP has been determined to be between 2 and 3 in aqueous solutions as indicated by its solubility. Since the reported pK_a of phenazine is 1.2,(*96*) the acid-base color change observed near pH 2 is postulated to be that of free-base porphyrin, i.e., -[PH_2-Pz]-$_n$

to -[PH_4^{2+}-Pz]-$_n$. Protonated TAPP generates a strong hyperporphyrin spectrum(*70*)(*71*)(*72*) similar to that observed for oxidized TAPP or oxidized pTAPP.

Horizontal lines in a Pourbaix diagram correlate to a change dependent only on potential. The oxidation of pTAPP at about +0.5 V behaves in this way at all pH values tested and would appear to be completely independent of the protonation state. On the other hand the reduction of the polymer films shows a multiple electron/proton transition that does vary with pH. The reduction of pTAPP shows a slope of 49 mV per pH unit where a single electron/proton coupled process would give a slope of 59 mV per pH unit. We observe that the reduction of phenazine to dihydrophenazine is considerably variable, which we attribute to the neutral polymer being in an inhomogeneous and relatively resistive state.

Transitions outside of a pH range of 2 to 8 are not readily observed but are added to the diagram for completeness. The oxidation of the protonated porphyrin would be increasingly difficult, and we expect the transition from -[PH_4^{2+}-Pz]-$_n$ to -[PH_2^{2+}-Pz]-$_n$ to be a two-electron and two-proton process. Likewise the oxidation of porphyrin from -[PH_2^{2+}-Pz]-$_n$ to -[P^{2+}-Pz]-$_n$ would also be a two-electron and two-proton process. The pK_a of -[PH_2^{2+}-Pz]-$_n$ to -[P-Pz]-$_n$ is placed at approximately 8 in order to correlate with the transition observed at higher pH. Note that the lowest R_{CT} values (highest conductivity) occur with the presence of a mixed state, depicted by the brownish color in the Pourbaix diagram. Coexistence of both -[PH_2-Pz]-$_n$ and -[PH_2^{2+}-Pz]-$_n$ (i.e., at +0.4 V,

pH 2-8) is analogous to the half-oxidized emeraldine salt form of polyaniline that shows maximum conductivity.

3.6 Conclusions

Tetra(4-aminophenyl)porphyrin can be oxidatively polymerized with a variety of methods, including electropolymerization, chemical oxidation, and interfacial polymerization. pTAPP displays a nanofibrous morphology and interesting properties of electroactivity and electrochromism. Charge-transfer resistance (oxidative doping and dedoping) can be very low under optimum conditions at pH 4 and +0.4 V vs. Ag/AgCl, where we propose a mixed state of neutral and oxidized porphyrin units exist in the polymer, electronically connected by phenazine bridges. EIS data are similar to electrochemically characterized pAni. pTAPP is a strong candidate for all of the similar applications of pAni and more considering its added light adsorption as well as the ability to contain metals. Data collected from cyclic voltammetry and electrochemical impedance spectroscopy allowed for creation of a novel polymer Pourbaix diagram correlating the proposed states of the system with observed color, pH, and potential.

4 CHARACTERIZATION OF METALLATED pTAPP

Monomeric porphyrins as well as porphyrin polymers are often metallated with transition metals in order to add functionality. The added bonding orbitals supplied by transition metal centers can be used for catalysis, coordination, and modifying excited state properties.(*105*) Porphyrins are commonly metallated with metal ions in the two plus oxidation state. Upon metallation the metal adopts a square planar geometry leaving orbitals on either side of the planar porphyrin ring available for further bonding.(*106*) While typically these open orbitals are targeted for coordination with substrates, they can also cause unexpected coordination with other neighboring porphyrin units. This type of coordination typically leads to extended networks and a decrease in solubility.(*59*)

Upon metallation of pTAPP there is both expected changes in the absorption spectrum and solubility as well as an unexpected change in the morphology. This chapter describes the characterization of pTAPP metallated with either zinc or cobalt.

4.1 Changes in UV-Visible Absorbance upon Metallation

Metallation was optimized using cobalt acetate, cobalt chloride, zinc acetate, or zinc chloride dissolved in methanol or isopropyl alcohol. Typically metallation occurs rapidly and completely by simply immersing the pTAPP film electrodes into the metal salt/alcohol solution and heating to reflux. Refluxing with times as short as five minutes shows complete metallation of the film based on the absorption spectrum. Both methanol

and isopropyl alcohol work well as orthogonal solvents for the metallation reaction i.e., solvents that dissolve the metal salt but had minimal effect on the polymer.

The rapid metallation can be monitored by the UV-Vis absorption spectrum. The facile nature of this reaction, along with the completeness of metallation, was determined by disappearance of the band at 791 nm in pTAPP films as well as the appearance of the two Q bands at 605 and 558 nm. The absorbance spectra of the free base polymer and the cobalt metallated polymer are shown in Figure 4.1. The spectra are of the same film before and after metallation.

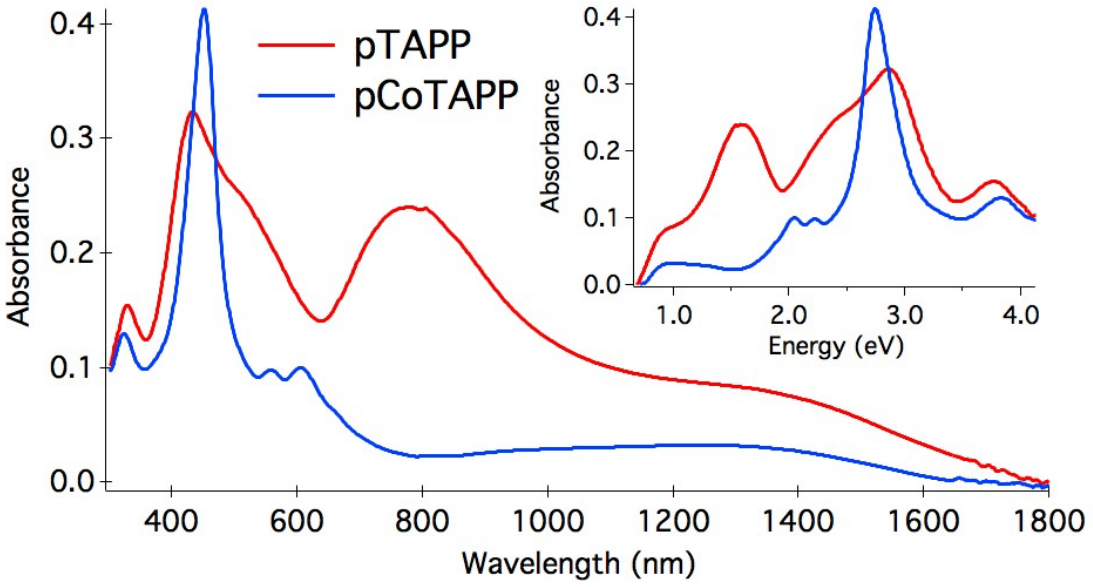

Figure 4.1 UV-Vis absorbance spectra of pTAPP and pCoTAPP films. The same film was used for both spectra, before metallation in red and after metallation in blue. The inset shows the same spectrum but with the x-axis as energy in eV.

There are two long wavelength absorptions in pTAPP films not seen in neutral porphyrin spectra. Long wavelength absorptions have been correlated with polaron and bipolaron conductivity mechanisms in polymers.(*107*)(*108*) The first is around 791 nm and can be attributed to a hyperporphyrin spectrum in which the phenyl and/or phenazine substituents are planarized and conjugated with the porphyrin ring.(*70*)(*71*)(*72*) Hyperporphyrin spectra are often seen in porphyrins with +2 charges and strongly electron-donating groups such as amino (Figure 4.2). In a polymer this can be considered equivalent to a bipolaron state. Bipolarons are two singly occupied molecular orbitals (SOMO) which associate with each other as the distortions caused within the conjugated polymer are minimized in energy through association.(*109*)(*107*) All electrons are paired in bipolarons. In pCoTAPP, the disappearance of the band at 791 nm in Figure 4.1 suggests that the individual porphyrin units in the polymer are significantly less electronically conjugated. In this case association of polarons into a bipolaron do not appear to occur. The presence of delocalized bipolarons, as shown in Figure 4.2, is considered one mechanism for electronic conductivity. After metallation the polymer does not show the same electrochromic or redox behavior as the free base polymer and is not considered to have the same mechanism of conduction.

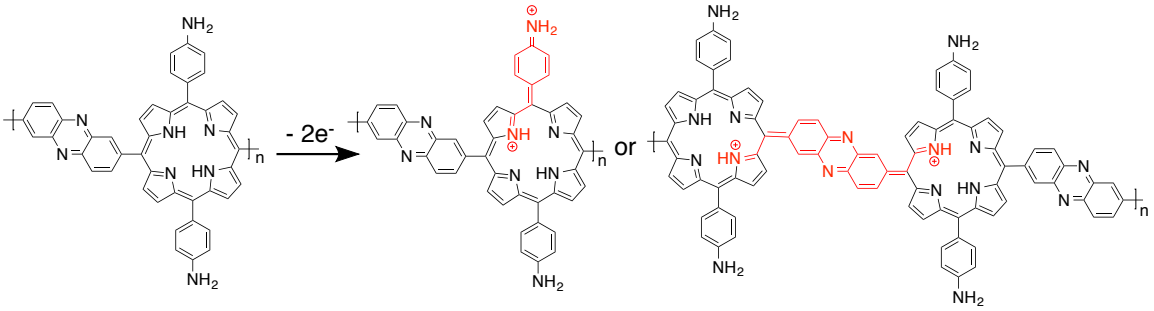

Figure 4.2 Partially oxidized pTAPP polymer showing planarization of meso-position units leading to the characteristic hyperporphyrin absorbance at 791 nm. Planarized meso-substituents are highlighted in red.

The second long-wavelength absorption is centered at 1300 nm. Near IR absorptions are typically attributed to additional states found within the band gap after doping and unpaired electron conduction known as polarons.(*107*)(*109*)(*110*) A polaron exists in a SOMO and even though multiple polarons can exist in one polymer the polarons do not always associate with each other. Polarons have been proposed to remain unassociated when conjugated polymer systems are large enough to separate the charges and two separate SOMOs can exist independently at lower energy. Depending upon the distortion and extent of conjugation either bipolarons or polarons are more energetically stable. Metallated derivatives of pTAPP do not lose the broad long-wavelength absorption centered near 1300 nm but do lose the 791 nm absorption indicating the possible presence of polarons and not bipolarons. While we have proposed that pTAPP has a bipolaron mechanism of conduction,(*63*) any conductivity in pCoTAPP

would follow a conduction mechanism via polarons. Interactions between the metal and substituents are proposed to explain this continued conductivity.

If these absorptions are due to polarons and bipolarons distributed within the films, then the absorbances should correlate with the relative concentration of doping within the polymers. In order to test this, the degree of oxidative doping can be performed both on an electrode and with the polymer dissolved in solution. pTAPP is readily dissolved in DMSO. When the polymer dissolves, it does not return to monomeric units; monomeric TAPP dissolved in DMSO fluoresces but dissolved polymer does not. With a single sample of pTAPP dissolved in DMSO, the absorption at 791 nm was monitored as APS was titrated. As can be seen in Figure 4.3, with greater concentrations of APS the band at 791 nm grows larger until a maximum is reached in an excess of APS.

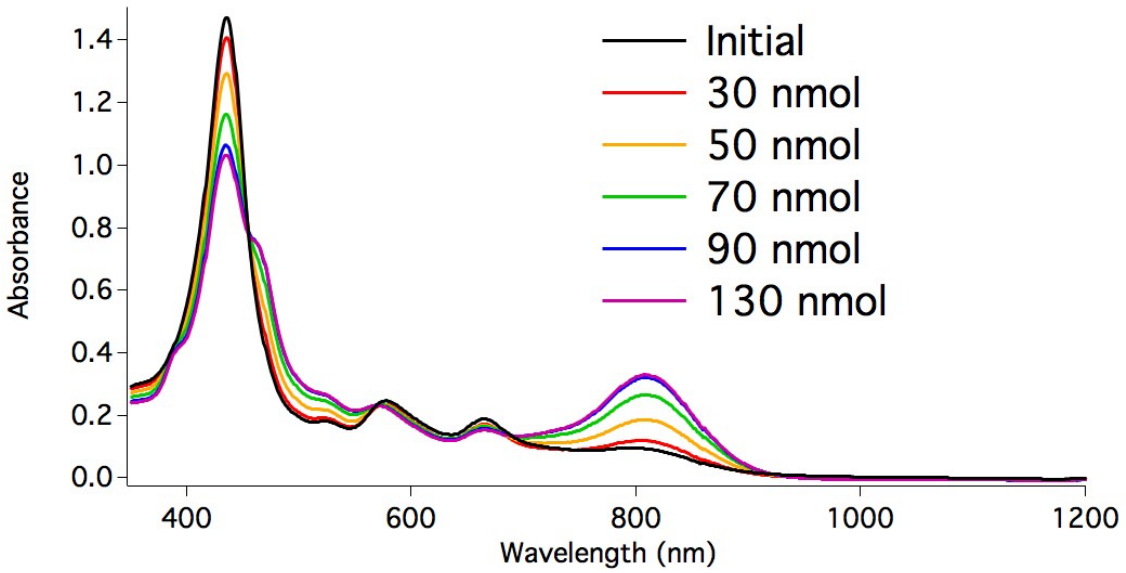

Figure 4.3 Change in absorbance of pTAPP dissolved in DMSO with oxidative doping by APS.

A similar experiment performed on a solid sample of pTAPP on an FTO electrode showed the absorption at 791 nm increased with the oxidative doping, Figure 4.4. The polymer film was first completely oxidized with APS and shows a large absorption at 791 nm and a small absorption near 1300 nm. Using small reduction steps, both the peak at 1300 nm as well as the peak at 791 nm decrease in intensity. The decrease near 1300 nm is too small to definitely correlate with the doping of the polymer. The fully reduced film shows no absorption at 791 nm, but a small absorption near 1300 nm is still present under fully reduced conditions. These results indicate that pTAPP films have bipolarons but the presence of polarons distributed within the film is still questionable. The polymer is inhomogeneous and made up of systems with different numbers of polymerized

monomeric units, which may cause both the bipolaron and polaron states to coexist simultaneously. Hyperporphyrins are stable monomeric systems with a +2 charge, and pTAPP is stable with +2 charge on a single porphyrin unit. Individually created polarons on pTAPP are likely to be stabilized by association within a single porphyrin macrocycle. The tendency for association of polarons within pTAPP would lead to a large increase in the absorbance at 791 nm with minimal increase in the absorbance near 1300 nm with a higher level of doping.

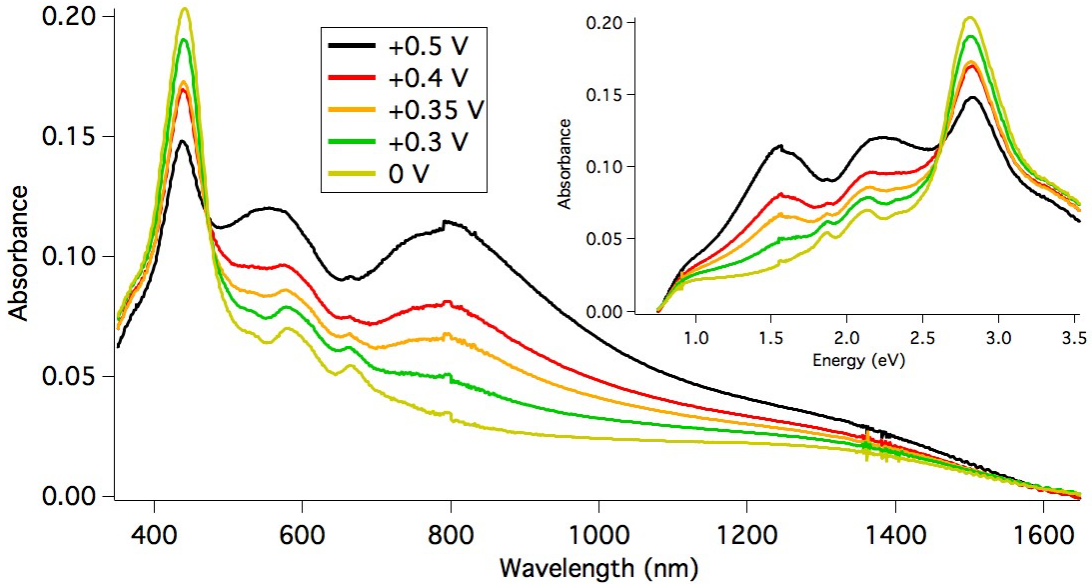

Figure 4.4 Change in absorbance of pTAPP on FTO with initial oxidative doping by APS at +0.5 V, followed by small steps of electrochemical reduction. A clean FTO slide was used for the reference beam. The inset window shows the same data with energy in electron volts as the x-axis.

The metallated films are highly cross-linked and completely insoluble. This leads to an inability to monitor doping in solution. In addition the absorption spectrum shows the absence of the bipolaron absorbance from 700 to 800 nm. The addition of cobalt leads to a redox center that can accept or donate a single electron. It is believed that this leads to the loss of a bipolaron lowest energy state and a conduction mechanism based solely on polarons. An absorption around 1300 nm corresponds to a band gap of only 0.95 eV. This relatively small band gap helps to explain both the conductive nature of pTAPP and pCoTAPP as well as its lack of fluorescence.

4.2 Morphology of Metallated pTAPP Films

SEM images of pTAPP films were taken before and after metallation with cobalt in methanol. The film in Figure 4.5a was electropolymerized using the fixed potentiometery method as compared to the cycling method. This confirms that the fixed potentiometry method (Figure 4.5a) as well as the cycling method (Figure 1.5a) both produce nanofibrous morphology. After metallation, the film maintains its nanofibrous structure(Figure 4.5b). This is important as it suggests the metallation procedure does not modify the polymer in any significant way as would be expected for a system conjugated with a stable linkage such as the proposed phenazine linkage.

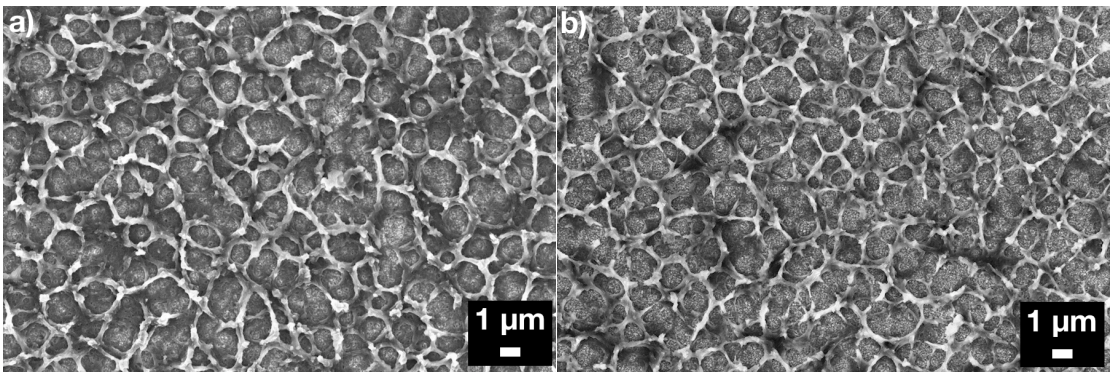

Figure 4.5 The same pTAPP sample before (a) and after metallation with cobalt (b).

4.3 Fluorescence with pZnTAPP

Monomeric TAPP and ZnTAPP show strong fluorescence between 600-800 nm, but pTAPP shows no fluorescence out to 900 nm. pZnTAPP shows absorption and morphological changes identical to pCoTAPP but has much better solubility in DMSO. Therefore the fluorescence experiments for metallated derivatives of pTAPP were performed with pZnTAPP. Fluorescence quenching experiments are often used as a way to determine excited state electron transfers. Oxygen is known to quench the fluorescence of porphyrins and often leads to the production of singlet oxygen. If fluorescence could be detected using pTAPP or pZnTAPP, then quenching and detection of oxygen reduction would be useful tools for studying the polymer as a photocatalyst. Unfortunately no fluorescence was detectable using pZnTAPP.

Upon sonication the metallated particles become disconnected from one another. We were hopeful this would allow for fluorescent behavior. Unfortunately pZnTAPP particles in solution also show no detectable fluorescence out to 900 nm.

4.4 Conductivity of pCoTAPP

A conductive structure is highly desirable for porous polymers with immobilized catalytic centers such as pCoTAPP. EIS measurements of pCoTAPP were performed and analyzed with an equivalent circuit model analogously to pTAPP.

pCoTAPP behaved much more like a typical electroactive polymer than pTAPP during EIS measurements. Nyquist plots of pCoTAPP are shown in Figure 4.8. The Nyquist plot at +0.5 V vs. Ag/AgCl shows a single RC circuit followed by a clear Warburg element. At this potential the film shows a charge transfer resistance around 65 ohms, comparable to what would be expected for unmetallated pTAPP films.

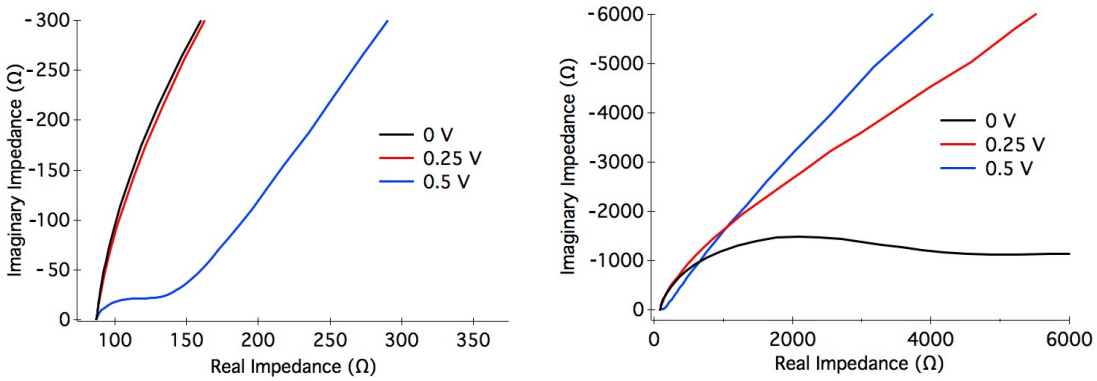

Figure 4.6 Nyquist plots of pCoTAPP film at three potentials in aqueous 5 M NaCl at pH 4. The two figures are the same data at different scales in order to emphasize the interpretable elements at each potential.

The pCoTAPP films show much larger charge transfer resistances at lower potentials. Upon initial testing at +0.5 V vs. Ag/AgCl films show around 70 ohms of resistance, at +0.25 V vs. Ag/AgCl the resistance is extremely large and is estimated to be

between 8-10 kohms and at 0 V vs. Ag/AgCl the resistance is close to 4 kohms. The increase in resistance can be caused by less porosity or more resistance to charge transfer from the electrode through the film. Most interesting is that at a potential of +0.25 V vs. Ag/AgCl the film has a larger charge transfer resistance than at 0 V. Kellett and Spiro have found the Co^{III} to Co^{II} transition in Co-5,10,15,20-tetrakis-(p-trimethylammoniophenyl)porphyrin occurs at +0.3 V vs. the saturated calomel electrode (SCE) at pH 1, which would be approximately +0.1 V vs Ag/AgCl at pH 4.(*111*) This transition introduces additional redox states within the polymer leading to the lower charge transfer resistance at 0 V.

The increased charge transfer resistance below +0.5 V vs. Ag/AgCl may be related to the decreased conjugation between the porphyrin units as proposed in Figure 4.7. Electronic and ionic conductivity can be coupled in these polymer systems as charge neutrality must be maintained within the film-solution interface.(*86*) If there is a decrease in the charge mobility in the polymer this may be seen in the charge transfer resistance to ions moving in and out of the film. Unfortunately without the typical redox behavior of the film that was present for pTAPP, the pCoTAPP system proved difficult to optimize for a conductive state and to find a second RC element in the Nyquist plots. Upon repeated cycling, there was only an increase in the charge transfer resistance with cycling. This indicates that as the film is cycled to oxidative and reductive potentials, an optimized stable state is reached in which the film becomes unresponsive to the electrode potential. Even though the film does not physically disconnect from the electrode surface

the system does become disconnected electronically. The resistive behavior of similar systems has been commented on previously with monomeric layers of CoTAPP films by Spiro et al.(*111*)(*112*) They found that for CoTAPP monolayers, the system worked as a hydrogen evolution catalyst but only for one cycle. More recently this was commented on by Lokesh et al. who found that a self-adsorbed monolayer of CoTAPP on a gold electrode was able to completely block the ferricyanide redox couple during electrochemical cycling.(*113*) The polymeric film after metallation behaves similarly to the CoTAPP monolayers and quickly becomes a blocking layer to the electrode after electrochemical cycling.

This resistive nature of the film also brings about difficulty in determining the redox potential of the cobalt ion in the porphyrin polymer network. Typically the cobalt redox couples can be determined relatively easily in porphyrins using cyclic voltammetry.(*58*) In CoTAPP films the Co^{II} to Co^{III} redox couple can act extremely sluggish.(*112*) Previously Kellet et al. determined the Co^{III} to Co^{II} redox couple to be at +0.3 V vs. SCE at pH 1 and -0.2 V vs. SCE at pH 7.2 with adsorbed monolayers of CoTAPP films. pCoTAPP films on gold electrodes show a small reduction peak around 0 V vs Ag/AgCl at pH 5 (Figure 4.9). This correlates well with the expected reduction of Co^{III} to Co^{II} from Kellet's report.(*111*)

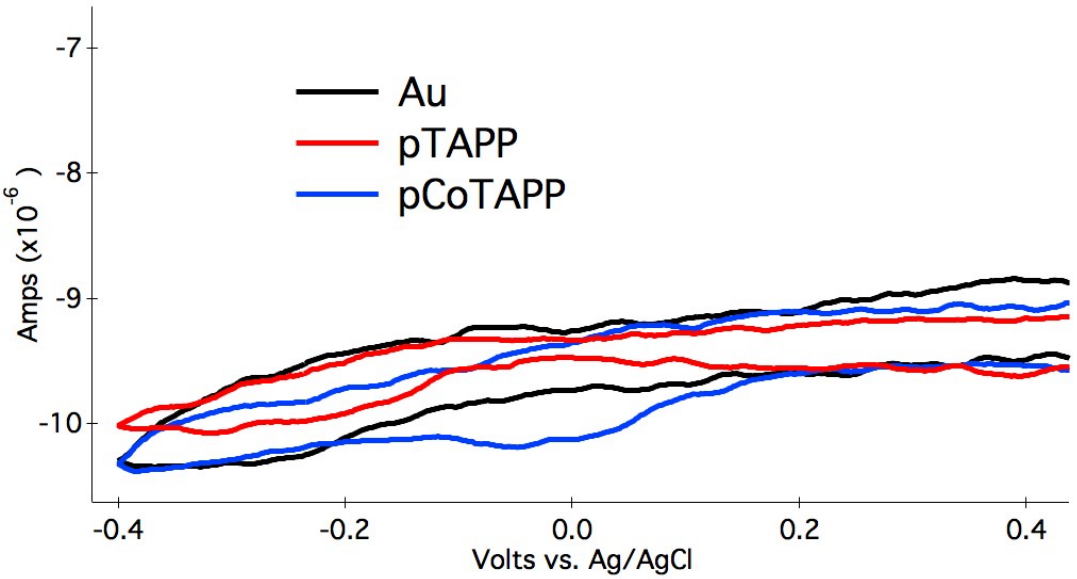

Figure 4.7 Cyclic voltammograms of pTAPP and pCoTAPP on 0.3 cm^2 area gold electrode in aqueous 0.5 M KCl saturated with N_2 at pH 5.

4.5 Conclusions

The successful metallation of pTAPP showed no morphological changes; in particular the nanofiber structure remained indicating no change in the polymers linkages. In addition conductivity of metallated pTAPP is retained as signified by EIS measurements. However, the proposed mechanism of conductivity does not appear to occur via bipolarons as the loss of conjugation between the meso substituents prevents the conduction of electrons through fully conjugated substituents. Unfortunately the strong fluorescence often seen with metallated porphyrins was not detected. Without fluorescence, testing substrates for photocatalytic activity would continue to be relatively problematic. In addition because of the difficulty with pCoTAPP as an electroactive film

redox properties of the film are unable to be determined. To probe catalytic activity, pTAPP and its metallated derivatives were tested for electrocatalysis as electrode films.

5 CATALYTIC TESTING OF pTAPP AND pCoTAPP FILMS

pTAPP can be grown on electrodes and metallated, allowing for testing as an electrocatalyst. Determining electrocatalytic behavior is preliminary to testing for photocatalytic potential. In order for a polymer-modified electrode to optimally perform as an electrocatalyst, the polymer must first be conductive and able to transport charge carriers to immobilized catalytic sites within the film, and secondly the catalytic sites must be open to diffusion of reactants. This is typically accomplished using a conductive polymer optimized for catalytic conditions by including dispersions of proven catalysts such as enzymes, Pt nanoparticles or other catalysts.(*114*) Since pTAPP is the main polymer of this study, the goal is to use pTAPP and its metallated derivatives as both the conductive polymer and the catalyst.

pCoTAPP was briefly tested before for oxygen reduction reaction (ORR) and showed a small overpotential.(*115*) In general metal-free catalysis is more desirable because metal-free catalysts for ORR are more resistive to catalyst poisoning.(*116*) Unfortunately, the overpotential was rather significant with unmetallated pTAPP films so both pTAPP and pCoTAPP films will be evaluated for the ORR.

Many metallated polymeric tetrakis(aminophenyl)porphyrin films were previously tested for the ORR by Bettelheim et al.(*49*)(*117*)(*118*) Early in this body of work it was found that the ortho-substituted derivative, poly-cobalt-tetrakis-5,10,15,20-(2-aminophenyl)porphyrin (pCoT2APP) outperformed pCoTAPP. As such the majority

of their work concentrates on pCoT2APP and neglected to further test pCoTAPP. This work will concentrate solely on pCoTAPP for testing.

Recently nitrogen-doped carbon nanotubes have shown ORR catalytic behavior even better than Pt.(*119*) This was attributed to the electron-withdrawing effect of nitrogen on neighboring carbon atoms. pTAPP has two types of conjugated nitrogen heterocyclic structures, both the porphyrin core and the phenazine linkage. This makes it a promising material for metal-free ORR and thus will be evaluated even though it shows high overpotential.

5.1 Electrocatalytic Testing with Cyclic Voltammetry

Figure 5.1a shows cyclic voltammograms of pTAPP films on glassy carbon electrodes in the presence of oxygen. The catalytic peak in the solid blue curve has a half wave reduction potential of -370 mV vs. Ag/AgCl. The significant overpotential for oxygen reduction with pTAPP films encouraged us to look at pCoTAPP films as shown in Figure 5.1b. pCoTAPP showed a significant reduction in the overpotential for oxygen reduction, with a half-wave reduction potential of -50 mV. In addition a clean glassy carbon electrode and a clean glassy carbon electrode which was treated with Co^{2+} solution identically to the metallation of pTAPP were also tested for ORR. The glassy carbon electrode and the glassy carbon electrode treated with cobalt have significantly later onset potentials than the pTAPP and pCoTAPP electrodes and showed significantly less activity at identical potentials.

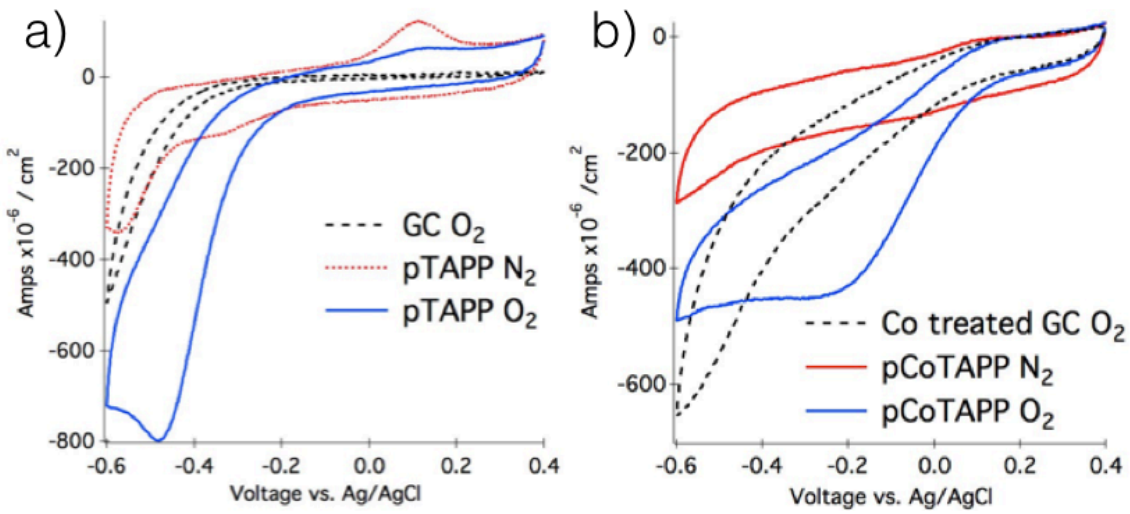

Figure 5.1 Oxygen reduction at glassy carbon (GC) electrodes coated with pTAPP (a) and pCoTAPP (b) taken in aqueous solutions at pH 4 with a scan rate of 100 mV/s. The GC electrode in (b) was treated identically to the metallation procedure of pCoTAPP.

In order to determine the over-potential under identical conditions, samples were also compared to the catalysis peak with a platinum electrode. Currently commercial polymer electrolyte membrane fuel cells use Pt/C electrodes for the oxygen reduction electrode. In this system platinum works as the catalyst and the carbon support network is used to keep the amount of platinum as low as possible. Testing a platinum electrode should give us a benchmark for the potential desired for catalytic systems. Figure 5.2 shows O_2 reduction at four different electrodes including glassy carbon (black), pCoTAPP on glassy carbon (GC) (blue), pTAPP on glassy carbon (red), and a platinum electrode (green) all at pH 3. Platinum shows a half-wave reduction potential of +0.34 V vs. Ag/AgCl, while glassy carbon has a half-wave reduction potential of -0.58 V vs.

Ag/AgCl. The difference of 0.92 V is due to glassy carbon's poor catalytic activity and shows why many electrochemists use GC electrodes to study the catalytic behavior of many reactions. A GC electrode coated with pCoTAPP shows a half-wave reduction potential of -0.05 V vs. Ag/AgCl at pH 3, indicating that there is still an overpotential of 0.39 V as compared to the Pt electrode. pTAPP shows a half-wave reduction potential of +0.4 V indicating an overpotential of 0.74 V.

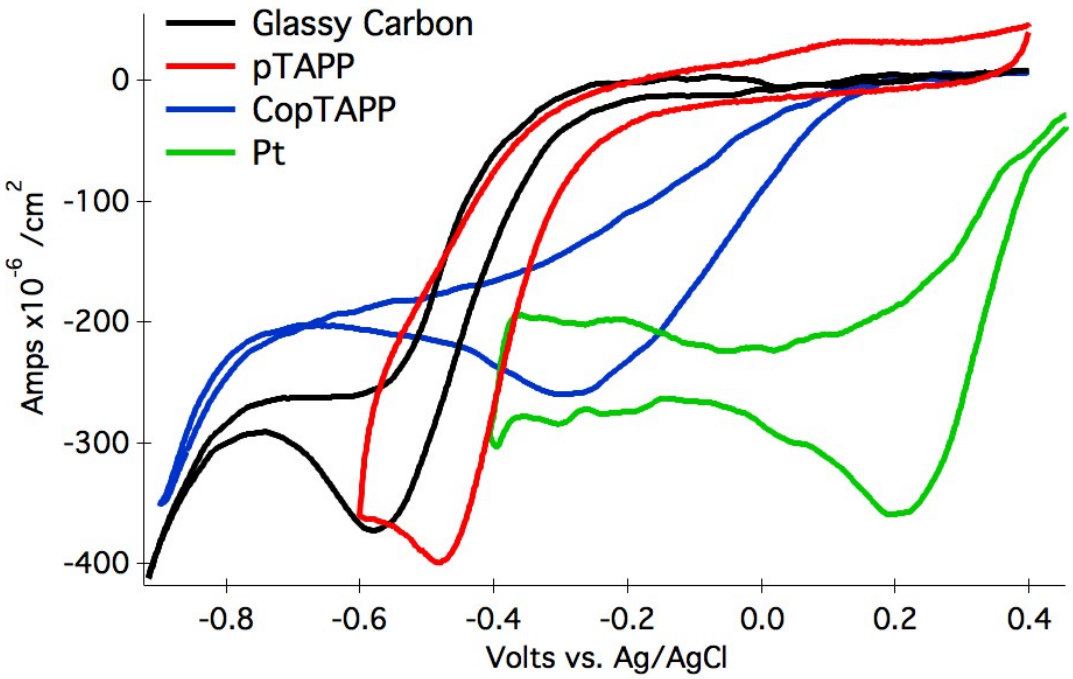

Figure 5.2 CVs of oxygen reduction at four electrodes in pH 3 acetate buffer. All curves were run at 20 mV/s in a O_2 saturated solution (approx. 1.0 mM). GC electrode is in black, pCoTAPP coated on GC is in blue, pTAPP on GC is red, and Pt is in green. Currents were normalized to an electrode size of 1 cm^2.

5.2 Electrocatalytic Testing with Linear Sweep Voltammetry

A common method to determine the number of electrons transferred electrocatalytically is the rotating disk electrode (RDE). RDE experiments are performed by rotating the working electrode at varied speeds in order to clarify the diffusion limitations associated with typical CV experiments.(*86*)(*120*) By rotating a circular electrode around the center of the active surface, solvent is drawn towards the electrode and flung outward towards the edges (Figure 5.3). The flow of electrolyte and electroactive species allows diffusion-limiting currents to be associated with the speed at which the working electrode is rotated. This permits distinguishing the mass transport limitations associated with current from the experimental catalytic data.

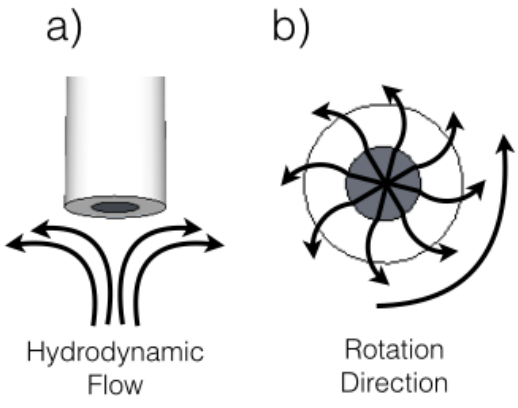

ω	X_D (mm)
50	1
200	0.5
800	0.3
1600	0.2

Figure 5.3 a) RDE-induced hydrodynamic flow of solution towards and away from the electrode caused by rotation. b) Hydrodynamic flow of electrolyte viewed from the electrode surface and as a function of the direction of rotation of the RDE. c) Stationary diffusion layer (X_D) at the electrode surface which is a function of the rotation speed (ω). The table shows X_D values in mm from the surface of the electrode in an aqueous system saturated with oxygen. (*86*)(*120*)

Typical linear sweep voltammograms (LSV) obtained at an RDE are analyzed using the Koutecky-Levich equation (Equation 5.1). Here i is the limiting current at a designated overpotential, i_K is the heterogeneous modified electrode rate constant which represents the current without any mass transfer limitations, n is the number of electrons transferred at the designated overpotential to the substrate, F is Faraday's constant, A is the area of the electrode, D_S is the substrate diffusion coefficient, ω is the rotation speed of the electrode, ν is the kinematic viscosity, and C_S is the concentration of substrate in the bulk electrolyte. A common way to solve the Koutecky-Levich equation is to make a plot of the inverse of the current vs. the inverse of the square root of the rotation speed.

This plot, termed a Koutecky-Levich plot, should be linear and allows the extrapolation of the data to infinite diffusion, at which i_K can be determined and all other parameters can be solved.

$$\frac{1}{i} = \frac{1}{i_K} + \frac{1}{0.62nFAD_S^{2/3}\omega^{1/2}\upsilon^{-1/6}C_S} \qquad \text{Eq. 5.1}$$

In order to gain the most accurate results using an RDE and Koutecky-Levich analysis, the polymer film should be as close as possible to a 2D structure. As such, thin films were formed on the GC RDE electrode using short polymerization times. From the data plotted in Figure 5.4, the y intercept determines that $1/i_K$ is 0.52 and thus i_K, the heterogeneous rate constant, is 1.92 mA. This is representative of the current that can be achieved in the absence of any mass transfer effects and with the concentration of oxygen remaining at the bulk concentration. Which is equivalent to the current that would flow with only kinetic limitations. With i_K determined the rest of the equation parameters can be solved.

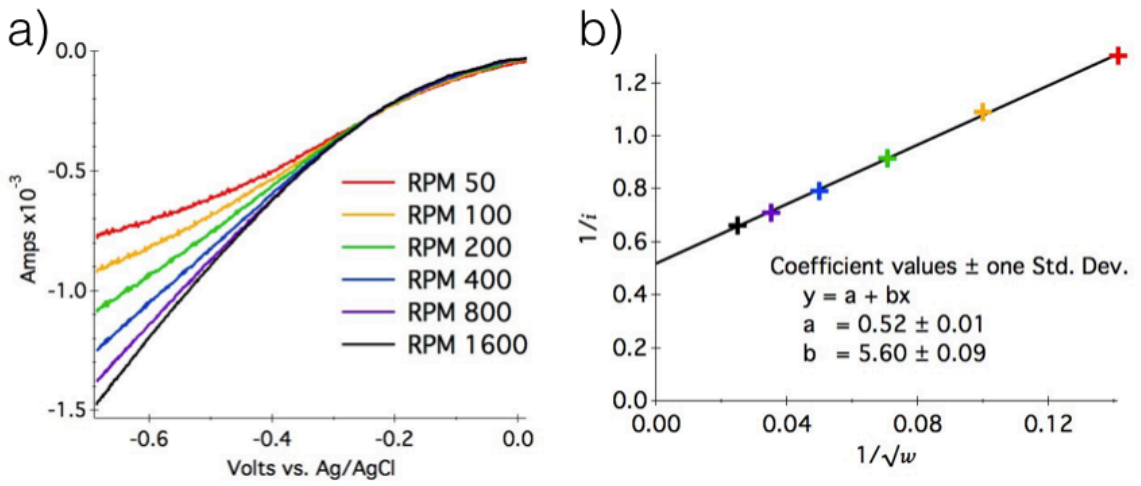

Figure 5.4 a) RDE LSVs of thin pCoTAPP films in aqueous solution at pH 3 buffered with 0.2 M acetate saturated with oxygen. b) Koutecky-Levich plot of the limiting currents from RDE LSVs at 0.7 V vs. Ag/AgCl shown. The color of the +-markers in the Koutecky-Levich plot on the right correlate with the color of the RDE experiments on the left.

Since oxygen has a diffusion coefficient (D_s) of approximately 1.9 x 10^{-4} cm^2/s,(*86*) the kinetic viscosity (ν) of water is approximately 0.01 cm^2/s(*121*) and the solubility of O_2 in a saturated aqueous solution is approximately 1.0 mM(*120*) we calculate the number of electrons transferred at an overpotential of between 0.55 and 0.7 V using equation 5.1. Table 5.1 shows the calculated number of electrons transferred (η) at several potentials, all close to two electrons. A two-electron transfer predicts the creation of H_2O_2 as the main product. In comparison, if a four-electron transfer was seen, the direct reduction of O_2 to water would be predicted, and if a single electron transfer was seen, then superoxide would have been the predicted product. Often the numbers

derived from Koutecky-Levich plots contain considerable more variability. This may be an indicator that pCoTAPP is a very specific catalyst and only catalyzes the two-electron reduction of O_2. However other reactions that are also two-electron transfers would not be differentiated. In order to test how specific the reaction is for H_2O_2, the Faradaic efficiency will be determined in the next section.

Table 5.1 Calculation of the number of electrons transferred during catalysis at various potentials vs. Ag/AgCl using pCoTAPP.

	Bias Potential vs. Ag/AgCl				
	0.6 V	0.65 V	0.7 V	0.75 V	Avg. n
Number of e^- Transferred (n)	2.2	2.1	2.0	1.9	2.0

Once thin films of pCoTAPP have proven catalytic for H_2O_2, by testing thicker films on RDEs it can be determined where the reaction is taking place in the polymeric system. Electroactive polymer catalysts can be thought of as a 3D matrix with immobilized catalysts imbedded throughout the film. Typically the polymer is optimized for conductivity at an appropriate potential to give electrons to the catalyst. This allows for optimal use of the large surface area that polymers can provide to give good substrate diffusion to a large number of imbedded catalysts. Lyon(*86*) as well as Albery and Hillman(*122*) define six areas, termed reaction zones, in which an electroactive polymer

film with immobilized catalysts can show catalytic activity. Figure 5.5 shows four of the six cases for which pCoTAPP was able to be classified and highlights the area of the film in which the catalysis takes place. Thin films of the type studied in Figure 5.4 fall into case 2.

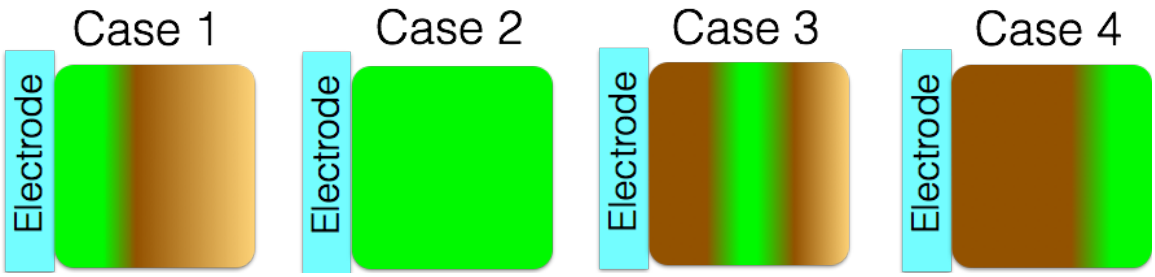

Figure 5.5 Four reaction zones as classified by Lyons.(*86*) Green indicates the region of the polymer where the catalytic reaction is taking place while brown indicates inactive regions of the polymer.

To determine the active catalytic area in the film, the thickness and thus the total surface area of the film can be varied and retested using the RDE. Figure 5.6 defines the relevant processes in a systematic fashion, enabling a better understanding of how RDE experiments with thicker films can isolate the reaction area of the film.

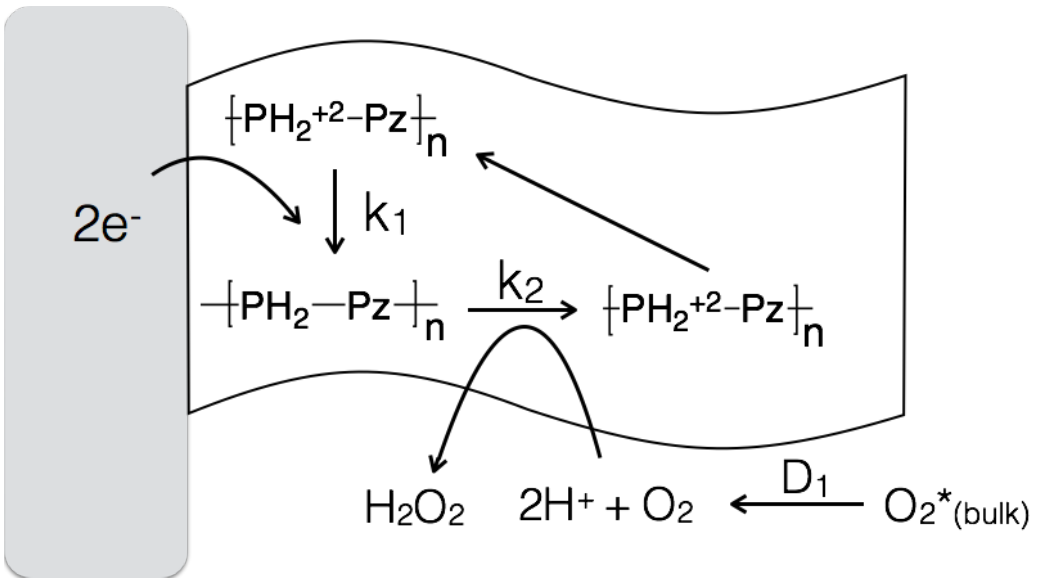

Figure 5.6 Schematic diagram of reaction processes necessary for catalysis within the film, where -[-PH_2^{+2}-Pz-]-$_n$ represents an oxidized polymer unit and -[-PH_2-Pz-]-$_n$ represents a reduced polymer unit.

Considering that the reaction of O_2 to H_2O_2 is a reduction reaction, pTAPP or pCoTAPP must be in a reduced form for catalytic activity, represented by -[-PH_2-Pz-]-$_n$. This brings about two reactions defined in equations 5.1 and 5.2.

$$\left[PH_2^{+2}-Pz\right]_n + 2e^- \xrightarrow{k_1} \left[PH_2-Pz\right]_n \qquad \text{Eq. 5.1}$$

$$\left[PH_2-Pz\right]_n + O_2 + 2H^+ \xrightarrow{k_2} \left[PH_2^{+2}-Pz\right]_n + H_2O_2 \qquad \text{Eq. 5.2}$$

Rate constant k_1 is a function of applied voltage (*E*) because it is related to the rate of charge transfer from the electrode to the polymer as well as the electronic

conductivity through the film. k_2 represents of the rate constant of the catalytic reaction throughout the film. D_1 is related to the diffusion of oxygen into the polymer pores and reaching the catalytic centers of the polymer. It can be seen that the overall catalytic rate can be limited by either k_1 or D_1 and that we can define the rate of each of the reactions involved as R_1 and R_2 in Equations 5.3 and 5.4.

$$R_1 = k_1(E)\ [\text{—}PH_2^{+2}\text{—}Pz\text{—}]_n \qquad \text{Eq. 5.3}$$

$$R_2 = k_2[\text{—}PH_2\text{—}Pz\text{—}]_n\ [O_2]\ [H^+]^2 \qquad \text{Eq. 5.4}$$

Finally from chapter 3 it was determined that pTAPP films are most conductive when they are in a mixed redox state where the numbers of oxidized units are equal to the numbers of reduced units. Since it is proposed that the reduced form of pTAPP is needed to reduce O_2 to H_2O_2 and in the process the oxidized form is created, and the reduced form is regenerated from the electrode in Equation 5.1, this means that when R_1 is equal to R_2, pTAPP will stay in its most conductive form as the balance between oxidized and reduced units is maintained. This will allow the highest catalytic efficiency as the greatest number of catalytic sites within the film will be active. Setting R_1 and R_2 equal to each other is shown in equation 5.5.

$$k_1(E)\ [\text{—}PH_2^{+2}\text{—}Pz\text{—}]_n = k_2\ [\text{—}PH_2\text{—}Pz\text{—}]_n\ [O_2]\ [H^+]^2 \qquad \text{Eq. 5.5}$$

From Equation 5.5 we see that by modifying the potential at which the electrode is poised to regenerate the reduced form of pTAPP, R_1 can be optimized and the

degradation of the catalyst will determine the end of the reaction as will be seen in section 5.4. Before that we will use thick films of pCoTAPP and the limiting rates of diffusion and electron transfer to to classify the reaction area of the films based on the overall rate R_2.(*86*)

Thicker films of pCoTAPP show identical limiting currents that do not vary with rotation speed as can be seen in Figure 5.7. This indicates that regardless of the rate at which O_2 reaches the surface of the polymer it is reduced before it can reach the electrodes surface. As outlined by Albery and Hillman this indicates that the reaction is occurring at the interface between the polymer film and the electrolyte (Figure 5.5, case 4).(*86*) This has many implications, most important of which is that pCoTAPP is indeed the catalytic system.

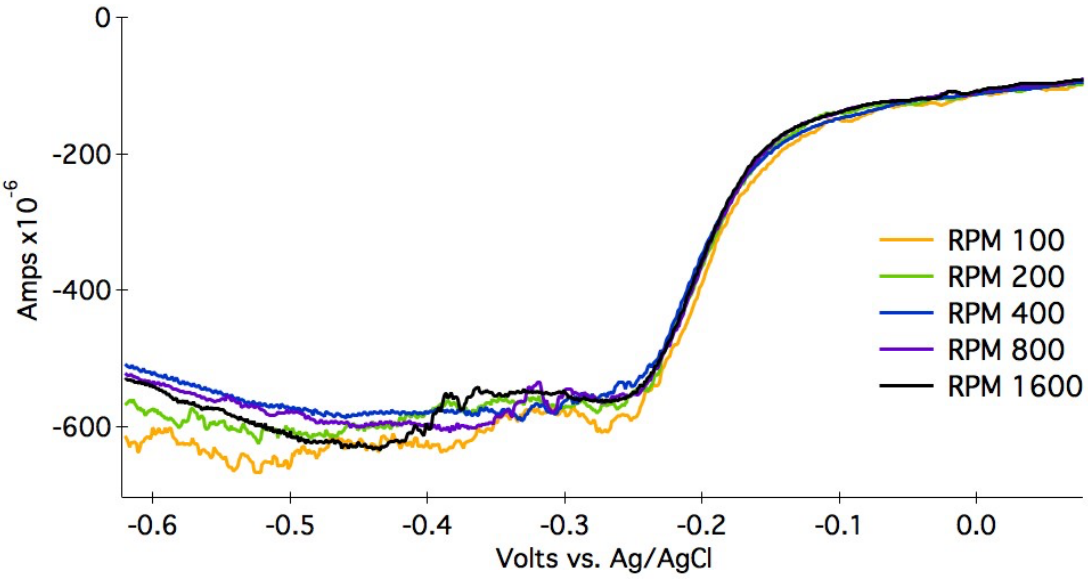

Figure 5.7 RDE LSVs of thick pCoTAPP films in aqueous solution at pH 3 buffered with 0.2 M acetate saturated with oxygen.

RDE voltammetry is a useful technique that allows the determination of a purely kinetic catalysis by isolating diffusional parameters. Using an RDE with a glassy carbon electrode it has been shown that pCoTAPP thin films fall in Lyon's case 2 and largely facilitate a two-electron transfer, significant of producing H_2O_2. In addition, thicker pCoTAPP films can be classified in Lyon's case 4 which clearly identified that the polymer film is doing the catalysis and not the electrode. Knowing the polymer is the catalytic system, determining its ability to use light as an energy source, and determining its efficiency will indicate its usefulness as a photocatalyst.

5.3 Photocatalytic Testing of pTAPP Films

With films showing good electrocatalytic behavior for the reduction of oxygen to hydrogen peroxide, photocatalytic experiments could be performed. Photocatalysis can be considered much more difficult with a system such as pTAPP and pCoTAPP as the conductivity of the system indicates a small band gap. This in turn suggests that there will also be very short excited state lifetimes. Low-energy excited states are typically considered undesirable for photocatalysis as the excited state electrons are needed to overcome the activation energy of the reaction. Short-lived excited states may not exist long enough to encounter reactants; short-lived excited states often show low photocatalytic turnover number and turnover frequency. Furthermore, when excited states are forced to recombine, photosensitizers typically begin to degrade.

5.3.1 Photoresponse of pTAPP and pCoTAPP

pTAPP and pCoTAPP films show an increase in current when under illumination, i.e., a photoresponse. This was first determined by running cyclic voltammograms under dark and illuminated conditions as shown in Figure 5.8. Photoresponses can be measured in different ways including a decrease in the resistivity of the material or increased activity of redox reactions in solution, both of which were observed with pTAPP and pCoTAPP samples. Because of the difficulty in accurately measuring the decrease in resistivity of films and the interest in using pTAPP and pCoTAPP as a heterogeneous catalyst, the photoresponse as a function of redox reactions in solution was measured. In particular, the photoresponse as a function of the ORR was targeted. Measuring the photoresponse can be done in multiple ways. Cyclic voltammetry, as shown in Figure 5.8, is good for determining the range of potentials under which there is a response. Light can also be pulsed for very short durations during a CV, but this does not help show if the photoresponse can be sustained for any length of time. In order to test for both the largest photoresponse obtainable and if it is sustainable, further photoresponse testing was done at different bias potentials. Since this is a catalytic reaction which is being partially or completely driven by light absorption, it is termed a photoassisted catalysis.(*123*)

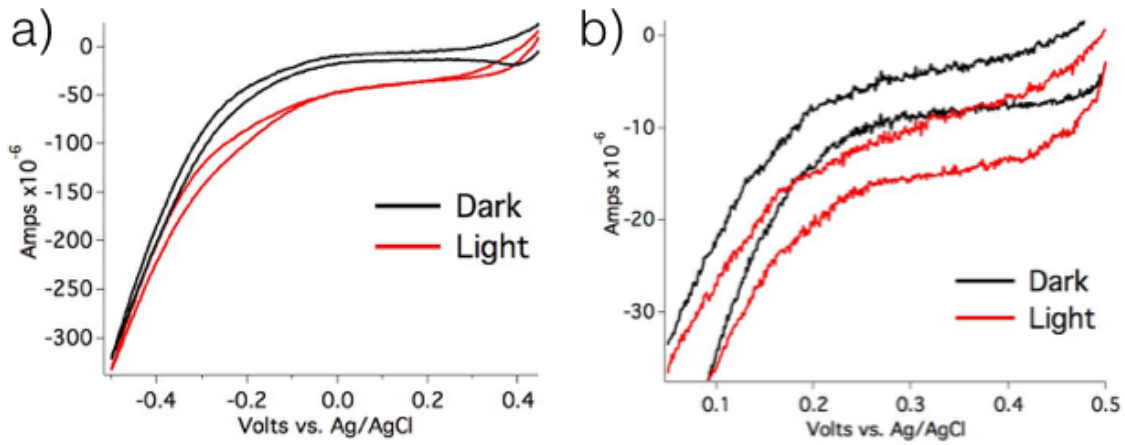

Figure 5.8 CVs of pTAPP (a) and pCoTAPP (b) in saturated O_2 solutions of 0.1 M acetate buffer at pH 3.0 with and without illumination.

Depending on conditions the photoresponse can range from almost no increase in current to around 50 μamps per cm^2 (Figure 5.9). The largest photoresponse was seen in the presence of oxygen. The photoresponse is not linked to the potential at which oxygen reduction is catalyzed by pTAPP (-0.37 V vs. Ag/AgCl). It is clear from the results that a photoexcited electron has enough energy to catalyze the reduction of oxygen to hydrogen peroxide. This may allow the reduction of oxygen even at underpotentials.

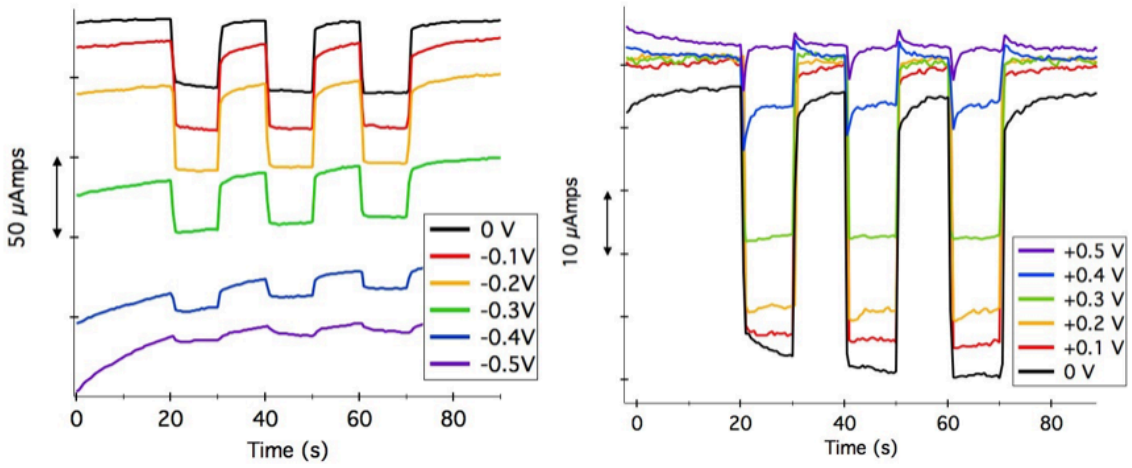

Figure 5.9 Photoresponse of 1 cm^2 pTAPP films at different bias potentials vs. Ag/AgCl. All films were tested at pH 3.0 in 0.1 M acetate buffer saturated with oxygen and under 0.8 sun illumination by an 5000 K LED lamp rated for 500 lumens. The system was allowed to equilibrate for 30 seconds before the light was turned on for 10 second intervals starting at 20, 40 and 60 seconds. The bias voltage is vs. Ag/AgCl and the counter electrode was a Pt coil electrode.

The photoresponse linked closely with the band gap of the material. As can be seen in Figure 5.9 the photoresponse is basically absent when the film is at potentials near +0.5V to around -0.5 V. This corresponds closely with the oxidation and reduction potentials for pTAPP determined by cyclic voltammetry in Chapter 3.2. This clearly shows that the electrons are being photoexcited into the lowest occupied molecular orbital (LUMO) of the film at which point they have enough energy to reduce oxygen in solution. If the potential bias applied is not within the band gap then the electrons are

either not excited into the LUMO of the polymer or the LUMO of the polymer is already filled, in the latter case electrocatalysis takes place.

The photoresponse of pCoTAPP films can be seen in Figures 5.10 and 5.11. Here even when the film was in pH 3 acetate buffer saturated with argon, a photoresponse was seen. This indicates that there are solution species which pCoTAPP is passing electrons to other than oxygen. This may also be indicative that pCoTAPP will be a less specific catalyst as compared with pTAPP. Figure 5.10 shows the photoresponse of pCoTAPP in an argon atmosphere. pCoTAPP shows a maximum photoresponse of approximately 5 μAmps in an argon atmosphere between potentials of +0.1 V and -0.6 V vs. Ag/AgCl.

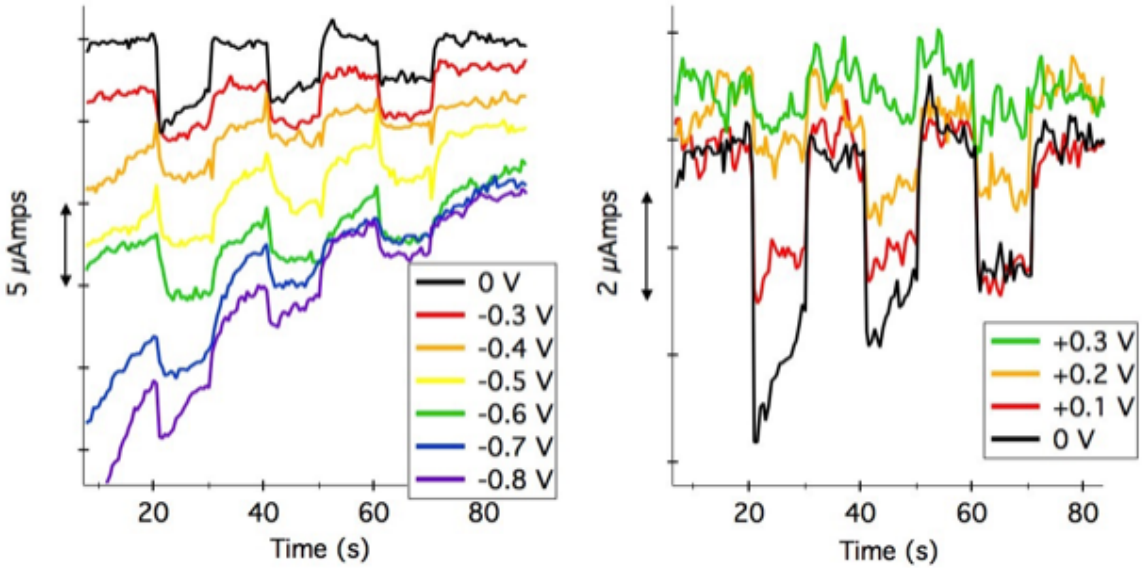

Figure 5.10 Photoresponse of 1 cm^2 pCoTAPP films at different biases vs Ag/AgCl. All films were tested at pH 3.0 in 0.1 M acetate buffer saturated with argon and under 0.8 sun illumination by a 5000 K LED lamp rated for 500 lumens. The system was allowed to equilibrate for 30 seconds before the light was turned on for 10 second intervals starting at 20, 40 and 60 seconds. The bias voltage is vs. Ag/AgCl and the counter electrode was a Pt coil electrode.

When pCoTAPP films are placed in a solution saturated with oxygen, the photoresponse increases significantly. This indicates that pCoTAPP films are more readily able to pass electrons into solution with oxygen as a substrate. The maximum photoresponse of pCoTAPP is approximately 10 μAmps, doubling the amount of current seen in an argon atmosphere. Surprisingly this is only approximately one fifth of the photoresponse seen with pTAPP under the same conditions. Apparently pTAPP is a better photocatalyst than pCoTAPP for the reduction of oxygen to hydrogen peroxide.

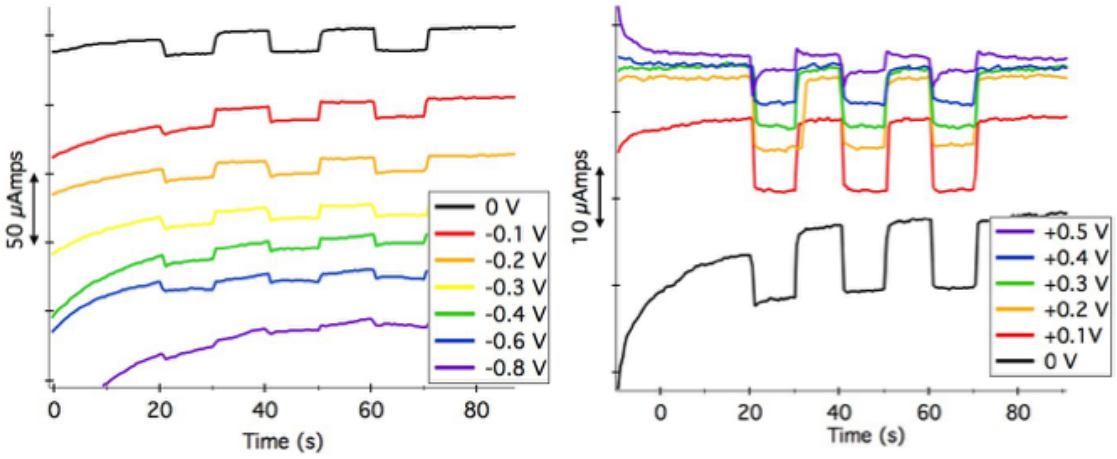

Figure 5.11 Photoresponse of 1 cm^2 pCoTAPP films at different biases vs Ag/AgCl. All films were tested at pH 3.0 in 0.1 M acetate buffer saturated with oxygen and under 0.8 sun illumination by a 5000 K LED lamp rated for 500 lumens. The system was allowed to equilibrate for 30 seconds before the light was turned on for 10 second intervals starting at 20, 40 and 60 seconds. The bias voltage is vs. Ag/AgCl and the counter electrode was a Pt coil electrode.

The meaning of a photoresponse in relation to band gap theory is shown in Figure 5.12. In this photocatalytic system, electrons are being excited by light from the HOMO to the LUMO and leaving the LUMO to perform the ORR. The electrons holes in the HOMO are filled by electrons from the electrode. Then the process can repeat reducing oxygen to hydrogen peroxide. Photoelectrocatalysts such as pTAPP and pCoTAPP may prove useful in future applications in order to lower the overpotential of reactions. Lower overpotentials lead to less energy loss during catalysis.

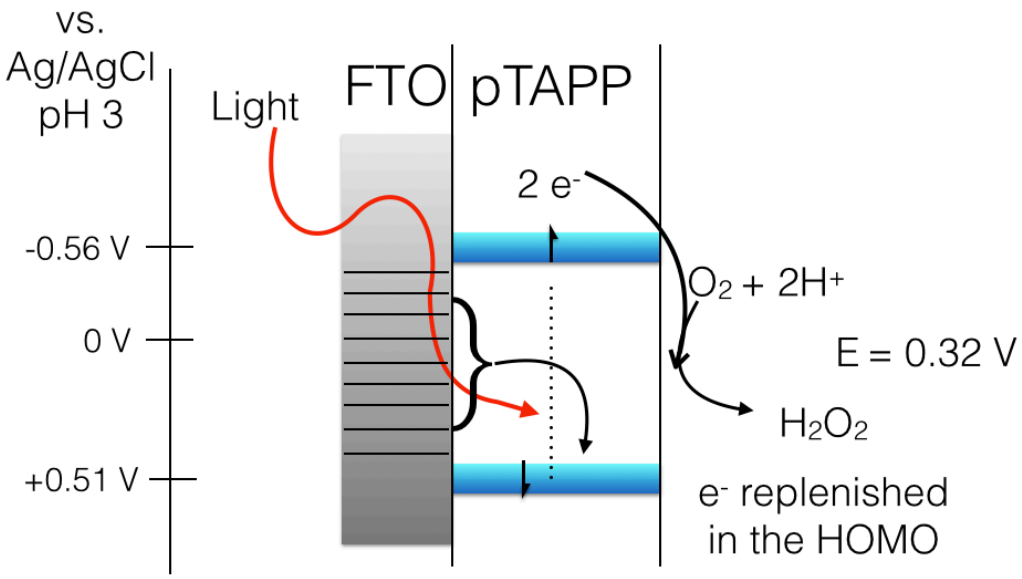

Figure 5.12 Band gap diagram showing the photoresponse behaviors in catalyzing the reduction of oxygen by pTAPP or pCoTAPP.

5.4 Catalytic Efficiency

In order to test the catalytic efficiency, the number of electrons transferred into solution and the number of catalytic sites available will need to be compared to the quantity of H_2O_2 produced. Using pTAPP and pCoTAPP samples on FTO glass in a cuvette the systems were measured at different biases vs. Ag/AgCl while being irradiated with light. It is important to note that FTO can also show catalytic activity for the ORR with a turn-on bias potential of -0.1 V. In order to isolate reduction of O_2 due to FTO from reduction due to the polymers, all results reported are at bias potentials at 0 V and more positive vs. Ag/AgCl.

pTAPP was tested for catalytic efficiency at a range of potentials between 0 V to +0.4 V vs. Ag/AgCl. The catalytic activity between 0 V to +0.2 V vs. Ag/AgCl was found to be independent of the potential as was suggested by the photoresponse experiments. The catalytic activity at +0.3 V was lower and variable depending on the sample, and at +0.4 V no reduction of O_2 was detectable. It was concluded that the catalytic activity at these potentials is dependent on the irradiance. pTAPP samples tested without irradiation at these potentials show no activity towards the production of H_2O_2 over a one-hour time period

By quantitating the amount of pTAPP deposited from solution during polymerization the number of monomeric units of TAPP in a pTAPP film can be calculated. Using an identical polymerization method, seven samples of pTAPP were electropolymerized and all electropolymerizations were integrated for the quantity of pTAPP deposited. Over the seven polymerizations an average of 60 ± 6 nmols of TAPP was oxidized in solution most of which can be assumed to have been deposited on the electrode. Using this quantity of monomeric units and assuming each monomeric unit is catalytic, the turnover numbers (TON) and turnover frequencies (TOF) for pTAPP catalysis can be determined. TON is the number of products produced divided by the number of catalysts in the system. TOF is simply the TON divided by a unit of time. In all experiments the TOFs are divided by the number of minutes the system has been in solution under illumination with bubbling oxygen.

Regardless of the bias potential applied pTAPP samples maintained a relatively constant TON. From seven of the samples tested at bias potentials between 0 V to +0.2 V vs. Ag/AgCl the average TON was 5.6 ± 1. Figure 5.14a shows TONs over time for samples at +0.2, +0.1 and 0 V vs. Ag/AgCl.

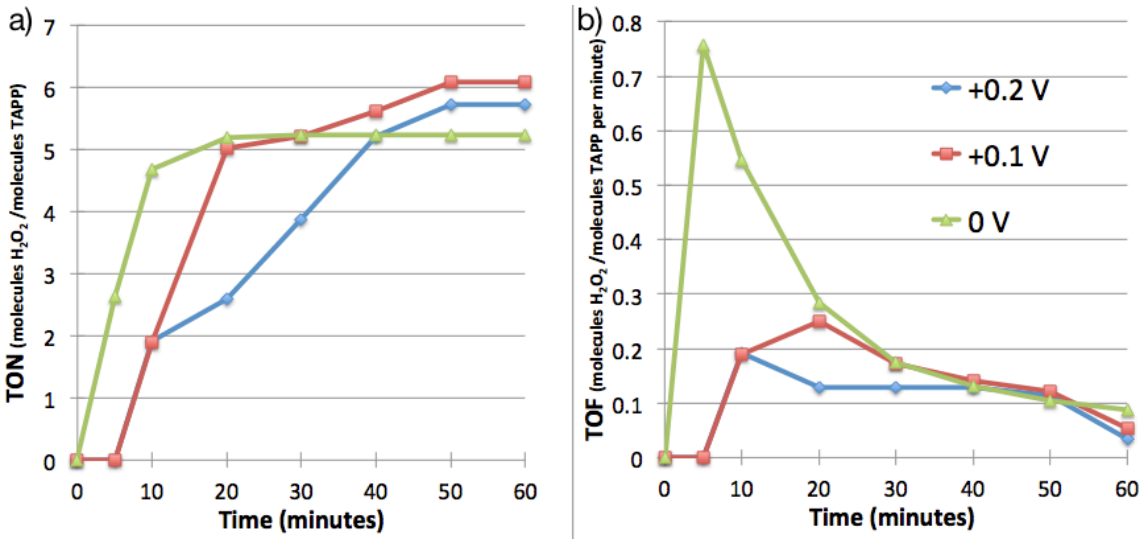

Figure 5.13 TON (a) and TOF (b) vs. time for samples of pTAPP with 2 suns illumination at bias potentials of +0.2 V (blue), +0.1 V (red), and 0 V (green) vs. Ag/AgCl. All samples tested were approximately 2 cm^2 in a cuvette with aqueous 0.1 M acetate buffer at pH 3 with a graphite counter electrode and constant O_2 bubbling.

No clear correlation was seen between the bias potential and the TOF. For samples held at positive biases vs. Ag/AgCl the average turnover frequency after ten minutes of irradiation was only 0.3 H_2O_2 per minute.

Faradaic efficiency was calculated by integrating the current passed during the ORR experiment. Current was measured using chronoamperometry for the entire

duration of the experiment. By calculating the number of moles of electrons passed and using a molar ratio of two electrons per mole of H_2O_2 the theoretical amount of H_2O_2 that could have been was determined. By dividing the number of moles of H_2O_2 produced by the theoretical number of moles the Faradaic efficiency was obtained.

Faradaic efficiency showed no correlation with bias potentials applied between 0 V to +0.2 V vs. Ag/AgCl. The average Faradaic efficiency of eight pTAPP samples tested under 2 suns irradiation after the first ten minutes was 49 percent (Figure 5.14). These results suggest that pTAPP is not a specific catalyst for the reduction of O_2 to H_2O_2. It is very possible that pTAPP also catalyzes the further reduction of H_2O_2 to H_2O.

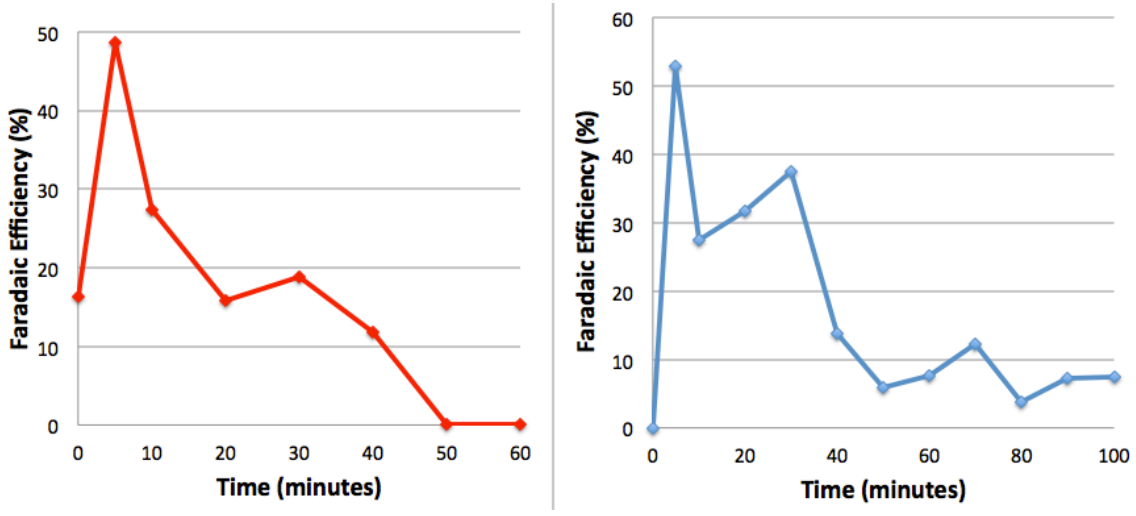

Figure 5.14 Average Faradaic efficiency over time of all samples tested for pTAPP (red) and pCoTAPP (blue).

pCoTAPP proved to be a better photoelectrocatalyst for the reduction of O_2 at the potentials tested as compared to pTAPP. The average TON for samples tested between 0 V and +0.3 V under 2 suns irradiation and saturated oxygen was 17.5 ± 4, as shown in

Figure 5.15a. pCoTAPP at 0 V vs. Ag/AgCl produces much of the H_2O_2 in the first five minutes, while at +0.3 V the TON grows steadily producing H_2O_2 over an hour. These same trends can be seen in Figure 5.15b as the TOF. The rate of production of H_2O_2 at +0.3 V vs. Ag/AgCl is steadily increasing and may not have stopped production even after one hour. This suggests the rates of R_1 and R_2, as described earlier, may have been optimized. Since +0.3 V is much higher than the -0.05 V half-wave catalytic potential determined for electrocatalysis, it is clear that pCoTAPP is driven at this potential primarily photocatalytically. Since pCoTAPP can produce H_2O_2 at +0.3 V vs. Ag/AgCl there is almost no overpotential compared to platinum or the thermodynamic potential for ORR making pCoTAPP a promising material for further study.

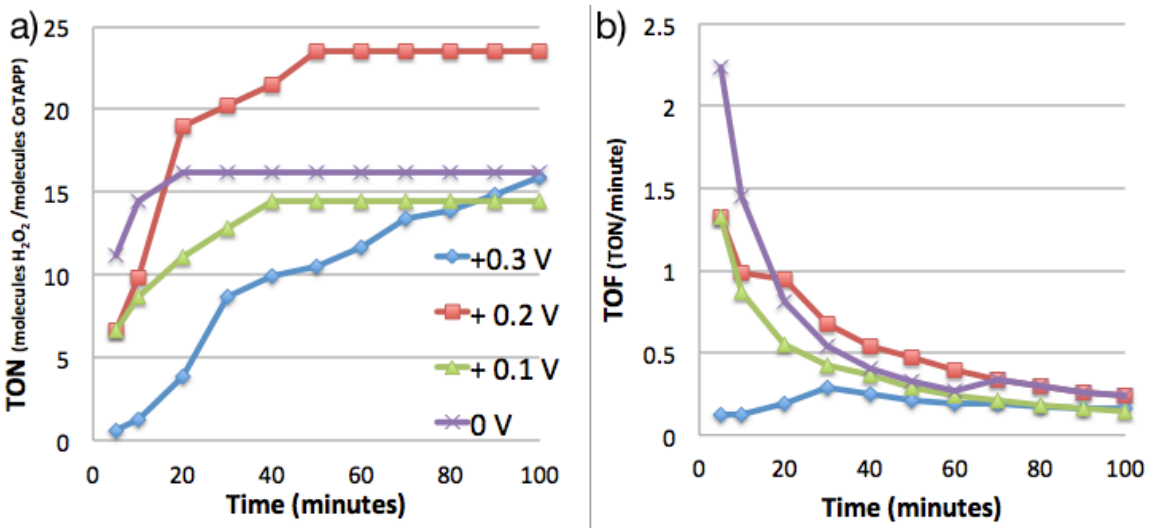

Figure 5.15 TON (a) and TOF (b) vs. time for pCoTAPP with 2 suns illumination at bias potentials of +0.3 V (blue), +0.2 V (red), +0.1 V (green), and 0 V (purple) vs. Ag/AgCl. All samples tested were approximately 2 cm^2 in a cuvette with aqueous 0.1 M acetate buffer at pH 3 with a graphite counter electrode and constant O_2 bubbling.

Faradaic efficiency for pCoTAPP was also higher than that of pTAPP with an average Faradaic efficiency through the first five minutes at 53 percent (Figure 5.14 blue). The highest Faradaic efficiency seen was just over 70 percent on samples held at 0 V and +0.1 V bias vs. Ag/AgCl and suggests the system is a good electrocatalyst for ORR. Both pTAPP and pCoTAPP pass more current than is necessary for the quantity of H_2O_2 produced, indicative of non-specific catalysis. Some of the other reactions that are likely to be occurring are the reduction of H_2O_2 to H_2O and the reduction of protons to H_2. As mentioned earlier the RDE experiments would differentiate from these reactions as both of these alternative reactions also require two electrons. The RDE experiment does rule out the four-electron transfer in which O_2 goes directly to H_2O.

Considering pCoTAPP as a photocatalyst as well as an electrocatalyst at the potentials tested two identical samples were tested for production of hydrogen peroxide under illumination and in the dark. An identical test was performed with pTAPP but without light no generation of H_2O_2 was seen. Figure 5.16 shows pCoTAPP in the light produces approximately twice as much H_2O_2 as pCoTAPP in the dark.

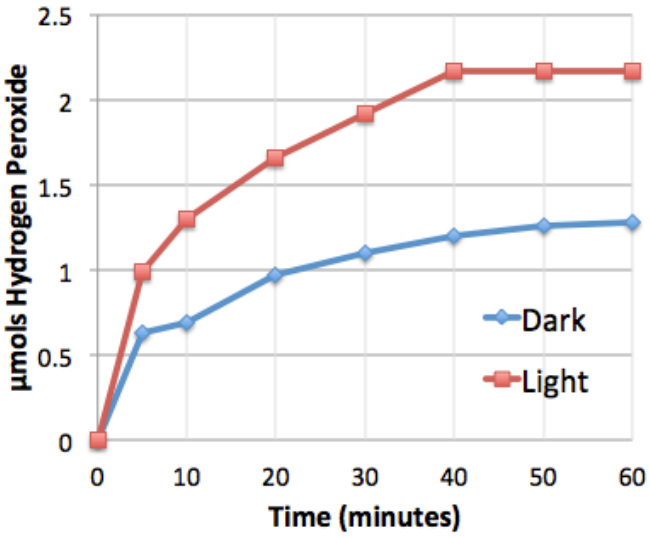

Figure 5.16 Production of H_2O_2 by pCoTAPP samples in the dark (blue) and under 2 suns irradiation (red) at +0.1 V vs Ag/AgCl in saturated oxygen at pH 3 in 0.1 M aqueous sodium acetate buffer.

Clearly both pTAPP and pCoTAPP are reducing O_2 to H_2O_2. pCoTAPP can even achieve close to the thermodynamic potential of O_2 reduction under irradiation making it a good photoelectrocatalyst. Unfortunately neither pTAPP nor pCoTAPP can achieve high Faradaic efficiencies indicating that they are non-specific catalysts. Further research needs to be done in order to increase the selective catalysis of O_2 to H_2O_2 and the TON of both systems if use for industrial purposes were to be economically feasible.

6 CONCLUSIONS

Tetra(4-aminophenyl)porphyrin (pTAPP) can be oxidatively polymerized with a variety of methods, including electropolymerization, chemical oxidation, and interfacial polymerization. pTAPP left in a mixed oxidation state was shown to have both its minimum charge transfer resistance to movement of ions in and out of the film as well as its minimum impedance to electronic conductivity in the film. The pTAPP absorbance spectrum with increased doping is similar to a hyperporphyrin and is characteristic of a two-plus charge localized on a single porphyrin unit. This strongly indicates the presence of a bipolaron on the individual porphyrin units, and thus a bipolaron conduction mechanism has been proposed. pTAPP also shows a longer wavelength near-IR absorbance which is still present upon metallation. The longer wavelength absorbance is ascribed to polarons within the film and suggests a different conduction mechanism for pCoTAPP, which does not show the characteristic bipolaron absorption.

pTAPP changes color depending on its oxidation state and therefore is a promising material for electrochromic devices. pTAPP can reversibly change color from yellow to black and thus is able to block out the majority of blue light (when yellow) all the way to all visible wavelengths including some near infrared radiation (when black).

As a summary of pTAPP redox states, changes in pH, electrochromic behavior, and its conductivity, a novel Pourbaix diagram was created which is able to show all characteristics determined for pTAPP. Pourbaix diagrams for electroactive polymers rarely appear in the literature, but we propose that they can be useful tools for the

illustration of many properties in one figure. The Pourbaix diagram of pTAPP conveniently portrays its color, redox state, and conductivity as a function of pH and potential.

pTAPP worked as a metal-free catalyst for the reduction of oxygen although more work will need to be done in order to optimize pTAPP for future use as the catalysis required a high overpotential. The catalytic reduction of O_2 by pTAPP occurs near the potential at which the phenazine linkage is reduced. This suggests that phenazine may prove to be a good ORR catalyst

pCoTAPP proved to be a better catalyst than pTAPP for the ORR. This is not surprising as similar systems have been shown to be good ORR catalysts before. pCoTAPP when irradiated performs the ORR reaction close to the thermodynamic potential of the reduction of oxygen to hydrogen peroxide. Catalysts with low overpotentials are promising systems for storage of solar energy for future use.

7 OUTLOOK

pTAPP as a polymer has now been well characterized and may prove useful as a conductor/insulator, capacitor, electrochromic or catalytic material. Organic polymers are interesting conductors as they need to be in a specific state for conduction, lending to applications in which rapid or selective switching may be useful. The large surface area of organic polymers gives them very large theoretical capacitances, so that organic polymers such as polyaniline and pTAPP may hold great potential for future supercapacitor applications.

The Pourbaix diagram created in this work is intended to encourage more researchers to create and make use of similar figures with other conductive polymers. The utility of this figure is in helping scientists and engineers find the right conductive polymers for their application. There are many aspects such as working potential range and redox properties that need to be considered when using an organic polymer as a conductive substrate for displays, solar cells, or other technology. The ability to have a single figure communicate all of the necessary parameters can be highly informative.

Electrochromic devices are of interest for a variety of uses, and the larger the range of wavelength absorption the more potential uses a system may prove to have. As pTAPP does not have a completely clear state, window coatings are not likely to be a significant application for pTAPP electrochromic properties. On the other hand the broad absorbance near 1300 nm would be useful for blocking out near IR radiation.

It has been postulated that the catalytic activity of pTAPP in oxygen reduction coincides with the reduction of the phenazine linkages. Further testing should be done in order to look at just phenazine as an ORR catalyst. Recently researchers have found N-doped carbon nanotubes to be highly efficient for oxygen reduction.(*119*) Phenazine is a simple N-containing aromatic molecule which may prove to be a good theoretical model for the mechanism by which N-doped carbon nanotubes reduce oxygen.

Further optimization may allow pCoTAPP to be a realistic way to make or harvest energy from hydrogen peroxide. Reducing oxygen without an overpotential makes it a good candidate for industrial scale production using solar irradiation as an energy source.

pTAPP and pCoTAPP are promising materials for future energy storage devices both as photocatalysts for fuel cells as well as capacitors. Hopefully the characterization performed on these systems will encourage more researchers to continue testing pTAPP and related systems for further applications.

REFERENCES

(1) Carbon dioxide passes symbolic mark. *BBC* **2013**.
(2) Climate Milestone: Earth's CO_2 Level Nears 400 ppm. http://news.nationalgeographic.com/news/energy/2013/05/130510-earth-co2-milestone-400-ppm/ (accessed October 6, 2015).
(3) Ice-Free Arctic in Pliocene, Last Time CO_2 Levels above 400 PPM: Scientific American. http://www.scientificamerican.com/article.cfm?id=ice-free-arctic-in-pliocene-last-time-co2-levels-above-400ppm (accessed October 6, 2015).
(4) Publication: Key World Energy Statistics 2014. http://www.iea.org/publications/freepublications/publication/key-world-energy-statistics-2014.html (accessed October 6, 2015).
(5) Ayres, R. U.; Warr, B. *The Economic Growth Engine: How Energy and Work Drive Material Prosperity*; Edward Elgar Publishing, 2010.
(6) Lewis, N. S.; Nocera, D. G. Powering the planet: Chemical challenges in solar energy utilization. *Proc. Natl. Acad. Sci.* **2006**, *103*, 15729–15735.
(7) Voigt, A.; Walls, B.; McKerney, M.; Bakogiannis, D.; Williams, A.; Morley, C.; Warga, R.; Bronstein, R. *Drowning in Oil: Indicators of Instability in a Low Price Environment*; American University, 2015.
(8) Wiser, R.; Bolinger, M. *2012 Wind Technologies Market Report*; Department of Energy, 2013.
(9) Fenton, J. M. *The Electrochemical Society's Interface*. Spring 2015, pp. 41–42.
(10) Marshall, M. Solar electricity is now cheaper than diesel in India. *New Sci.* **2012**, *213*, 12.
(11) Solar PV Becoming Cheaper than Gas in California? http://www.renewableenergyworld.com/rea/news/article/2011/02/solar-pv-becoming-cheaper-than-gas-in-california (accessed October 6, 2015).
(12) Kristen Ardani, Dan Seif, Robert Margolis, Jesse Morris, Carolyn Davidson, Sarah Truitt, Roy Torbert Non-Hardware ('Soft') Cost-Reduction Roadmap for Residential and Small Commercial Solar Photovoltaics, 2013-2020 **2013**.
(13) Jacobson, M. Z.; Delucchi, M. A. Providing all global energy with wind, water, and solar power, Part I: Technologies, energy resources, quantities and areas of infrastructure, and materials. *Energy Policy* **2011**, *39*, 1154–1169.
(14) Fthenakis, V.; Mason, J. E.; Zweibel, K. The technical, geographical, and economic feasibility for solar energy to supply the energy needs of the US. *Energy Policy* **2009**, *37*, 387–399.
(15) Eltawil, M. A.; Zhao, Z. Grid-connected photovoltaic power systems: Technical and potential problems—A review. *Renew. Sustain. Energy Rev.* **2010**, *14*, 112–129.
(16) Luo, C.; Banakar, H.; Shen, B.; Ooi, B.-T. Strategies to Smooth Wind Power Fluctuations of Wind Turbine Generator. *IEEE Trans. Energy Convers.* **2007**, *22*, 341–349.

(17) Farhangi, H. The path of the smart grid. *IEEE Power Energy Mag.* **2010**, *8*, 18–28.
(18) Hargreaves, T.; Nye, M.; Burgess, J. Making energy visible: A qualitative field study of how householders interact with feedback from smart energy monitors. *Energy Policy* **2010**, *38*, 6111–6119.
(19) Kuwano, Y. The PV Era is coming — the way to GENESIS. *Sol. Energy Mater. Sol. Cells* **1994**, *34*, 27–39.
(20) Greenblatt, J. B.; Succar, S.; Denkenberger, D. C.; Williams, R. H.; Socolow, R. H. Baseload wind energy: modeling the competition between gas turbines and compressed air energy storage for supplemental generation. *Energy Policy* **2007**, *35*, 1474–1492.
(21) Wald, M. L. Energy-Storage Plans Gain Ground in California. *N. Y. Times* **2014**.
(22) Will Tesla's Battery for Homes Change the Energy Market? http://www.scientificamerican.com/article/will-tesla-s-battery-for-homes-change-the-energy-market/ (accessed June 5, 2015).
(23) Jain, I. P. Hydrogen: the fuel for 21st century. *Int. J. Hydrog. Energy* **2009**, *34*, 7368–7378.
(24) Veziroğlu, T. N.; Barbir, F. Hydrogen: the wonder fuel. *Int. J. Hydrog. Energy* **1992**, *17*, 391–404.
(25) Olah, G. A. Beyond Oil and Gas: The Methanol Economy. *Angew. Chem. Int. Ed.* **2005**, *44*, 2636–2639.
(26) Walter, M. G.; Warren, E. L.; McKone, J. R.; Boettcher, S. W.; Mi, Q.; Santori, E. A.; Lewis, N. S. Solar water splitting cells. *Chem. Rev.* **2010**, *110*, 6446–6473.
(27) International Journal of Hydrogen Energy. http://www.journals.elsevier.com/international-journal-of-hydrogen-energy/ (accessed June 9, 2015).
(28) Chaubey, R.; Sahu, S.; James, O. O.; Maity, S. A review on development of industrial processes and emerging techniques for production of hydrogen from renewable and sustainable sources. *Renew. Sustain. Energy Rev.* **2013**, *23*, 443–462.
(29) Thomas, G. Overview of Storage Development: DOE Hydrogen Program. http://www1.eere.energy.gov/hydrogenandfuelcells/pdfs/storage.pdf (accessed August 24, 2015).
(30) Mikkelsen, M.; Jørgensen, M.; Krebs, F. C. The teraton challenge. A review of fixation and transformation of carbon dioxide. *Energy Environ. Sci.* **2010**, *3*, 43–81.
(31) Yin, X.; Moss, J. R. Recent developments in the activation of carbon dioxide by metal complexes. *Coord. Chem. Rev.* **1999**, *181*, 27–59.
(32) Campos-Martin, J. M.; Blanco-Brieva, G.; Fierro, J. L. G. Hydrogen peroxide synthesis: an outlook beyond the anthraquinone process. *Angew. Chem. Int. Ed Engl.* **2006**, *45*, 6962–6984.

(33) Fukuzumi, S.; Yamada, Y.; Karlin, K. D. Hydrogen peroxide as a sustainable energy carrier: Electrocatalytic production of hydrogen peroxide and the fuel cell. *Electrochimica Acta* **2012**, *82*, 493–511.
(34) Disselkamp, R. S. Can aqueous hydrogen peroxide be used as a stand-alone energy source? *Int. J. Hydrog. Energy* **2010**, *35*, 1049–1053.
(35) Mekhilef, S.; Saidur, R.; Safari, A. Comparative study of different fuel cell technologies. *Renew. Sustain. Energy Rev.* **2012**, *16*, 981–989.
(36) Steele, B. C. H.; Heinzel, A. Materials for fuel-cell technologies. *Nature* **2001**, *414*, 345–352.
(37) Jena, P. Materials for Hydrogen Storage: Past, Present, and Future. *J. Phys. Chem. Lett.* **2011**, *2*, 206–211.
(38) Schlapbach, L.; Züttel, A. Hydrogen-storage materials for mobile applications. *Nature* **2001**, *414*, 353–358.
(39) Li, X.; Faghri, A. Review and advances of direct methanol fuel cells (DMFCs) part I: Design, fabrication, and testing with high concentration methanol solutions. *J. Power Sources* **2013**, *226*, 223–240.
(40) Leung, P.; Li, X.; León, C. P. de; Berlouis, L.; Low, C. T. J.; Walsh, F. C. Progress in redox flow batteries, remaining challenges and their applications in energy storage. *RSC Adv.* **2012**, *2*, 10125–10156.
(41) Skyllas-Kazacos, M.; Chakrabarti, M. H.; Hajimolana, S. A.; Mjalli, F. S.; Saleem, M. Progress in Flow Battery Research and Development. *J. Electrochem. Soc.* **2011**, *158*, R55–R79.
(42) Huskinson, B.; Marshak, M. P.; Suh, C.; Er, S.; Gerhardt, M. R.; Galvin, C. J.; Chen, X.; Aspuru-Guzik, A.; Gordon, R. G.; Aziz, M. J. A metal-free organic-inorganic aqueous flow battery. *Nature* **2014**, *505*, 195–198.
(43) Van Noorden, R. The rechargeable revolution: A better battery. *Nature* **2014**, *507*, 26–28.
(44) Simon, P.; Gogotsi, Y. Materials for electrochemical capacitors. *Nat. Mater.* **2008**, *7*, 845–854.
(45) Barringer, F. Warren Buffett's Big Bet on Renewables in Nevada. *N. Y. Times* **2014**.
(46) Kato, S.; Jung, J.; Suenobu, T.; Fukuzumi, S. Production of hydrogen peroxide as a sustainable solar fuel from water and dioxygen. *Energy Environ. Sci.* **2013**, *6*, 3756–3764.
(47) Kudo, A.; Miseki, Y. Heterogeneous photocatalyst materials for water splitting. *Chem. Soc. Rev.* **2008**, *38*, 253–278.
(48) Choudhury, N. A.; Raman, R. K.; Sampath, S.; Shukla, A. K. An alkaline direct borohydride fuel cell with hydrogen peroxide as oxidant. *J. Power Sources* **2005**, *143*, 1–8.
(49) Bettelheim, A.; Ozer, D.; Harth, R.; Ydgar, R. Dioxygen reduction and hydrogen peroxide dismutation using electropolymerized bilayers of cobalt + manganese tetrakis(o-aminophenyl)porphyrins. *J. Electroanal. Chem. Interfacial Electrochem.* **1990**, *281*, 147–61.

(50) Mokrushina, A. V.; Heim, M.; Karyakina, E. E.; Kuhn, A.; Karyakin, A. A. Enhanced hydrogen peroxide sensing based on Prussian Blue modified macroporous microelectrodes. *Electrochem. Commun.* **2013**, *29*, 78–80.
(51) Wang, B. Recent development of non-platinum catalysts for oxygen reduction reaction. *J. Power Sources* **2005**, *152*, 1–15.
(52) Nie, Y.; Li, L.; Wei, Z. Recent advancements in Pt and Pt-free catalysts for oxygen reduction reaction. *Chem. Soc. Rev.* **2015**, *44*, 2168–2201.
(53) Mase, K.; Ohkubo, K.; Fukuzumi, S. Efficient Two-Electron Reduction of Dioxygen to Hydrogen Peroxide with One-Electron Reductants with a Small Overpotential Catalyzed by a Cobalt Chlorin Complex. *J. Am. Chem. Soc.* **2013**, *135*, 2800–2808.
(54) Song, E.; Shi, C.; Anson, F. C. Comparison of the Behavior of Several Cobalt Porphyrins as Electrocatalysts for the Reduction of O_2 at Graphite Electrodes. *Langmuir* **1998**, *14*, 4315–4321.
(55) Han, L.; Guo, S.; Wang, P.; Dong, S. Light-Driven, Membraneless, Hydrogen Peroxide Based Fuel Cells. *Adv. Energy Mater.* **2015**, *5*.
(56) Yamada, Y.; Fukunishi, Y.; Yamazaki, S.; Fukuzumi, S. Hydrogen peroxide as sustainable fuel: electrocatalysts for production with a solar cell and decomposition with a fuel cell. *Chem. Commun.* **2010**, *46*, 7334–7336.
(57) Milgrom, L. R. *The Colours of Life: An Introduction to the Chemistry of Porphyrins and Related Compounds*; 1 edition.; Oxford University Press: Oxford ; New York, 1997.
(58) Kadish, K.; Smith, K. M.; Guilard, R. *The Porphyrin Handbook, Volumes 1-10*; 1 edition.; Academic Press, 1999.
(59) Day, N. U.; Wamser, C. C.; Walter, M. G. Porphyrin polymers and organic frameworks. *Polym. Int.* **2015**, *64*, 833–857.
(60) Walter, M. G.; Rudine, A. B.; Wamser, C. C. Porphyrins and phthalocyanines in solar photovoltaic cells. *J. Porphyr. Phthalocyanines* **2010**, *14*, 759–792.
(61) Walter, M. G.; Wamser, C. C. Synthesis and Characterization of Electropolymerized Nanostructured Aminophenylporphyrin Films. *J. Phys. Chem. C* **2010**, *114*, 7563–7574.
(62) Li, W.; Wamser, C. C. Synthesis and Characterization of Interfacially Polymerized Films of Tetraphenylporphyrin Derivatives. *Langmuir* **1995**, *11*, 4061–4071.
(63) Day, N. U.; Walter, M. G.; Wamser, C. C. Preparations and Electrochemical Characterizations of Conductive Porphyrin Polymers. *J. Phys. Chem. C* **2015**, *119*, 17378–17388.
(64) Huang, J.; Kaner, R. B. A General Chemical Route to Polyaniline Nanofibers. *J. Am. Chem. Soc.* **2004**, *126*, 851–855.
(65) Huang, J.; Virji, S.; Weiller, B. H.; Kaner, R. B. Polyaniline Nanofibers: Facile Synthesis and Chemical Sensors. *J. Am. Chem. Soc.* **2003**, *125*, 314–315.

(66) Tran, H. D.; D'Arcy, J. M.; Wang, Y.; Beltramo, P. J.; Strong, V. A.; Kaner, R. B. The oxidation of aniline to produce "polyaniline": a process yielding many different nanoscale structures. *J. Mater. Chem.* **2011**, *21*, 3534–3550.
(67) Mathew, R.; Mattes, B. R.; Espe, M. P. A solid state NMR characterization of cross-linked polyaniline powder. *Synth. Met.* **2002**, *131*, 141–147.
(68) Inamo, M.; Funahashi, S.; Tanaka, M. Kinetics of the reaction of hydrogen peroxide with some oxotitanium (IV) complexes as studied by a high-pressure stopped-flow technique. *Inorg. Chem.* **1983**, *22*, 3734–3737.
(69) Matsubara, C.; Kawamoto, N.; Takamura, K. Oxo[5, 10, 15, 20-tetra(4-pyridyl)porphyrinato]titanium(IV): an ultra-high sensitivity spectrophotometric reagent for hydrogen peroxide. *The Analyst* **1992**, *117*, 1781.
(70) Weinkauf, J. R.; Cooper, S. W.; Schweiger, A.; Wamser, C. C. Substituent and Solvent Effects on the Hyperporphyrin Spectra of Diprotonated Tetraphenylporphyrins. *J. Phys. Chem. A* **2003**, *107*, 3486–3496.
(71) Wang, C.; Wamser, C. C. Hyperporphyrin Effects in the Spectroscopy of Protonated Porphyrins with 4-Aminophenyl and 4-Pyridyl Meso Substituents. *J. Phys. Chem. A* **2014**, *118*, 3605–3615.
(72) Rudine, A. B.; DelFatti, B. D.; Wamser, C. C. Spectroscopy of protonated tetraphenylporphyrins with amino/carbomethoxy substituents: hyperporphyrin effects and evidence for a monoprotonated porphyrin. *J. Org. Chem.* **2013**, *78*, 6040–6049.
(73) Ojadi, E. C. A.; Linschitz, H.; Gouterman, M.; Walter, R. I.; Lindsey, J. S.; Wagner, R. W.; Droupadi, P. R.; Wang, W. Sequential protonation of meso-[p-(dimethylamino)phenyl]porphyrins: charge-transfer excited states producing hyperporphyrins. *J. Phys. Chem.* **1993**, *97*, 13192–13197.
(74) Ransdell, R. A.; Wamser, C. C. Solvent and substituent effects on the redox properties of free-base tetraphenylporphyrins in DMSO and aqueous DMSO. *J. Phys. Chem.* **1992**, *96*, 10572–10575.
(75) Bailey, D. N.; Hercules, D. M.; Roe, D. K. Electrochemistry and Photopotentials of Phenazine in Methanol Solutions. *J. Electrochem. Soc.* **1969**, *116*, 190–195.
(76) Ćirić-Marjanović, G. Recent advances in polyaniline research: Polymerization mechanisms, structural aspects, properties and applications. *Synth. Met.* **2013**, *177*, 1–47.
(77) Das, T. K.; Prusty, S. Review on Conducting Polymers and Their Applications. *Polym.-Plast. Technol. Eng.* **2012**, *51*, 1487–1500.
(78) MacDiarmid, A. G. "Synthetic Metals": A Novel Role for Organic Polymers (Nobel Lecture). *Angew. Chem. Int. Ed.* **2001**, *40*, 2581–2590.
(79) Heeger, A. J. Nobel Lecture: Semiconducting and metallic polymers: The fourth generation of polymeric materials. *Rev. Mod. Phys.* **2001**, *73*, 681–700.
(80) Rubinstein, I.; Sabatani, E.; Rishpon, J. Electrochemical Impedance Analysis of Polyaniline Films on Electrodes. *J. Electrochem. Soc.* **1987**, *134*, 3078–3083.

(81) Rubinson, J. F.; Kayinamura, Y. P. Charge transport in conducting polymers: insights from impedance spectroscopy. *Chem. Soc. Rev.* **2009**, *38*, 3339–3347.
(82) Mondal, S. K.; Prasad, K. R.; Munichandraiah, N. Analysis of electrochemical impedance of polyaniline films prepared by galvanostatic, potentiostatic and potentiodynamic methods. *Synth. Met.* **2005**, *148*, 275–286.
(83) Garcia-Belmonte, G.; Bisquert, J.; Pereira, E. C.; Fabregat-Santiago, F. Anomalous transport on polymeric porous film electrodes in the dopant-induced insulator-to-conductor transition analyzed by electrochemical impedance. *Appl. Phys. Lett.* **2001**, *78*, 1885–1887.
(84) Bisquert, J.; Garcia-Belmonte, G.; Bueno, P.; Longo, E.; Bulhões, L. O. S. Impedance of constant phase element (CPE)-blocked diffusion in film electrodes. *J. Electroanal. Chem.* **1998**, *452*, 229–234.
(85) Fletcher, S. Contribution to the theory of conducting-polymer electrodes in electrolyte solutions. *J. Chem. Soc. Faraday Trans.* **1993**, *89*, 311–320.
(86) Lyons, M. *Electroactive Polymer Electrochemistry: Part 1: Fundamentals*; Springer Science & Business Media, 2013.
(87) A. Sezai Sarac; Murat Ates; Bilge Kilic Electrochemical Impedance Spectroscopic Study of Polyaniline on Platinum, Glass Carbon and Carbon Microelectrodes. *Int. J. Electrochem. Sci.* **2008**, *3*, 777–786.
(88) Jorcin, J.-B.; Orazem, M. E.; Pébère, N.; Tribollet, B. CPE analysis by local electrochemical impedance spectroscopy. *Electrochimica Acta* **2006**, *51*, 1473–1479.
(89) Córdoba-Torres, P.; Mesquita, T. J.; Nogueira, R. P. Relationship between the Origin of Constant-Phase Element Behavior in Electrochemical Impedance Spectroscopy and Electrode Surface Structure. *J. Phys. Chem. C* **2015**, *119*, 4136–4147.
(90) Zoltowski, P. On the electrical capacitance of interfaces exhibiting constant phase element behaviour. *J. Electroanal. Chem.* **1998**, *443*, 149–154.
(91) Albery, W. J.; Mount, A. R. Dual transmission line with charge-transfer resistance for conducting polymers. *J. Chem. Soc. Faraday Trans.* **1994**, *90*, 1115–1119.
(92) Burgmayer, P.; Murray, R. W. Ion gate electrodes. Polypyrrole as a switchable ion conductor membrane. *J. Phys. Chem.* **1984**, *88*, 2515–2521.
(93) Feldman, B. J.; Burgmayer, P.; Murray, R. W. The potential dependence of electrical conductivity and chemical charge storage of poly(pyrrole) films on electrodes. *J. Am. Chem. Soc.* **1985**, *107*, 872–878.
(94) Li, H.; Wang, J.; Chu, Q.; Wang, Z.; Zhang, F.; Wang, S. Theoretical and experimental specific capacitance of polyaniline in sulfuric acid. *J. Power Sources* **2009**, *190*, 578–586.
(95) Kipnis, N. A Law of Physics in the Classroom: The Case of Ohm's Law. *Sci. Educ.* **2009**, *18*, 349–382.
(96) Albert, A.; Goldacre, R.; Phillips, J. The strength of heterocyclic bases. *J. Chem. Soc.* **1948**, 2240–2249.

(97) MacDiarmid, A. G.; Epstein, A. J. Polyanilines: a novel class of conducting polymers. *Faraday Discuss. Chem. Soc.* **1989**, *88*, 317–332.
(98) Scully, J. R.; Silverman, D. C.; Kendig, M. W. *Electrochemical Impedance: Analysis and Interpretation*; ASTM International, 1993.
(99) Albery, W. J.; Elliott, C. M.; Mount, A. R. A transmission line model for modified electrodes and thin layer cells. *J. Electroanal. Chem. Interfacial Electrochem.* **1990**, *288*, 15–34.
(100) Lvovich, V. *Interface*. pp. 62–66.
(101) Monk, P.; Mortimer, R.; Rosseinsky, D. *Electrochromism and Electrochromic Devices*; Cambridge University Press, 2007.
(102) Dong, Q.; Su, J.-H.; Gong, S.; Li, Q.-S.; Zhao, Y.; Wu, B.; Yang, X.-J. Nickel Complexes with Two Types of Noninnocent Ligands: α-Diimine and Phenazine. *Organometallics* **2013**, *32*, 2866–2869.
(103) Kaye, R. C.; Stonehill, H. I. 619. The polarographic reduction of pyridine, quinoline, and phenazine. *J. Chem. Soc. Resumed* **1952**, 3240–3243.
(104) Laviron, E.; Roullier, L. Electrochemical reactions with protonations at equilibrium: Part IX. Comparison between the surface and heterogeneous electrochemical rate constants in the system phenazine/dihydrophenazine. *J. Electroanal. Chem. Interfacial Electrochem.* **1983**, *157*, 7–18.
(105) Kadish, K. M.; Guilard, R. *Handbook of Porphyrin Science: With Applications to Chemistry, Physics, Materials Science, Engineering, Biology and Medicine, Vol 1-35*; 1st edition.; World Scientific Publishing Company: Hackensack, N.J. ; London, 2010.
(106) *Iron Porphyrins: Pts. 1 & 2 in 1v*; Lever, A. B. P.; Gray, H. B., Eds.; Wiley-VCH Verlag GmbH, 1989.
(107) Zaikowski, L.; Kaur, P.; Gelfond, C.; Selvaggio, E.; Asaoka, S.; Wu, Q.; Chen, H.-C.; Takeda, N.; Cook, A. R.; Yang, A.; Rosanelli, J.; Miller, J. R. Polarons, Bipolarons, and Side-By-Side Polarons in Reduction of Oligofluorenes. *J. Am. Chem. Soc.* **2012**, *134*, 10852–10863.
(108) Pomerantz, Z.; Zaban, A.; Ghosh, S.; Lellouche, J.-P.; Garcia-Belmonte, G.; Bisquert, J. Capacitance, spectroelectrochemistry and conductivity of polarons and bipolarons in a polydicarbazole based conducting polymer. *J. Electroanal. Chem.* **2008**, *614*, 49–60.
(109) Bredas, J. L.; Street, G. B. Polarons, bipolarons, and solitons in conducting polymers. *Acc. Chem. Res.* **1985**, *18*, 309–315.
(110) Skotheim, T. A.; Reynolds, J. *Handbook of Conducting Polymers, 2 Volume Set*; CRC Press, 2007.
(111) Kellett, R. M.; Spiro, T. G. Cobalt porphyrin electrode films as hydrogen catalysts. *Inorg. Chem.* **1985**, *24*, 2378–2382.
(112) Jester, C. P.; Rocklin, R. D.; Murray, R. W. Electron Transfer and Axial Coordination Reactions of Cobalt Tetra(Aminophenyl)Porphyrins Covalently Bonded to Carbon Electrodes. *J. Electrochem. Soc.* **1980**, *127*, 1979–1985.

(113) Lokesh, K. S.; De Keersmaecker, M.; Adriaens, A. Self Assembled Films of Porphyrins with Amine Groups at Different Positions: Influence of Their Orientation on the Corrosion Inhibition and the Electrocatalytic Activity. *Molecules* **2012**, *17*, 7824–7842.
(114) Benaglia, M.; Puglisi, A.; Cozzi, F. Polymer-Supported Organic Catalysts. *Chem. Rev.* **2003**, *103*, 3401–3430.
(115) Bettelheim, A.; White, B. A.; Raybuck, S. A.; Murray, R. W. Electrochemical polymerization of amino-, pyrrole-, and hydroxy-substituted tetraphenylporphyrins. *Inorg. Chem.* **1987**, *26*, 1009–1017.
(116) Dai, L.; Xue, Y.; Qu, L.; Choi, H.-J.; Baek, J.-B. Metal-Free Catalysts for Oxygen Reduction Reaction. *Chem. Rev.* **2015**, *115*, 4823–4892.
(117) Bettelheim, A.; White, B. A.; Murray, R. W. Electrocatalysis of dioxygen reduction in aqueous acid and base by multimolecular layer films of electropolymerized cobalt tetra(o-aminophenyl)porphyrin. *J. Electroanal. Chem. Interfacial Electrochem.* **1987**, *217*, 271–286.
(118) Ozer, D.; Harth, R.; Mor, U.; Bettelheim, A. Electrochemistry of various substituted aminophenyl iron porphyrins. Part II. Catalytic reduction of dioxygen by electropolymerized films. *J. Electroanal. Chem. Interfacial Electrochem.* **1989**, *266*, 109–23.
(119) Gong, K.; Du, F.; Xia, Z.; Durstock, M.; Dai, L. Nitrogen-Doped Carbon Nanotube Arrays with High Electrocatalytic Activity for Oxygen Reduction. *Science* **2009**, *323*, 760–764.
(120) Bard, A. J.; Faulkner, L. R. *Electrochemical Methods: Fundamentals and Applications*; Wiley, 2000.
(121) Fernandez, F.; Quigley, R. M. Viscosity and dielectric constant controls on the hydraulic conductivity of clayey soils permeated with water-soluble organics. *Can. Geotech. J.* **1988**, *25*, 582–589.
(122) Linford, R. G. *Electrochemical science and technology of polymers*; Elsevier Applied Science, 1987.
(123) Wang, C. M.; Heller, A.; Gerischer, H. Palladium catalysis of O_2 reduction by electrons accumulated on TiO_2 particles during photoassisted oxidation of organic compounds. *J. Am. Chem. Soc.* **1992**, *114*, 5230–5234.